Higher order sinusoidal input describing functions : extending linear techniques towards non-linear systems analysis

Document Version:
Publisher's PDF, also known as Version of Record (includes final page, issue and volume numbers)

Please check the document version of this publication:

• A submitted manuscript is the version of the article upon submission and before peer-review. There can be important differences between the submitted version and the official published version of record. People interested in the research are advised to contact the author for the final version of the publication, or visit the DOI to the publisher's website.
• The final author version and the galley proof are versions of the publication after peer review.
• The final published version features the final layout of the paper including the volume, issue and page numbers.

[Link to publication](#)

Higher Order Sinusoidal Input Describing Functions

Extending linear techniques towards non-linear systems analysis

Higher Order Sinusoidal Input Describing Functions

Extending linear techniques towards non-linear systems analysis

PROEFSCHRIFT

ter verkrijging van de graad van doctor
aan de Technische Universiteit Eindhoven,
op gezag van de Rector Magnificus, prof.dr.ir. C.J. van Duijn,
voor een commissie aangewezen door het College voor Promoties
in het openbaar te verdedigen
op woensdag 29 augustus 2007 om 16.00 uur

door

Pieter Waltherus Jozef Maria Nuij

geboren te Eindhoven

Dit proefschrift is goedgekeurd door de promotoren:

prof.dr.ir. M. Steinbuch
en
prof.ir. O.H. Bosgra

Contents

Nomenclature

Acronyms

CD	Compact Disc
DAC	Digital to Analog Convertor
DC	Direct Current
DF	Describing Function
DVD	Digital Versatile Disc
FFT	Fast Fourier Transform
FRF	Frequency Response Function
GFRF	Generalized Frequency Response Function
HOSIDF	Higher Order Sinusoidal Input Describing Functions
HOSODF	Higher Order Sinusoidal Output Describing Functions
IQ	In-phase Quadrature-phase
OLFRF	Open Loop Frequency Response Function
OLTF	Open Loop Transfer Function
PSD	Power Spectral Density
RLDS	Related Linear Dynamic System
RMS	Root Mean Square
SFRF	Sensitivity Frequency Response Function
SIDF	Sinusoidal Input Describing Function
SODF	Sinusoidal Output Describing Function
STF	Sensitivity Transfer Function
VHC	Virtual Harmonics Compressor
VHE	Virtual Harmonics Expander
ZPETC	Zero Phase Error Tracking Controller

List of operators

Operator	Description
$floor(X)$	rounds the elements of X to the nearest integers towards minus infinity
G_{XX}	auto-power spectrum of x(t)
G_{XY}	cross-power spectrum of x(t) and y(t)
$\hat{H}_{1n}$	estimated value of H_{1n}
$\|x\|$	magnitude of a complex number x
$\angle x$	phase of the complex number x
$xdBV$	$20 \cdot^{10} \log x/V$
$\delta y/\delta x$	partial derivative of y with respect to x

List of symbols

Symbol	Description	Unit
A_n	amplitude of nth harmonic signal component	
a_i, b_i	i^{th} Fourier coefficients	
$\hat{a}$	amplitude of sinusoidal input signal	
b	damping	[Ns/m]
$C(s)$	transfer function of controller	
C_G	amplitude gradient	
C_{11}	complex value of the linear controller C at ω	
C_{n1}	complex value of the linear controller C at $n\omega$	
$D(j\omega)$	Fourier transform of d(t)	
$DC(z)$	transfer function of the DC reconstruction filter	
$d(t)$	external disturbance time signal	
$e(t)$	error time signal	
F_c	Coulomb friction force	[N]
F_f	restoring friction force	[N]
F_h	friction force with hysteretic behavior	[N]
F_s	static friction force	[N]
F_ω	tangential force frequency signal	[N]
f	frequency	[Hz]
f_k	frequency of kth line of an FFT	[Hz]
f_{res}	resonance frequency	[Hz]
f_s	sampling frequency	[Hz]

f_{max}	maximum frequency in multisine excitation signal	[Hz]
$G(f_k)$	leakage free FRF of a Volterra system	
$G_B(f_k)$	leakage free systematic bias due to non-linear distortion	
$G_O(f_k)$	leakage free FRF of the underlying linear system	
$G_R(f_k)$	leakage free FRF of the Related Linear Dynamic System	
$G_S(f_k)$	leakage free stochastic non-linear contribution to $G(f_k)$	
$Gen(t)$	Generator time signal with non-constant amplitude	
$H(\hat{a}, \omega)$	sinusoidal input describing function	
$H_k(\hat{a}, \omega)$	k^{th} order sinusoidal input describing function	
$H(s)$	transfer function of a plant	
H_{nm}	complex value of the mth HOSIDF at $n\omega$	
$h(\tau)$	impulse response function	
I	class of stable, time-invariant non-linear systems with a harmonic response to a sinusoidal excitation	
I_k	k^{th} in-phase component of IQ demodulator	
I_m	motor current	[A]
I_s	sensed motor current	[A]
J	inertia	[kgm^2]
k	stiffness	[N/m]
$L(z)$	transfer function of the learning filter	
l	delay caused by L filter	
l_{window}	length of weighting function	[s]
M	repetitive controller	
$M_s(z)$	transfer function of the modified complementary sensitivity function	
m	mass	[kg]
N	number of components	
$N(j\omega)$	Fourier transform of n(t)	
$\mathbb{N}$	set of natural numbers	
$N_G(f_k)$	Impact of output noise on leakage free FRF measurement of $G(f_k)$	
$n(t)$	external generator time signal	
O	class of stable, time-invariant non-linear systems with a sinusoidal response to a harmonic excitation	
P	generalized contact point	
$P(j\omega)$	Fourier transform of p(t)	
$p(t)$	excitation time signal	
$Q(z)$	transfer function of the robustness filter	
Q_k	k^{th} quadrature-phase component of IQ demodulator	
q	delay caused by Q filter	

$R(\hat{a}, \omega)$	sinusoidal output describing function	
$R_k(\hat{a}, \omega)$	k^{th} order sinusoidal output describing function	
$R(j\omega)$	Fourier transform of r(t)	
$r(t)$	setpoint time signal	
$S(s)$	sensitivity transfer function	
s	Laplace transform variable	
T	torque	[Nm]
T_0	periode time	[s]
t	time variable	[sec]
T_b	length of data block	[s]
$U(j\omega)$	Fourier transform of u(t)	
U_n	n^{th} harmonic component of $U(\omega)$	
$u(t)$	input time signal	
$\breve{u}(t)$	virtual harmonics expander output time signal	
$\tilde{u}$	fundamental component of the system excitation time signal	
V_n	n^{th} excitation level	
v_s	Stribeck velocity	[m/s]
$x(t)$	displacement time signal	[m]
$\dot{x}(t)$	velocity time signal	[m/s]
$\ddot{x}(t)$	acceleration time signal	[m/s^2]
$Y(j\omega)$	Fourier transform of y(t)	
Y_n	n^{th} harmonic component of $Y(\omega)$	
$y(t)$	output time signal	
$y_l(t)$	linear part of output time signal	
$y_{nl}(t)$	non-linear part of output time signal	
$\breve{y}(t)$	virtual harmonics compressor input time signal	
$\tilde{y}(t)$	fundamental component of output time signal	
$\mathbb{Z}$	set of integer numbers	
z	Z-transform variable	
z	state variable describing average asperity deflection	[m]
γ	constant gain value	[-]
Δf	frequency spacing	[Hz]
ζ_i	state variable in Maxwell Slip model	[m]
σ_1	the micro-viscous damping coefficient	[Ns/m]
σ_2	the viscous damping coefficient	[Ns/m]
τ	time delay	[s]
φ	phase angle	[rad]
$\varphi_k(\hat{a}, \omega)$	phase of the kth order SIDF	[rad]
$\varphi_{k_{in}}$	phase of the kth harmonic component of the VHE	[rad]

$\varphi_{k_{out}}$	phase of the kth harmonic component in $Y(j\omega)$	[rad]
$\omega = 2\pi f$	angular frequency	[rad]
ω_{out}	angular velocity	[rad/s]
ω_{ps}	pre-sliding displacement frequency signal	[m]

Introduction

Abstract / In this chapter a brief introduction is given into the analysis of precision motion systems. The consequences of non-linear system behavior with respect to system identification are illustrated. In order to position this thesis, a short review is presented of the existing techniques for non-linear identification. The problem formulation and main contributions of the thesis are stated and an outline is presented.

This thesis is about the definition and application of a new technique for frequency response identification of non-linear systems. The technique is a generalization of the describing function concept and as such applicable for the analysis of a wide range of non-linear system behavior. We believe that this technique is a useful addition to the already wide family of analysis technique of non-linear system behavior.

1.1 Introduction to the analysis of precision motion systems

In many high precision positioning systems, position accuracy is a key performance objective. During the last three decades, accuracy requirements have changed from the micrometer range to the sub micron and even nanometer range. Examples of high precision systems are wafer scanners for lithographic applications, laser beam recorders for CD/DVD mastering, lathes for the production of optical components like contact lenses, electron microscopes and coordinate-measuring machines (Fig. 1.1). But also in consumer products, subcomponents like hard disc drives (Fig. 1.2) and optical storage devices can not function without extreme positioning accuracy. The operating conditions under which these products have to perform are changing from laboratory environment to an environment as hostile as a car on an unmetalled road. This poses extra challenges to both the mechanical and the control design. The mechanical design must be predictable and stable in time, often it must accommodate a wide temperature range and still be as

cheap as possible. The control design must be robust with respect to changes in mechanical behavior, but with a minimum of extra costs i.e. additional sensors. For both the mechanical and the control aspects, this can only be achieved by the use of advanced design techniques, often necessitating the incorporation of non-linear phenomena in the design.
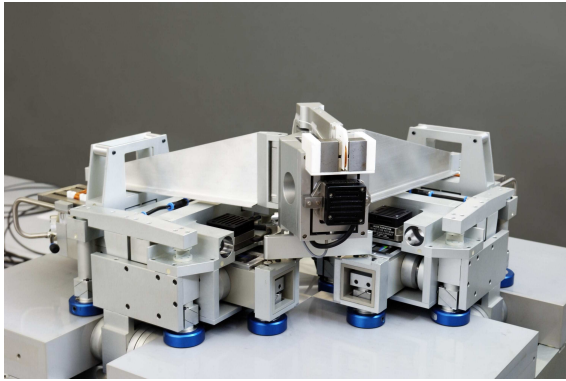
Figure 1.1 / Coordinate-measuring machine (van Seggelen, 2007).

Figure 1.2 / Hard disc drive.

1.2 Analysis of motion systems with linear techniques

The majority of high performance motion systems consists of a plant operating in feedback. The modern control theory and design procedures applied for the design and evaluation of these systems are frequency domain based. In this theory the *Sensitivity Transfer Function* (STF) plays a key role both in controller design and in loop performance evaluation. The STF is defined as (Skogestad and Postlethwaite, 2005)[1]:

$$S(s) = \frac{1}{1 + C(s)H(s)} \tag{1.1}$$

with $C(s)$ and $H(s)$ the transfer functions of respectively the controller and the plant, with s the Laplace operator. The product $C(s)H(s)$ is called the *Open Loop Transfer Function* (OLTF) and establishes the basis for stability analysis. For linear systems the OLTF can be determined from the STF as:

$$C(s)H(s) = S(s)^{-1} - 1 \tag{1.2}$$

For linear systems, thinking in terms of the Laplace transform and the transfer function is a powerful tool, especially when supported in practice with FRF measurements derived

---

[1]In order to present the concepts without unnecessary complexity, single input single output (SISO) descriptions are used in this thesis.
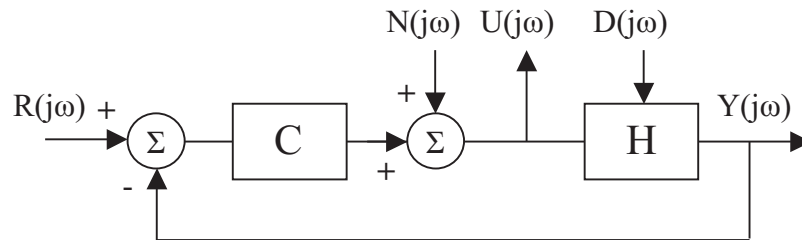
Figure 1.3 / Feedback system with additional summing node for determination of the sensitivity frequency response function.

under realistic operating conditions. The *Sensitivity Frequency Response Function* (SFRF) can be measured as depicted in Fig. 1.3. An external generator signal $N(j\omega)$, uncorrelated to both the setpoint $R(j\omega)$ and the external disturbances $D(j\omega)$, is inserted in the loop through a summing node. The output from the summing node is $U(j\omega)$. The H_1 Frequency Response Function (Randall, 1987) calculated from these signals yields the SFRF:

$$S(j\omega) = \frac{G_{NU}(j\omega)}{G_{NN}(j\omega)} \tag{1.3}$$

with $G_{NU}(j\omega)$ the cross spectrum between $N(j\omega)$ and $U(j\omega)$ and $G_{NN}(j\omega)$ the power spectrum of $N(j\omega)$. From the SFRF the *Open Loop Frequency Response Function* (OLFRF) can be calculated as:

$$C(j\omega)H(j\omega) = S(j\omega)^{-1} - 1 \tag{1.4}$$

As an example, a controlled motion system is measured. The system consists of a small DC motor driving a mass coupled through a torsion spring (Fig. 1.4).
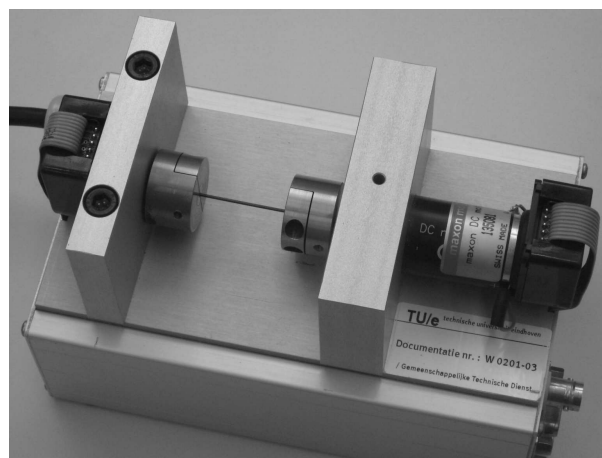
Figure 1.4 / System under test

Fig. 1.5 shows the Bode plots of both a measured SFRF (left column) and the calculated OLFRF (right column) of the controlled system measured under large signal conditions. The setpoint is a constant angular velocity of $2rev/sec$, the generator signal is band limited white noise of $5mV\,RMS$. The input signal of the measurement is the excitation signal $N(j\omega)$ inserted through the summing node amplifier. The output signal $U(j\omega)$ is the excitation voltage of the plant. The sampling frequency for this measurement is $1000Hz$, the block-size is 1024, a Hanning window is applied and the frequency domain results of 100 data-blocks are averaged.
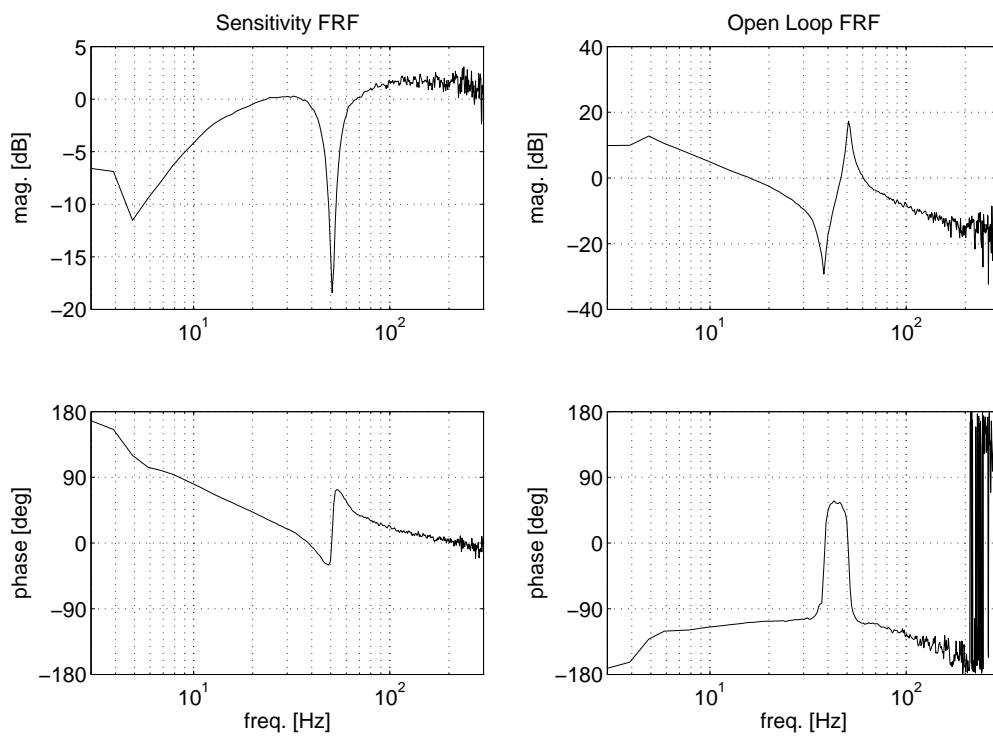
Figure 1.5 / Measured Sensitivity FRF and calculated Open Loop FRF. Conditions: $4\pi rad/sec$ setpoint, input: summing node excitation signal $5mV_{RMS}$, output: plant excitation voltage.

From the OLFRF we can conclude that the system is stable with a gain margin of approximately $15dB$ and a phase margin of approximately $80deg$ and has a bandwidth (first cross-over frequency) of approximately $15Hz$.

1.3 Non-linear behavior in motion systems

A limitation of using FRFs is the imperative assumption of linearity of the system behavior. Every real life system is non-linear although the implications are not always noticeable in the operating range. In Fig. 1.6 measurement results are presented of the same system as in Section 1.2. For these measurements the velocity setpoint is $0\,rev/sec$ and the band limited white noise generator signal is varied from $5mV\,RMS$ to $200mV\,RMS$. The sampling frequency, block-size, windowing and averaging remain unchanged. The differences between the results in Fig. 1.5 and Fig. 1.6 clearly indicate non-linear behavior. These differences are not only amplitude dependent, probably they are also caused by harmonic components from the output being fed back to the input of the system. From the SFRFs we see that depending on the operating conditions, error suppression of the control loop will vary more than $10dB$. From the OLFRFs we see large variations in the bandwidth, the phase margin and the low frequency gain, which results in a large variation in the performance of the controlled system. The causes of non-linear behavior are as numerous as their influences. Without being even remotely complete we mention causes like harmonic distortion in power amplifiers, quantization in analog to digital converters,
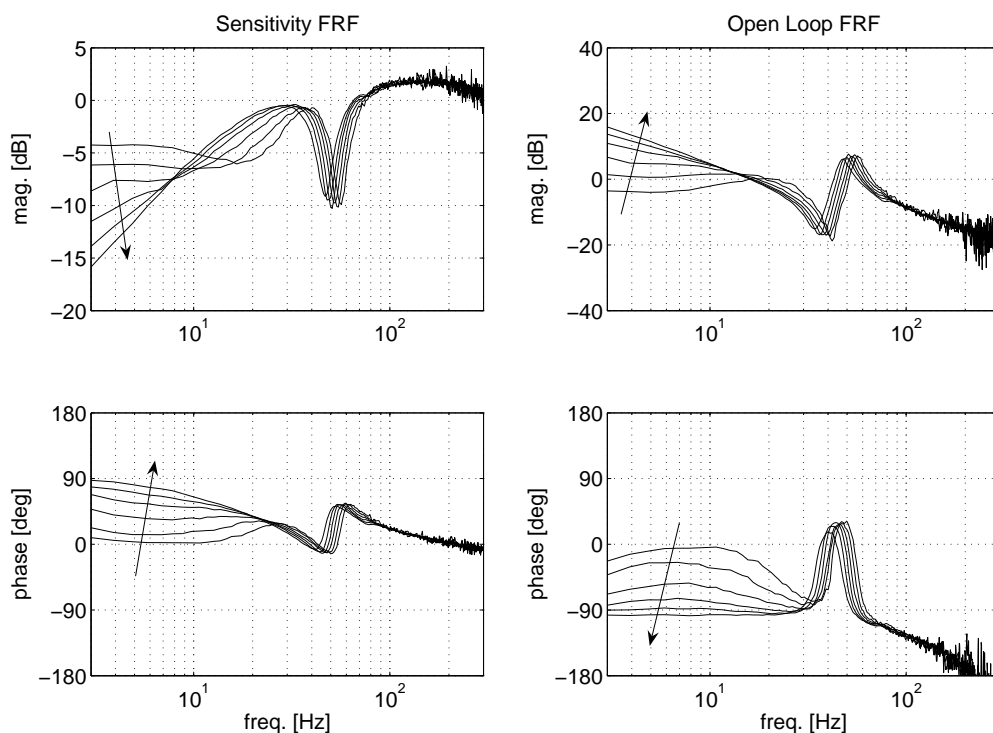
Figure 1.6 / Measured Sensitivity FRF and calculated Open Loop FRF. Conditions: $0\,rad/sec$ setpoint, input: summing node excitation signal $5mV_{RMS}$ to $200mV_{RMS}$, output: plant excitation voltage. The direction of the arrow indicates increasing excitation voltage.

saturation in magnetic material, play in kinematically over-constrained constructions and hysteresis in friction contacts. In precision motion systems, non-linear behavior can not be ignored, at best reduced with control loops. Control theory offers limited solutions for reducing the influences of non-linear system behavior on the performance of the controlled system. An example of an established technique is feedback linearisation of smooth non-linear systems, which can be implemented in motion control as computed torque control. With this technique the controlled system is linearized by implementing an inverted model of the non-linear system in the feedback loop (An et al., 1988; Nijmeijer and der Schaft, 1991; Slotine and Li, 1991; Sciavicco and Siciliano, 1996). For non-smooth systems (friction, hysteresis, etc.) feedback linearisation is not applicable and one has to resort to case specific approximative approaches for control. Non-linear system behavior has to be taken into consideration from the first pondering in the concept phase through the design and construction phase and even beyond the final release test for condition monitoring. As an example, let us consider the impact which a common phenomenon like friction has on positioning accuracy of these controlled motion systems and how friction influences the controller design process.

An example: Friction

In Fig. 1.7 the block-diagram of a motion system with friction is depicted. The system is non-linear due to the non-linear relation between the output and the resulting restoring friction force $F_f(t)$. This relation may be very complex and up to now not completely understood yet.
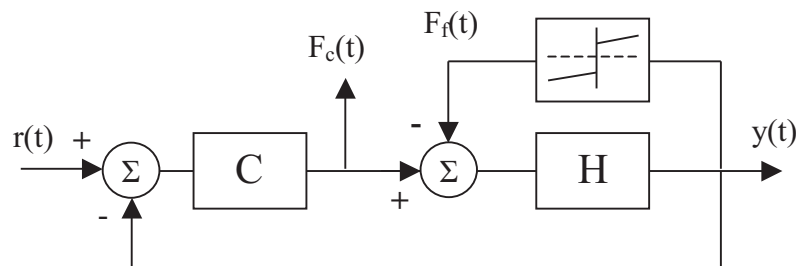
Figure 1.7 / Blockdiagram of non-linear feedback system

Friction has such a strong influence on positioning accuracy because it can lead to tracking errors, large settling times and limit cycling (Hensen, 2002; Hensen and van de Molengraft, 2002; Hensen et al., 2002b, 2003; Mihajlovic et al., 2004; Putra, 2004). In ultra precision motion systems the effect of friction is minimized by the application of gas bearings or fluid bearings. This results in rather complex and expensive mechanical constructions. In the majority of industrial positioning equipment however, the application of these ultra low friction bearings is too expen-

sive. Hence, the negative effects of friction on the dynamics of these machines have to be taken into account in the controller design. Advanced feedforward techniques are applied (de Jager, 1993; Armstrong-Hélouvry et al., 1994; Lee and Tomizuka, 1996; Kostic et al., 2004). These solutions are based on dynamic friction models like the Lu-Gre model and its modifications (de Wit et al., 1995; Swevers et al., 2000; Lampaert et al., 2002). These models include the Stribeck effect, non-local memory hysteresis, spring-like behavior for stiction and varying break-away force. Both for validating these friction models and for generating reliable friction parameters for the control algorithms, the dynamic friction model parameters must be identified with experiments on real systems. For this identification, time domain techniques are often used (de Wit and Lischinsky, 1997; Lampaert et al., 2004). Also linear frequency domain techniques are applied in order to estimate a Frequency Response Function (FRF) from which a number of friction parameters can be identified. The FRF concept however, presumes linear system behavior which is clearly not the case in this situation. This dilemma is dealt with by applying random noise excitation signals (Hensen et al., 2002a) or swept sine excitation (Sherif and Bassioni, 1994; Symens et al., 2002) which results in linearized (thus approximated) FRFs. It is clear that, although modern, thus frequency domain based, control theory still heavily draws on linear analysis techniques, a frequency domain based non-linear approach to analyse and synthese motion systems becomes inevitable.

1.4 Frequency domain techniques for non-linear system analysis

The measurements presented in the previous section showed that in case of a non-linear system, the Frequency Response Function is not a sufficient description of the system behavior. It has insufficient distinguishing and characterizing capabilities. The FRF measurement results of non-linear systems always have to be treated with caution because the characteristics of the excitation signal can have significant influence on the measured system characteristics (Nuij, 2002). Or even worse, the non-linear behavior is not detected and completely fools the experimenter (Billings and Tsang, 1990b). Many techniques exist for detecting non-linear system behavior (Wyckaert, 1992; Adams and Allemang, 1998; Vanhoenacker et al., 2002; Gloth and Göge, 2004) and in a realistic measurement situation a system linearity test should be the aim for the first measurement. Based upon the results of this initial test, the experimenter has to choose a suitable measurement technique to reveal the information he/she is looking for. In this section some commonly used frequency domain based techniques for the analysis of non-linear systems will be reviewed.

1.4.1 Linearisation

Frequency Response Functions are the starting point in modern control design and as such have their value. There are several approaches to approximate a non-linear system with a linear description. One approach assumes a weakly non-linear system to consist of a parallel connection of a true linear part and a non-linear part (Fig. 1.8). The contribution of the non-linear system $y_{nl}(t)$ to the output signal $y(t)$ is treated as distortion. If $y_l(t)$, the linear part of the response, dominates the system behavior for small excitations $u(t)$, the true linear system can be successfully identified. The influence of the non-linear distortion can be further minimized using odd multisine excitation signals with minimized crest factor and with an amplitude kept as small as possible (Evans and Rees, 2000b; Pintelon and Schoukens, 2001; Solomou et al., 2001). These multisine signals consist of N frequency components such that:

$$u(t) = \frac{1}{\sqrt{N}} \sum_{k=-N}^{N} U_k e^{jk2\pi f_{max}t/N} \tag{1.5}$$

with N the number of frequency components, $U_k = \overline{U}_{-k} = |\hat{U}(kf_{max}/N)|e^{j\varphi_k}$, f_{max} the maximum frequency of the excitation signal and φ_k the phase distribution to yield the minimized crest factor.
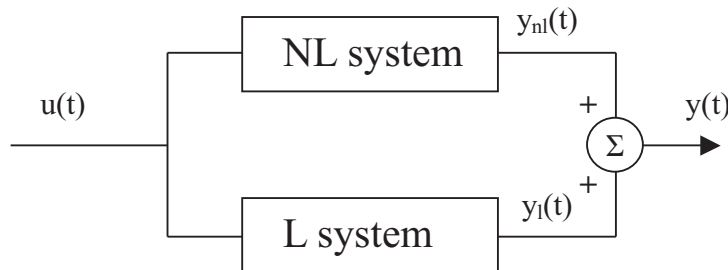
Figure 1.8 / Modeling a weakly non-linear system with a linear part and a non-linear part in parallel.

A second approach is to find the best linear approximation to the weakly non-linear system, i.e. the parallel connection of the truly linear part and the non-linear part (Fig. 1.8) (Schoukens et al., 1998; Weiss et al., 1998; Evans and Rees, 2000a; Pintelon and Schoukens, 2001; Dedene et al., 2002; Solomou et al., 2004; Schoukens et al., 2005). A system which response to a normalized random multisine excitation can be approximated by a Volterra series, has a measured FRF that be expressed as:

$$G(f_k) = G_R(f_k) + G_S(f_k) + N_G(f_k) \tag{1.6}$$

with f_k a multiple of the frequency spacing Δf of the FRF, $G_R(f_k)$ the Related Linear Dynamic System (RLDS), $G_S(f_k)$ the stochastic non-linear distortions and $N_G(f_k)$ the contribution of the measurement noise. The Related Linear Dynamic System consists of:

$$G_R(f_k) = G_O(f_k) + G_B(f_k) \tag{1.7}$$

with $G_O(f_k)$ the true linear system L and $G_B(f_k)$ the systematic bias due to non-linear distortion (Pintelon and Schoukens, 2001). The RLDS is a linearisation around an operating point so the test signals must be chosen similar to the signals under operating conditions for the approximation to be valid. The value of $G_B(f_k)$ depends the power spectrum and amplitude distribution of the excitation signals, the value of $G_S(f_k)$ also depends on the the actual phases of the multisine input signal. Averaging over several phase realizations will reduce $G_S(f_k)$. Averaging over several data blocks with equal phase realization will reduce $N_G(f_k)$. Apart from leakage free measurements, these multi-sine based signals also provide qualitative and quantitative information about the non-linear distortions. Generating only the $4k + 1$ frequency lines results in an odd-odd multisine. The response signal at frequency lines $4k + 1$ will consist of the linear contribution of the system and the odd non-linear distortion components. At frequency lines $4k + 2$ only the even non-linear distortion components will occur and the lines $4k + 3$ only contain the odd non-linear distortion components. The distribution is indicative for the non-linear behavior the system.

1.4.2 Describing Functions

For weakly non-linear systems the RLDS is a useful description of the system behavior. For systems with a stronger non-linear behavior, linearisation is only useful if the excursions of the system around its nominal operating point are small. Incorporating the excitation amplitude as a parameter in the (quasi)linear description can extend the range of operating points over which the non-linear system can be approximated. The resulting description, the Describing Function, is a function of the excitation signal characteristics. The Sinusoidal Input Describing Function and the Random Input Describing Function are well known (Gelb and Velde, 1968; Atherton, 1975; Slotine and Li, 1991; Taylor, 1999). The Describing Function concept extends the Frequency Response Function in the way that identification of amplitude dependency becomes possible. However this concept still does not describe the frequency transformation properties of non-linear systems. It is successfully used in the identification of strong non-linear behavior like the stick/sliding transition present in any common mechanical system with friction (Guvenc and Srinivasan, 1994; Olsson, 1995; Taylor and Jin, 1995; Armstrong and Amin, 1996; Olsson and Åström, 1996; Kang and Kim, 1997; Besançon-Voda and Blaha, 2002; Lim, 2003; Al-Bender and Symens, 2005a,b; Kim and Chung, 2006). An additional benefit of the describing function concept is its simplicity. It is an elegant and intuitively

apprehensible extension of linear techniques into the non-linear domain making it a useful and transparent analysis technique.

1.4.3 Generalized Frequency Response Functions

The dynamic behavior of a causal, stable, time-invariant linear system can be described by its impulse response function $h(\tau)$. The output $y(t)$ of the system is related to the input $u(t)$ through the convolution integral, assuming $u(t) = 0$ for $t < 0$,

$$y(t) = \int_0^\infty h(\tau) \cdot u(t - \tau) d\tau \tag{1.8}$$

The Fourier transform of this integral results in the Frequency Response Function $H(j\omega)$ which describes the system behavior in the frequency domain.

$$Y(j\omega) = H(j\omega)U(j\omega) \tag{1.9}$$

For the class of causal, stable, time-invariant, non-linear systems with analytic response functions, the convolution integral description of the linear system (Eq. 1.8) can be generalized to an infinite series called the Volterra series (Volterra et al., 1913; Volterra, 1959; Schetzen, 1980; Rugh, 1981). In that case the output $y(t)$ can be expressed as the sum of N components $y_n(t)$:

$$y(t) = \sum_{n=1}^N y_n(t) \tag{1.10}$$

with $y_n(t)$ the n-th order output component defined as:

$$y_n(t) = \int_0^\infty \ldots \int_0^\infty h_n(\tau_1, \tau_2, \ldots, \tau_n) \prod_{i=1}^n u(t - \tau_i) d\tau_i \tag{1.11}$$

where $h_n(\tau_1, \tau_2, \ldots, \tau_n)$ is the n-th order Volterra kernel (Bussgang et al., 1974; Lesiak and Krener, 1978; Chua and Ng, 1979; Boyd and Chua, 1985). Similar to the 1-dimensional Fourier transform of the impulse response function which yields the classical Frequency Response Function (Eq. 1.9), the n-dimensional Fourier transform of the n-th order Volterra kernel yields the n-th-order Frequency Response Function, the Generalized Frequency Response Function (GFRF) (George, 1959; Bedrosian and Rice, 1971).

$$Y_n(j\omega_1, j\omega_2 \ldots, j\omega_n) = H_n(j\omega_1, j\omega_2, \ldots, j\omega_n) \prod_{i=1}^n U(j\omega_i) \tag{1.12}$$

These GFRFs can be estimated with non-parametric methods under the assumption that the system can be described by a low order (truncated) Volterra kernel. The high numerical cost however limits these methods to the identification of GFRFs up to a maximum

order of three (Boyd et al., 1983; Chua and Liao, 1989). Parametric identification techniques ease the numerical requirements and allow analytical expressions for GFRFs up to any order (Billings and Tsang, 1989b,a, 1990a). The GFRFs also have their limitations as a tool to describe non-linear system behavior. Firstly, systems with non-fading memory (Boyd and Chua, 1985), like non-local memory hysteresis as seen in friction, can not be described with Volterra series, the basis of the GFRFs.[2] Secondly, the interpretation of the GFRFs is difficult due to their multidimensional nature (Jones and Billings, 1990; Yue et al., 2005a,b). To our opinion it is premature to conclude that the GFRFs are the ultimate tool for the analysis of non-linear system behavior because their visualization and interpretation is very demanding. For this technique to be successfully applicable it must at least provide useful information about the system behavior in a comprehensible format and connect to the background of the user.

1.5 Problem formulation

From the observations in the previous sections we may conclude that the ever increasing performance requirements of systems induce the relevance to address non-linear behavior. This necessitates the increase in capabilities of analysis techniques for non-linear system behavior and the design techniques for advanced control. This necessity is felt both in theoretical analysis techniques as well as in synthesis techniques and practical measurement techniques. We also conclude that there does not exist a comprehensive technique for frequency domain based analysis of non-linear systems.

In the field of classical system analysis, the linear concept of the Frequency Response Function displayed in Bode plots is well established. But its applicability in non-linear system analysis is confined to the identification of a linearized representation of the real system behavior. The Sinusoidal Input Describing Function concept extends the Frequency Response Function in the way that identification of amplitude dependency becomes possible. However, it ignores the excitation frequency transformation property of many non-linear systems. The Generalized Frequency Response Functions do not have these limitations but they are difficult to visualize which hampers the interpretation of the results. An additional limitation of the GFRFs is the fact that they only exist for non-linear systems with fading memory. This raises the question whether it is possible to formulate a new analysis technique for non-linear system behavior. A technique which (i) is applicable for a broad class of non-linear systems, (ii) combines the quasi linearisation principle of the Describing Function with (iii) the analysis capabilities of the GFRFs with respect to frequency transformation, (iv) characterizes transitions in non-linear system behavior in

---

[2]A system has fading memory if two input signals which are close in the recent past, but not necessarily close in the remote past yield present outputs which are close((Boyd and Chua, 1985), p.1152)

a structured way and finally (v) presents the information in an intuitively comprehensible format. An additional question which immediately comes to mind is about the applicability of such a new technique in practice. Can the usefulness of this new technique be demonstrated? In this thesis we will answer both questions affirmatively.

1.6 Expected contribution of this thesis

In this thesis the extension of the application of linear techniques towards non-linear systems analysis is studied. We focus on the class of time invariant non-linear systems with a harmonic response to a sinusoidal excitation. We show that systems belonging to this class can be modeled as a Virtual Harmonics Expander in series with a structure consisting of Higher Order Sinusoidal Input Describing Functions (HOSIDF) in parallel. The HOSIDF are the natural generalization of the Sinusoidal Input Describing Function and can be defined as the complex ratio of the nth harmonic component in the output signal to the virtual n^{th} harmonic signal derived from the sinusoidal excitation signal. Two measurement techniques are presented for the non-parametric identification of the HOSIDF. One technique is FFT based and the second technique is based on IQ (in-phase/quadrature-phase) demodulation. The selectivity and dynamic range of the two identification techniques are investigated. Both aspects are tested on the basis of simulation by comparing the HOSIDF estimates with the analytical expressions of the HOSIDF for a system with backlash. To our knowledge, both this modeling technique and the two non-parametric identification techniques of HOSIDF are new. They have first been presented in (Nuij and Steinbuch, 2004) and have been published in (Nuij et al., 2006, 2007b).

We concluded in the previous section that for an analysis technique to be successful, it must at least provide useful information about the system behavior. Although useful is a subjective measure and depends on the needs of the user, we make a reasonable case for the usefulness of this new analysis technique. From the odd HOSIDF identified in a real mechanical system with dry friction, we are able to determine the transition from the stick phase to the sliding phase as function of frequency and excitation amplitude (Nuij et al., 2007a). From these results the maximum tangential force in the friction contact is determined without the need of a dedicated force measurement. This opens new possibilities in for example machine condition monitoring.

To extend the area of applicability of the HOSIDF concept, we studied the implications feedback has on the estimation of HOSIDF. We present two techniques for reducing bias in the identification of HOSIDF of a non-linear plant operating in feedback. The first technique is a new numerical compensation algorithm which compensates for the harmonics fed back from the output of the non-linear system to the input. The second technique combines existing repetitive control strategies for harmonics suppression with a

new layout of the repetitive controller. Both techniques show excellent results (Nuij et al., 2007b).

The final contribution of this thesis is a new concept of a non-linear systems description. We name this concept the Higher Order Sinusoidal Output Describing Function (HOSODF) and define it as the dual of the HOSIDF. Where the HOSIDF is a description of non-linear behavior in the case of sinusoidal excitation, the HOSODF is the dual description of non-linear behavior in the case of a sinusoidal response. In this duality the Virtual Harmonics Expander is transformed into a Virtual Harmonics Compressor and positioned at the output of the non-linear systems model.

1.7 Outline

The outline of this thesis is as follows: in Chapter 2 the concept of the Higher Order Sinusoidal Input Describing Function is defined. Hereto the Virtual Harmonics Expander is introduced as a new non-linear function. In Chapter 3 two methods for the non-parametric identification of HOSIDF are described. Both methods are validated in Chapter 4. In Chapter 5 some practical aspects of both methods are demonstrated on the bases of a realistic measurement. In Chapter 6 we zoom in on a real application: the analysis of the stick/sliding transition in a bearing with friction. In Chapter 7 we expand our view again and present two techniques which enable the identification of HOSIDF of a non-linear plant operating in feedback. A possible application of HOSIDF in machine condition monitoring will be demonstrated in Chapter 8. Chapter 9 is the dual of Chapter 2. In this chapter we present the Higher Order Sinusoidal Output Describing Functions together with the Virtual Harmonics Compressor. In Chapter 10 conclusions are drawn and recommendations for further research are given. In the Appendix the Fourier coefficients of a system with backlash are presented, together with a short explanation of the Modified Leuven friction model and the parameters used in the measurements and simulation experiments.

Generalizing the Describing Function to Higher Order Describing Functions

Abstract / For a specific class of non-linear systems the Sinusoidal Input Describing Function can be generalized to Higher Order Sinusoidal Input Describing Functions. The concept of the Virtual Harmonics Expander is defined as the tool required for this generalization.

As stated in a Section 1.5, we will explore an extension of the well known (quasi) linear techniques for system analysis like FRF and Describing Functions towards non-linear systems analysis. Our strategy is the following:

1. Restrict the class of non-linear systems to be considered.

2. Separate the non-linear system in a highly non-linear part which can not be analyzed with (quasi) linear techniques but which can be successfully modeled and a part which can be analyzed with (quasi) linear techniques.

3. Merge the information gained from the non-linear modeling technique and from the (quasi) linear analysis technique.

2.1 Definition of the class of systems under consideration

Because the number of elements belonging to the class of non-linear systems is probably tending towards infinity, we have to restrict ourselves to a subset which can be successfully analyzed.

Definition 1. (Class of non-linear systems under consideration): The class *I* of causal, stable, time invariant non-linear systems which have a harmonic response to a sinusoidal excitation.

When we mention non-linear systems in the sequel of this thesis, we assume these systems to belong to **I**, unless mentioned otherwise.

2.2 Virtual Harmonics Expander

Consider a system which belongs to the class **I** as defined in the previous section. Let $u(t) = \hat{a}cos(\omega + \varphi)$ be the input signal. The system response $y(t)$ is considered to consist exclusively of harmonics of the fundamental frequency ω of the input signal $u(t)$, i.e. we assume that the transient behavior has vanished. Response $y(t)$ can be written as a summation of harmonics of the input signal $u(t)$, each with an amplitude and phase, which can depend on the amplitude $\hat{a}$, phase φ and frequency ω of the input signal (Fig. 2.1). This system can be modeled as a cascade of a so called Virtual Harmonics Expander and

$$u(t) = \hat{a}\cos(\omega t + \varphi) \qquad\qquad y(t) = \sum_{n=0}^{\infty} A_n(\hat{a},\omega)\cos(n(\omega t + \varphi) + \varphi_n(\hat{a},\omega))$$
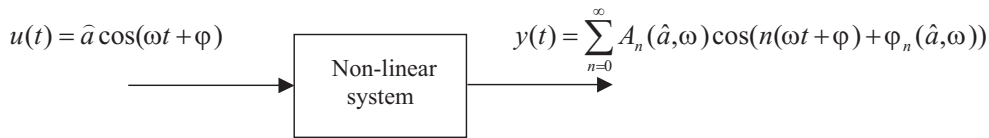
Non-linear system

Figure 2.1 / General sinusoidal input-output relation.

a (non) linear system (Fig. 2.2). The Virtual Harmonics Expander (VHE) is defined as a non-linear component which transforms a sinusoidal input signal $u(t)$ with frequency ω, amplitude $\hat{a}$ and phase φ, (Eq. 2.1), into a harmonic output signal $\breve{u}(t)$. This output signal

$$u(t) = \hat{a}\cos(\omega t + \varphi) \qquad\qquad y(t) = \sum_{n=0}^{\infty} A_n(\hat{a},\omega)\cos(n(\omega t + \varphi) + \varphi_n(\hat{a},\omega))$$

Non-linear system

$u(t)$
$\hat{a}\cos(\omega t + \varphi)$

Virtual harmonics expander

$$\breve{u}(t) \qquad \sum_{n=0}^{\infty} \hat{a}\cos(n(\omega t + \varphi))$$

(Non)linear system

$$y(t) \qquad \sum_{n=0}^{\infty} A_n(\hat{a},\omega)\cos(n(\omega t + \varphi) + \varphi_n(\hat{a},\omega))$$

Figure 2.2 / Virtual Harmonics Expander as separate block in the model of a non-linear system with harmonic response.

$\breve{u}(t)$ consists of an infinite amount of harmonics of the input signal $u(t)$ with frequency $n\omega$, amplitude $\hat{a}$ and phase $n\varphi$ with $n \in \mathbb{N}$:

$$u(t) = \hat{a}\cos(\omega t + \varphi) \tag{2.1}$$

$$\breve{u}(t) = \sum_{n=0}^{\infty} \hat{a}\cos(n(\omega t + \varphi)) \tag{2.2}$$

Remark: It is evident from Eq. 2.1, 2.2 that the VHE is not power invariant.

By defining a separate block for the generation of harmonics in modeling this class of non-linear systems, the complexity of the subsequent (non) linear block will be significantly less and linear approaches may become feasible depending upon the remaining non-linear behavior. The resulting model structure has strong similarities with a Hammerstein model. This structure however is not a Hammerstein model since the second block is not necessarily linear (Narendra and Gallman, 1966).

2.3 Higher Order Sinusoidal Input Describing Functions
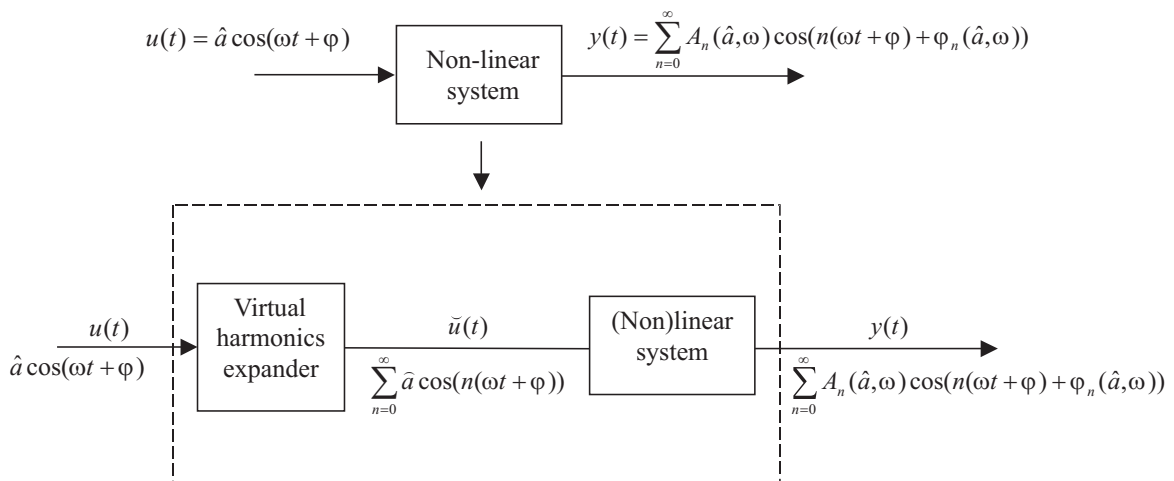
Consider a stable, non-linear time invariant system as described in Section 2.2 with $u(t)$ as the input signal and $y(t)$ as system response after the transient behavior has vanished (Fig. 2.1). The describing function $H(\hat{a}, \omega)$ of the system is defined as the complex ratio of the fundamental component $\tilde{y}(t)$ of the system response and the input sinusoid $u(t)$ (Fig. 2.3).

$$u(t) = \hat{a}\cos(\omega t + \varphi) \quad \boxed{H(\hat{a},\omega)} \quad \tilde{y}(t) = A_1(\hat{a},\omega)\cos(\omega t + \varphi + \varphi_1(\hat{a},\omega))$$
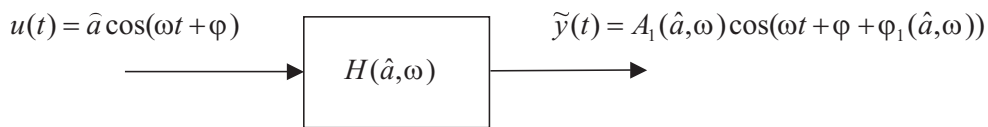
Figure 2.3 / Sinusoidal input describing function representation.

The describing function $H(\hat{a}, \omega)$ can be calculated as (Slotine and Li, 1991):

$$H(\hat{a}, \omega) = \frac{A_1(\hat{a}, \omega)e^{j(\omega t + \varphi + \varphi_1(\hat{a},\omega))}}{\hat{a}e^{j\omega t + \varphi}} = \frac{1}{\hat{a}}(b_1(\hat{a}, \omega) + ja_1(\hat{a}, \omega)) \tag{2.3}$$

The Fourier coefficients a_1 and b_1 are calculated as in Eq. 2.4, 2.5 with $T = \frac{2\pi}{\omega}$:

$$a_1 = \frac{2}{T} \int_{t_0}^{t_0+T} y(t)\cos(\omega t)dt \tag{2.4}$$

$$b_1 = \frac{2}{T} \int_{t_0}^{t_0+T} y(t)\sin(\omega t)dt \tag{2.5}$$

In Fig. 2.4 the block representation of the non-linear system with a harmonic response is redrawn by separating the Virtual Harmonics Expander from the system. The remaining system can be represented as a parallel connection of subsystems, each relating a harmonic component of the non-linear system output to the corresponding harmonic component of the Virtual Harmonics Expander. The subsystem $H_1(\hat{a}, \omega)$ is the sinusoidal
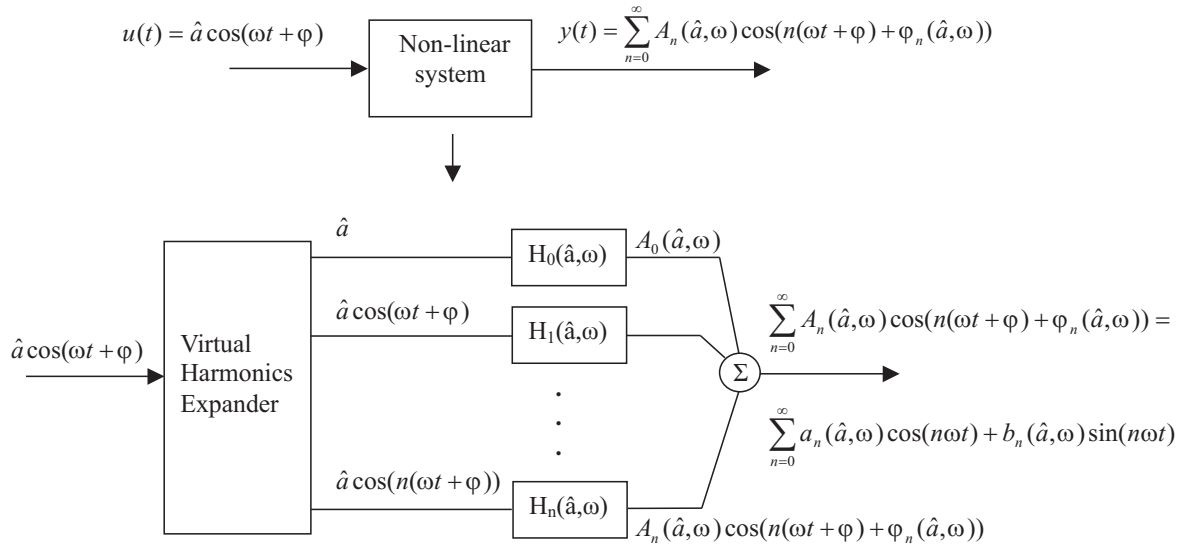
Figure 2.4 / Higher Order Sinusoidal Input Describing Functions representation.

input describing function of the system as defined in Eq. 2.3. This classical describing function can be interpreted as the first element of a set of higher order describing functions $H_k(\hat{a}, \omega)$. These functions can be defined as the complex ratio of the kth harmonic component in the output signal to the virtual k^{th} harmonic signal derived from the excitation signal. This virtual harmonic has equal amplitude as the fundamental sinusoid but its starting-phase is n times the starting phase of the excitation signal. Like the first order describing function (Eq. 2.3), the higher order describing functions are calculated from the corresponding Fourier coefficients:

$$
\begin{aligned}
H_k(\hat{a}, \omega) &= \frac{A_k(\hat{a}, \omega)e^{j(k(\omega t+\varphi)+\varphi_k(\hat{a},\omega))}}{\hat{a}e^{jk(\omega t+\varphi)}} \\
&= \frac{A_k(\hat{a}, \omega)e^{j(\varphi_k(\hat{a},\omega))}}{\hat{a}} = \frac{1}{\hat{a}}\left(b_k(\hat{a}, \omega) + ja_k(\hat{a}, \omega)\right)
\end{aligned} \tag{2.6}
$$

$H_k(\hat{a}, \omega)$ can be interpreted as a descriptor of the individual harmonic distortion components in the output of a time invariant non-linear system with a harmonic response as function of the amplitude and frequency of the driving sinusoid. In this thesis $H_k(\hat{a}, \omega)$ will be referred to as the Higher Order Sinusoidal Input Describing Functions (HOSIDF).

2.4 Discussion

In this chapter the key concepts of this thesis are presented. These concepts are defined for the class of causal, stable, time invariant non-linear systems that have a harmonic response to a sinusoidal excitation. This class, denoted as I, also contains systems with non-fading memory (Boyd and Chua, 1985) like for example non-local memory hysteresis. Systems with non-fading memory can not be described with (truncated) Volterra series which constitute the basis of non-linear analysis techniques like the Generalized Frequency Response Functions. The prime characteristic property of the non-linear systems belonging to the class I is the frequency transformation of a sinusoidal input signal into a harmonic output signal possibly also containing a DC component. This transformation property is concentrated as the essential characteristic of the Virtual Harmonics Expander. Although this property is highly non-linear, it also has linear aspects. Both the amplitude and the phase of the harmonics at the output of the Virtual Harmonics Expander have a linear relation with the amplitude and phase of the input sinusoid. This transformation function greatly extends the application of successful (quasi) linear concepts like the FRF and the Sinusoidal Input Describing Function towards the non-linear environment. The generalization of the Sinusoidal Input Describing Function to the Higher Order Sinusoidal Input Describing Functions is a logical result of this approach. By merging the Virtual Harmonics Expander and the HOSIDF concept, all non-linear systems belonging to this class I can be modeled as a parallel connection of weakly non-linear systems connected in series with one single highly non-linear system. The fact that the HOSIDF concept requires pure sinusoidal excitation both has advantages and disadvantages. The sinusoidal excitation results in simple non-parametric identification techniques of the HOSIDF which can be visualized easily. A disadvantage is the slow speed of identification and the inability to identify non-linear effects like intermodulation and desensitization (Billings and Tsang, 1989a).

Non-parametric identification of HOSIDF

Abstract / Two distinctly different methods for the non-parametric identification of HOSIDF are presented. The first method employs FFT techniques to determine the autospectrum and phase information and operates upon blocks of data. The second method uses IQ demodulation and is sample based.

In Section 2.2 the Virtual Harmonics Expander was presented. The frequency transformation property of this non-linear system is linear with respect to the amplitude and phase of the excitation sinusoid. In this Section we will use this property for the non-parametric identification of the HOSIDF of the systems belonging to the class defined in Section 2.1. Two identification methods will be described, both using the orthogonality properties of the $\sin$ and $\cos$ function. However, due to the way of implementation, the results are distinctly different.

3.1 Fourier based technique

The first identification technique is FFT based. Both the input signal $u(t)$ and output signal $y(t)$, (Fig. 2.1) are Fourier transformed with a transform size of $2m$. The resulting single sided spectra contain $m + 1$ frequency lines each with $0Hz$ in frequency line zero. The frequency spacing is $\Delta f = 1/T_b$ with T_b the length of the data block. T_b is chosen a multiple p times the period $T = 2\pi/\omega$ of the excitation signal. This assures that all the power of the excitation signal is concentrated in frequency-line p. The power of the response signal is fully concentrated in the frequency lines $n.p$ with $n \in \mathbb{N}$, so leakage is absent. In Fig. 3.1 the Virtual Harmonics Expander (VHE) and the kth order HOSIDF are highlighted. Let us consider the calculation of the k_{th} order HOSIDF. According to Eq. 2.6 this HOSIDF is calculated from the kth harmonic component in the output signal $y(t)$ of the system divided by the kth harmonic component $\breve{u}_k(t)$ of the output of the VHE.
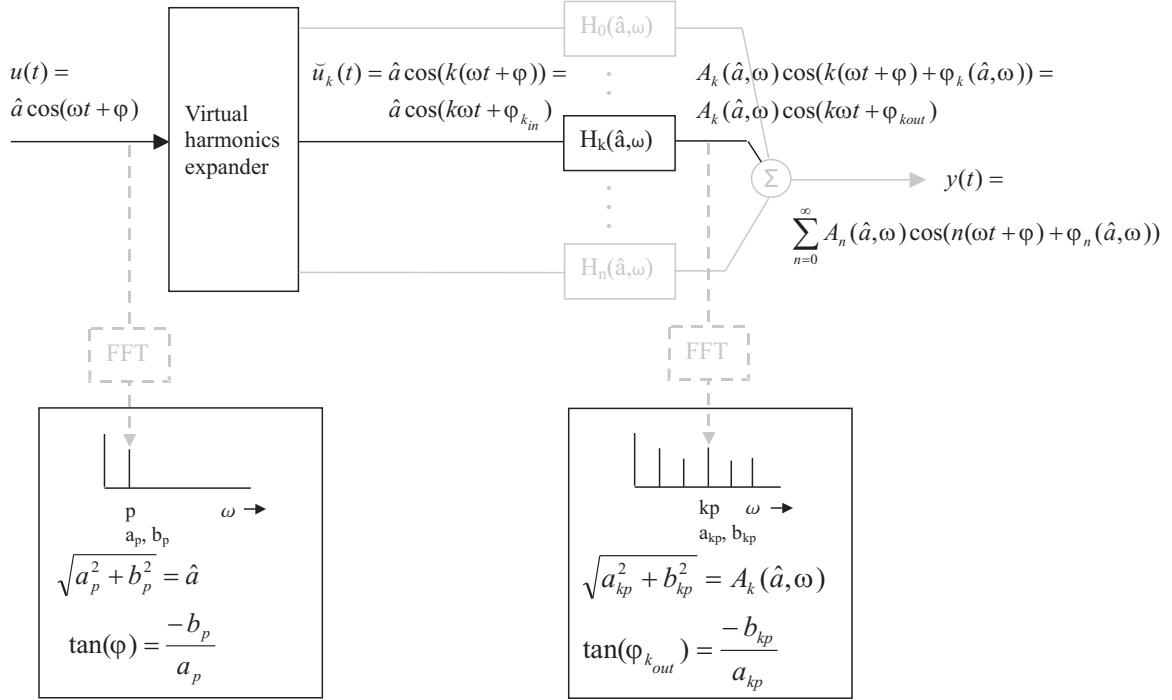
Figure 3.1 / Determination of the kth order HOSIDF using FFT techniques.

The signal $\breve{u}_k(t)$ however cannot be measured but has to be derived from the measurable input signal $u(t)$. Using Eq.2.1, 2.2 the frequency $n\omega$, amplitude $\hat{a}$ and phase $n\varphi$ of every component n from the output of the VHE can be calculated. In the frequency spectrum of $u(t)$ the frequency line p with complex value $a_p + jb_p$ represents the input signal. The square root of the power in this frequency line is the amplitude $\hat{a}$ and the phase angle of this frequency line equals phase φ:

$$\hat{a} = \sqrt{a_p^2 + b_p^2} \tag{3.1}$$

$$\begin{aligned}
\varphi &= \arctan(\tfrac{-b_p}{a_p}) & if & \quad a_p \geq 0 \\
\varphi &= \arctan(\tfrac{-b_p}{a_p}) + \pi & if & \quad a_p < 0
\end{aligned} \tag{3.2}$$

In the spectrum of the system output signal $y(t)$, the frequency line with number $k \cdot p$ and complex value $a_{kp} + jb_{kp}$ represents the output of the subsystem $H_k(\hat{a}, \omega)$. The square root of the power in this frequency line is the amplitude $A_k(\hat{a}, \omega)$:

$$A_k(\hat{a}, \omega) = \sqrt{a_{kp}^2 + b_{kp}^2} \tag{3.3}$$

The phase angle of this frequency line $\varphi_{k_{out}}$ is the sum of the phase of the kth component of the VHE $\varphi_{k_{in}}$ and the system phase $\varphi_k(\hat{a}, \omega)$:

$$\varphi_{k_{out}} = \varphi_{k_{in}} + \varphi_k(\hat{a}, \omega) = k\varphi + \varphi_k(\hat{a}, \omega) \tag{3.4}$$

From Eq. 3.1, 3.3 the magnitude of the kth order HOSIDF can be calculated as:

$$|H_k(\hat{a}, \omega)| = \frac{\sqrt{a_{kp}^2 + b_{kp}^2}}{\sqrt{a_p^2 + b_p^2}} \tag{3.5}$$

The phase $\varphi_k(\hat{a}, \omega)$ of the HOSIDF can be calculated from Eq. 3.2, 3.4:

$$
\begin{aligned}
\varphi_k(\hat{a},\omega) &= \arctan(\tfrac{-b_{kp}}{a_{kp}}) - [k\arctan(\tfrac{-b_p}{a_p})]_{mod2\pi} && if && a_p \geq 0, a_{kp} \geq 0 \\
&= \arctan(\tfrac{-b_{kp}}{a_{kp}}) - [k\{\arctan(\tfrac{-b_p}{a_p}) + \pi\}]_{mod2\pi} && if && a_p < 0, a_{kp} \geq 0 \\
&= \arctan(\tfrac{-b_{kp}}{a_{kp}}) + \pi - [k\arctan(\tfrac{-b_p}{a_p})]_{mod2\pi} && if && a_p \geq 0, a_{kp} < 0 \\
&= \arctan(\tfrac{-b_{kp}}{a_{kp}}) + \pi - [k\{\arctan(\tfrac{-b_p}{a_p}) + \pi\}]_{mod2\pi} && if && a_p < 0, a_{kp} < 0
\end{aligned}
\tag{3.6}
$$

3.2 IQ demodulation technique

An alternative to the FFT based technique is the IQ demodulation method (Rader, 1984; Mitchell, 1989). The signals $u(t)$ and $y(t)$ from which the HOSIDF are to be calculated only consist of the excitation sinusoid with frequency ω and its harmonics $n\omega$ respectively (Fig. 2.1). So their frequency spectra can be considered a collection of narrowband signals with bandwidth much less than ω. The magnitude and phase of these spectral components can be determined using IQ demodulation. In Fig. 3.2, IQ demodulation of the kth harmonic of the output signal is explained in more detail. The system output signal $y(t)$ is multiplied with $2\sin(k\omega)$ and $2\cos(k\omega)$ in two separate branches. These multiplications
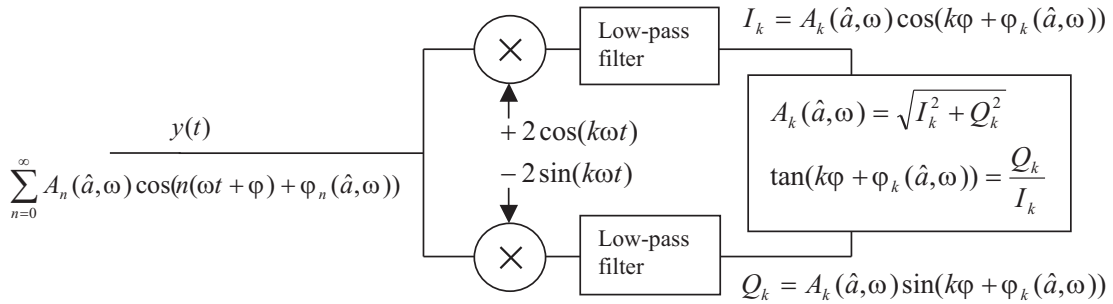
Figure 3.2 / Determining amplitude and phase of the kth order component of the system output signal using IQ demodulation.

result in the generation of two new signals, each consisting of the sum and difference frequencies of the original signal and the local oscillators signals. These new signals are $90°$ apart. After low-pass filtering with a cut-off frequency $\omega_{LP} \ll \omega$ the remaining signals representing the kth harmonic are $A_k(\hat{a}, \omega)\cos(k\varphi + \varphi_k(\hat{a}, \omega))$ called the I-signal (in phase) component and $A_k(\hat{a}, \omega)\sin(k\varphi + \varphi_k(\hat{a}, \omega))$ called the Q-signal (quadrature)

component. Because the frequency of the two local oscillators is $k\omega$, the I_k and Q_k components are the Fourier components of the IQ demodulated signal. So $|H_k(\hat{a},\omega)|$ and φ_k can be calculated from $\hat{a}$, φ, $A_k(\hat{a},\omega)$, and $\varphi_{k_{out}}$, (Fig. 3.3) with Eq. 3.1-3.6. The IQ demod-
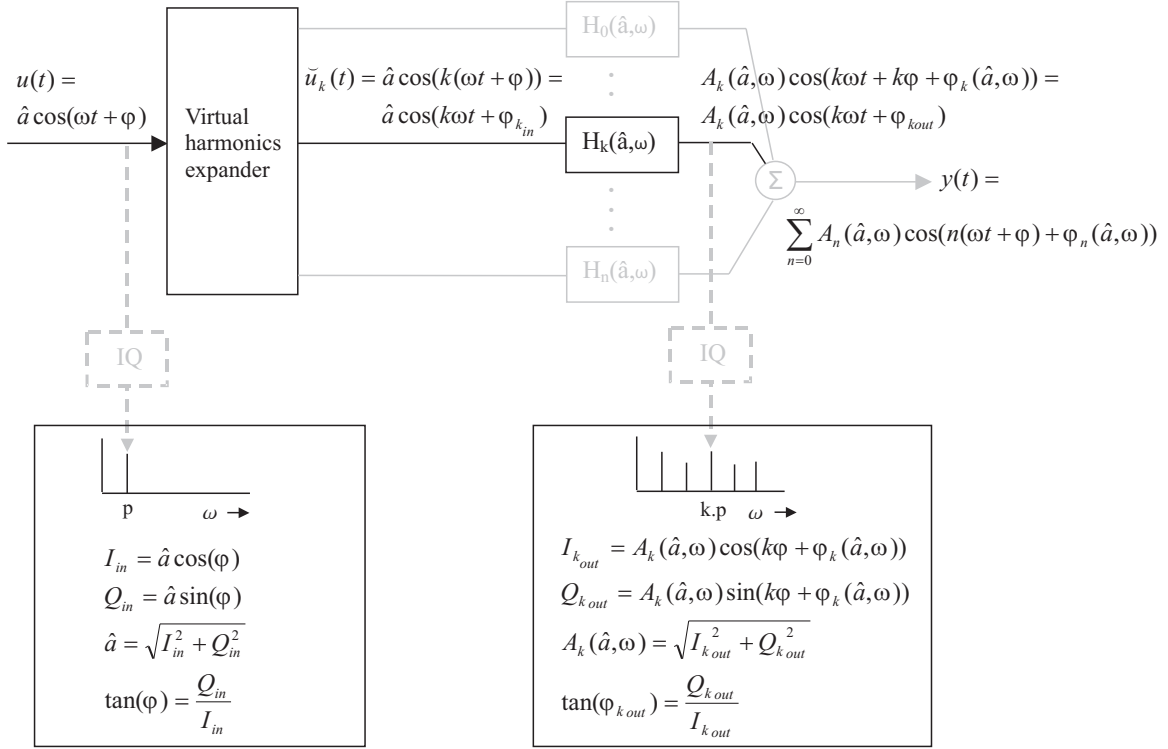
Figure 3.3 / Determining the kth order HOSIDF using IQ demodulation.

ulators for both signals $u(t)$ and $y(t)$ have identical lowpass filters, only the frequencies of the local oscillators differ. Because the filters are identical, their characteristics will not bias the results. However, any asymmetry between the filter characteristics will show up in the HOSIDF to be calculated.

3.3 Discussion

We defined two methods for non-parametric identification of the HOSIDF. Both methods have in common that they generate the complex values of the HOSIDF from which the magnitude and the phase information can be determined. The methods are distinctly different from a signal processing point of view. The FFT based method operates with data blocks where the IQ method is sample based. They also differ in the freedom of the design of their filter characteristics. In the FFT based method, the applied time weighting function dictates the effective filter characteristics of all frequency bins. In the IQ methode the selectivity is determined by the lowpass filters trailing the multipliers. Both

the type and the order of the I and the Q filter can be chosen freely as long as both filter characteristics are identical. This allows for optimization with respect to real-time performance which may be beneficial in applications where real-time, on-line information about HOSIDF is desirable. These aspects are not studied in this thesis. It is to be expected however that a characteristic with increased attenuation of the harmonics of the excitation frequency will lead to an increase in settling time of the filters. Once a filter characteristic is chosen, all frequencies analyzed are subjected to that specific filter characteristic. For the FFT based method each harmonic coincides with an FFT line and since all lines have equal selectivity, every harmonic is filtered with equal filter characteristics. In the IQ methode, after multiplication, each harmonic component is filtered by the same lowpass filter. Consequently, in both methods the effective filter shape for each individual harmonic is independent of frequency.

Validation of the proposed identification techniques

Abstract / In this chapter the proposed measurement techniques are tested in a simulation experiment to get a better understanding of their performance with respect to dynamic range and selectivity under extreme variations in the excitation amplitude. First, the HOSIDF of a known non-linear system will be derived analytically. These expressions serve as the reference for subsequent simulations. Time-sequences will be generated, simulating the dynamic behavior of this system. These time-sequences are processed both with the FFT technique and the IQ technique to derive the HOSIDF. A comparison between the analytically derived HOSIDF and the HOSIDF derived from the simulation experiment shows that the dynamic range of the IQ method suffers from limited selectivity.

In Chapter 3 two techniques for the non-parametric estimation of the HOSIDF were presented. Both techniques require frequency selectivity, either as the result of an FFT algorithm or from an analog or digital lowpass filter. In this Section we will investigate the influence of frequency selectivity on the estimates of the HOSIDF. As a first step the HOSIDF of a known and well defined non-linear process are derived analytically. Subsequently these HOSIDF serve as a reference in a simulation experiment over a wide range of excitation amplitudes.

4.1 Theoretical derivation of the HOSIDF for backlash

The reference system consists of a mass-less body m, connected to the surroundings by a spring with stiffness k (Fig. 4.1). The body experiences a Coulomb friction force F_c of magnitude b if $\dot{y} \neq 0$ (Fig. 4.2). Due to this friction in combination with the spring, the body will experience a backlash of $2b$ when excited with a periodic force $F(t) = A\sin(\omega t)$ if $A \geq b$. The non-linear relation between input force $F(t)$ and output displacement $y(t)$
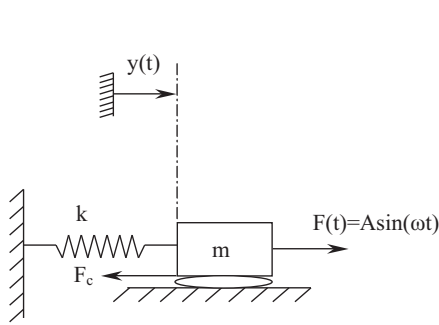
Figure 4.1 / System with Coulomb friction.
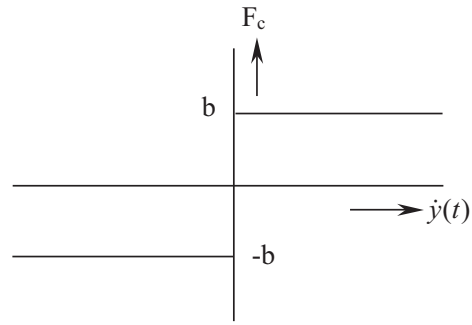
Figure 4.2 / Coulomb friction.

is an odd function and can be expressed analytically in steady state as:

$$
\begin{array}{llll}
y(t) = 0 \text{ if } A < b & else & \\
y(t) = (A - b)/k & \frac{\pi}{2} < \omega t \leq \pi - \gamma & mod\ 2\pi \\
y(t) = (A\sin(\omega t) + b)/k & \pi - \gamma < \omega t \leq \frac{3}{2}\pi & mod\ 2\pi \\
y(t) = -(A - b)/k & \frac{3}{2}\pi < \omega t \leq 2\pi - \gamma & mod\ 2\pi \\
y(t) = (A\sin(\omega t) - b)/k & 2\pi - \gamma < \omega t \leq \frac{5}{2}\pi & mod\ 2\pi
\end{array}
$$

$$(4.1)$$

with $\sin(\omega\gamma) = 1 - \frac{2b}{A}$. Fig. 4.3 shows the input-output relation for backlash. Using Eq. 2.4, 2.5, $y(t)$ can be decomposed in its Fourier coefficients a_n and b_n (Appendix 11.1). With Eq. 2.6 the HOSIDF are calculated as function of the excitation amplitude A. This
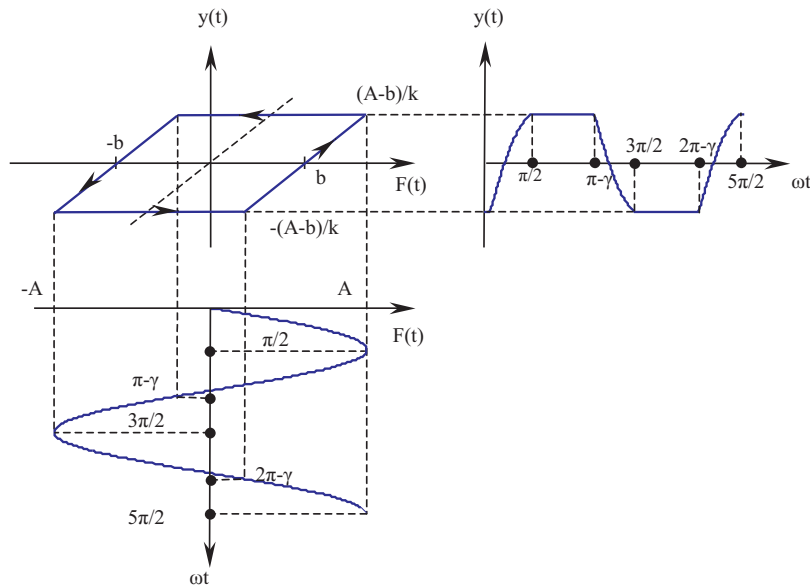
Figure 4.3 / Input-output relation for backlash

mass-less, non-linear system has no dynamics so the HOSIDF are independent of frequency. In Fig. 4.4 the magnitude and phase relations of the HOSIDF are displayed as function of the quotient of the magnitude of the resulting excitation force $A - b$ and the value of the Coulomb friction b. The top left graph shows the magnitude of the first order Describing Function. The top right plot shows the phase. In the subsequent rows the magnitudes and phases of the odd HOSIDF are shown. Obviously, the even orders are all zero because $y(t)$ is an odd function (Eq. 4.1). The HOSIDF clearly have a maximum in their magnitude. This maximum occurs when $A = 2b$. For this excitation value, the system has a maximum in its non-linear behavior and the harmonics in the output signal will reach maximum amplitude relative to the excitation amplitude. For much larger excitation magnitudes, the magnitude of the friction force relative to the excitation force decreases and the system tends to linear behavior. The magnitude of the first order SIDF becomes constant, while the magnitudes of the HOSIDF decrease. An interesting observation is the symmetry of the magnitude plots of the HOSIDF when $\log(A - b)/b$ is chosen as x-axis. In this thesis no further attempt is made to explain this symmetry.

Figure 4.4 / Theoretical odd HOSIDF of backlash.

4.2 Simulation experiments

In the simulation experiment, the system with backlash is solved numerically. The simulations are done in discrete time domain so in a perfect simulation the discrete-time series can be treated as the sampled representation of the theoretical continuous time series. Since the sampling frequen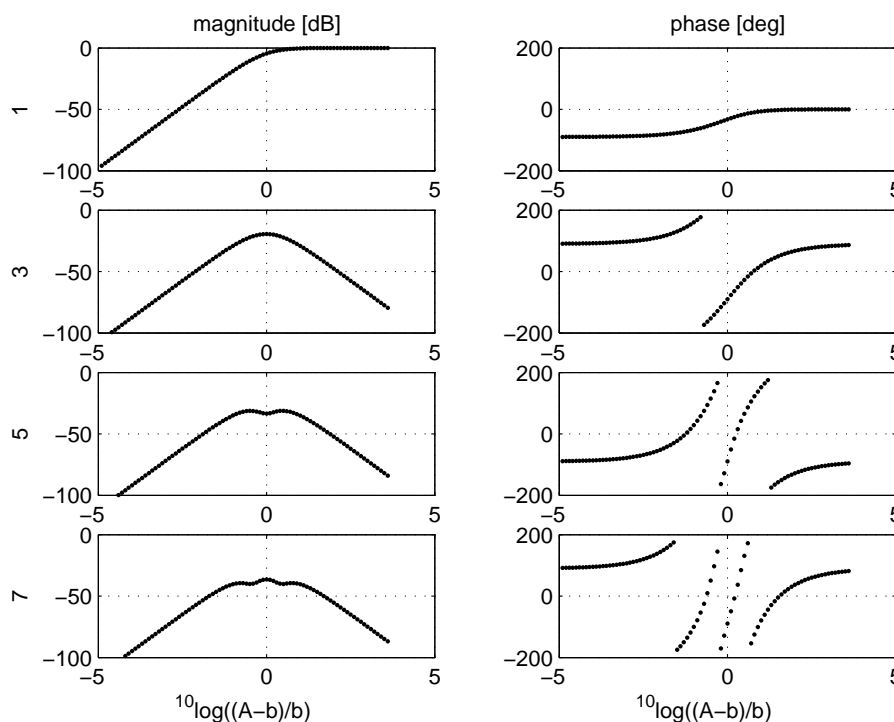cy is finite, aliasing will occur and can only be reduced by choosing the sampling frequency as high as practically possible. Leakage however can be prevented by choosing the sampling frequency a multiple of the excitation frequency. An additional pitfall apart from aliasing and leakage is the fact that the simulation results depend on the maximum values of the samples which represent each cycle of the sinusoidal excitation signal. Due to the discrete time behavior of the simulation, the maximum values of the calculated excitation signal samples in a cycle are not necessarily the peak value of the theoretical excitation signal f_0. Fig. 4.5 shows the influence of the phase of the sampling signal relative to the phase of the theoretical excitation signal. In
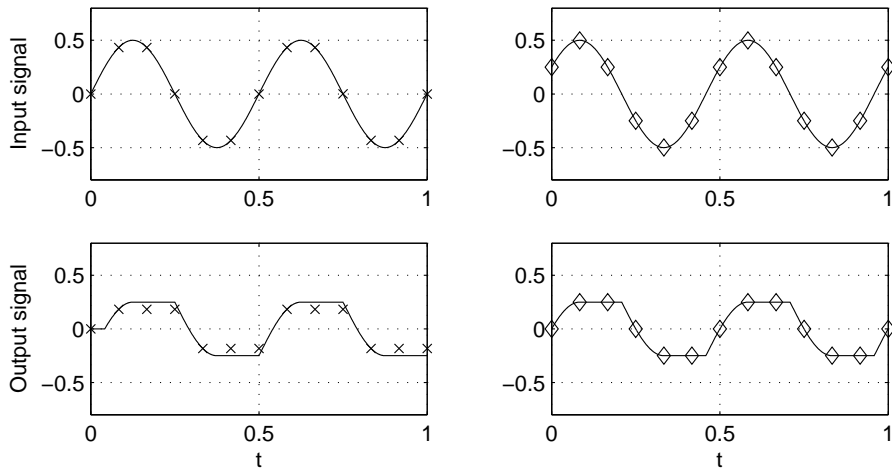
Figure 4.5 / Influence of sampling phase on the simulation results with backlash-width $b = 0.25$. Legend: - theory, $\times$ $f_s = 6f_0$ with $\phi(0) = 0$, $\diamond$ $f_s = 6f_0$ with $\phi(0) = \frac{\pi}{6}$

Fig. 4.6 an extreme example is given of the fact that the input sinusoid must be sampled at its maximum. The upper figure shows the theoretical input signal and its time discrete representation with three different sampling frequencies of $4f_0$, $8f_0$ and $10f_0$, all sufficiently high to correctly sample the input signal. The lower figure shows that a sampling frequency which is sufficiently high with respect to the Nyquist frequency of the input signal does not guarantee correct results of the output signal due to the non-linear system behavior. The figure shows that the results obtained with the highest sampling frequency are the poorest. This is due to the fact that for this frequency the input signal with an amplitude of 10^{-6} above the backlash-width was not sampled at its maximum value. Consequently the system remained within its backlash with zero output as result.
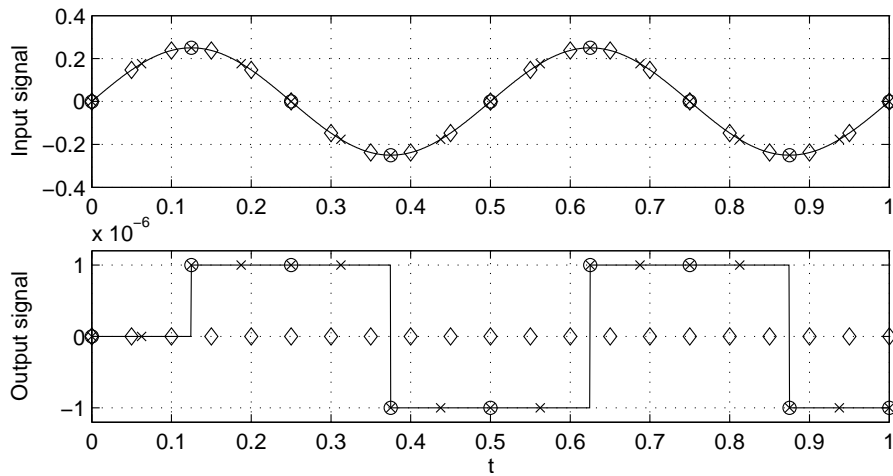
Figure 4.6 / Influence of sampling frequency and sampling phase on the simulation results with backlash-width $b = 0.25$ and $A = b + 10^{-6}$. Legend: - theory, $\times$ $f_s = 8f_0$ with $\phi(0) = 0$, $\circ$ $f_s = 4f_0$ with $\phi(0) = 0$, $\diamond$ $f_s = 10f_0$ with $\phi(0) = \frac{\pi}{6}$.

This phase influence can be minimized by synchronizing the phases of the sampling frequency and hypothetical excitation frequency such that the theoretical excitation frequency is sampled at its maximum values i.e. at $\phi = \frac{\pi}{2} + k\pi$ with $k \in \mathbb{Z}$. This can be done with a sampling frequency of $f_s = 4nf_0$ with $n \in \mathbb{N}$ and both $\varphi_{f_s}(0) = 0$ and $\varphi_{f_0}(0) = 0$. The analytical results were derived for a sinusoidal excitation with a constant amplitude in a range of $10^{-6} \leq (A - b) \leq 10^3$. In the simulation this signal is implemented as a sinusoid with a non-smooth stepped amplitude (staircase) with continuous phase transitions between the individual amplitude levels. This is implemented by changing the amplitude at the moment of zero phase (Fig. 4.7(a)). Changing the amplitude at other moments will result in large transients with a broad frequency content (Fig. 4.7(b)).
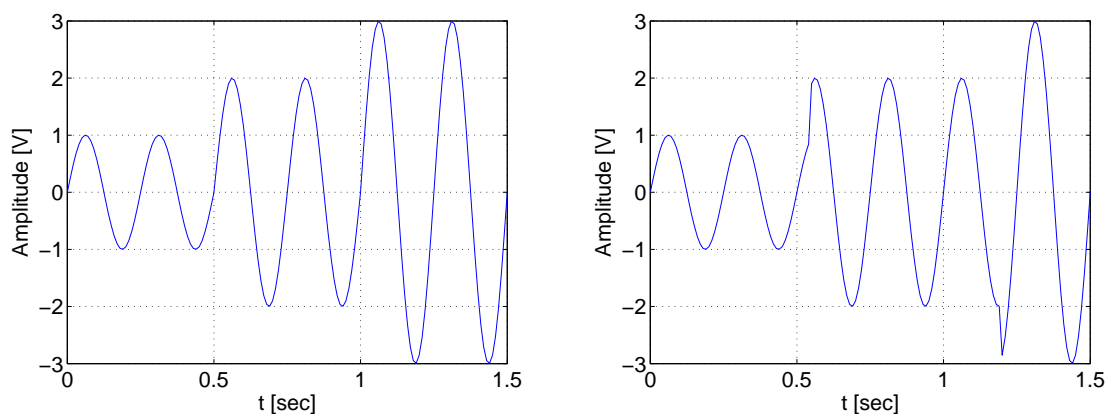
(a) Step in amplitude coincides with zero phase.

(b) Step in amplitude does not coincide with zero phase.

Figure 4.7 / Phase continuous stepped amplitude.

4.2.1   FFT based method

During this simulation experiment, every excitation level was kept constant during 3 periods of the excitation sinusoid. While processing the time series, the first period of every excitation level was skipped in order to suppress effects caused by the transition between subsequent excitation levels. Since the input signal for the simulation was free of noise, no signal averaging was applied. Table 4.1 gives the relevant measurement parameters for both measurement techniques.

FFT	IQ
$f_s = 2048f_0; 512f_0$	$f_s = 512f_0$
$\Delta f = \frac{f_0}{2}$	Butterworth LP filter
no leakage	$f_{-3dB} = \frac{f_0}{2}$
rect. window	4th order, 5th order
1 period settling	12 periods settling
$k = 1$	$k = 1$
$b = 0.25$	$b = 0.25$

Table 4.1 / Relevant measurement parameters

Fig. 4.8 shows the HOSIDF up to the 7th order for the staircase excitation when measured with the FFT method. The odd behavior of backlash is clearly reflected in the very low magnitude values of the even HOSIDF. The noise in the corresponding even order HOSIDF phase-plots is caused by the numeric resolution of the calculations. Fig. 4.9 shows the errors for both gain and phase between the simulated results and the analytically derived values for different sampling frequencies used in the simulation. The errors are calculated as:

$$magnitude\ error\ [dB] = 20\log\frac{|HOSIDF_{sim}|}{|HOSIDF_{an}|} \tag{4.2}$$

$$phase\ error\ [rad] = \angle(HOSIDF_{sim}) - \angle(HOSIDF_{an}) \tag{4.3}$$

with $HOSIDF_{sim}$, $HOSIDF_{an}$ the HOSIDF from the simulation experiment and the analytically derived results respectively. The errors induced by the simulation sampling frequency increase with the order number. The influence on the phase errors varies with the magnitude of the HOSIDF. The influence on the magnitude errors is excitation magnitude independent. From these results it may be concluded that the sampling frequency of $f_s = 2048f_0$ used in Fig. 4.8 for the simulation of the HOSIDF up to order 7 was sufficiently high to judge the dynamic range and selectivity of the analysis method.

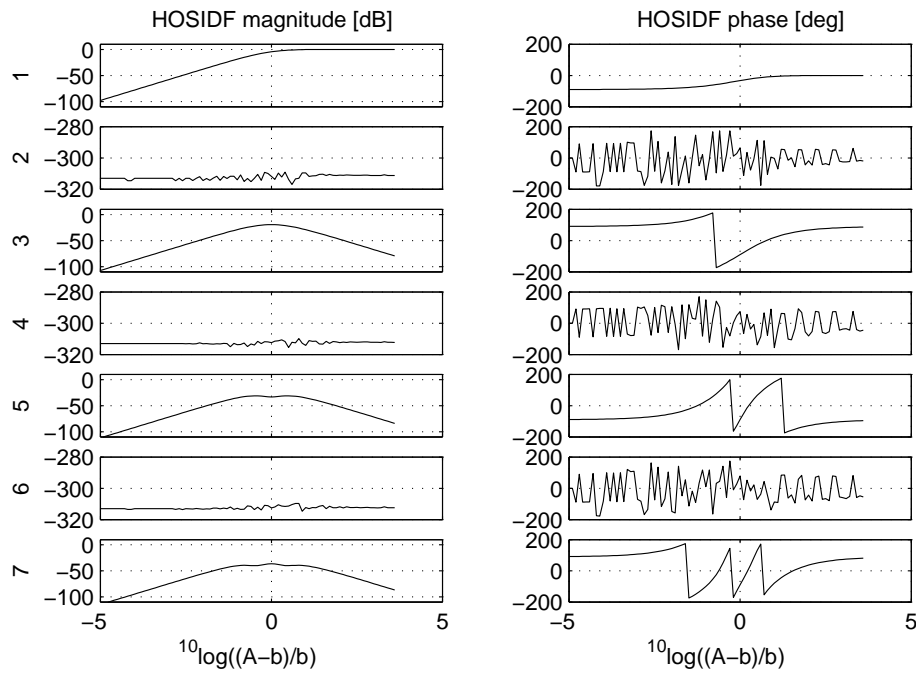**Figure 4.8 /** Simulation results using FFT with $f_s = 2048f_0$.
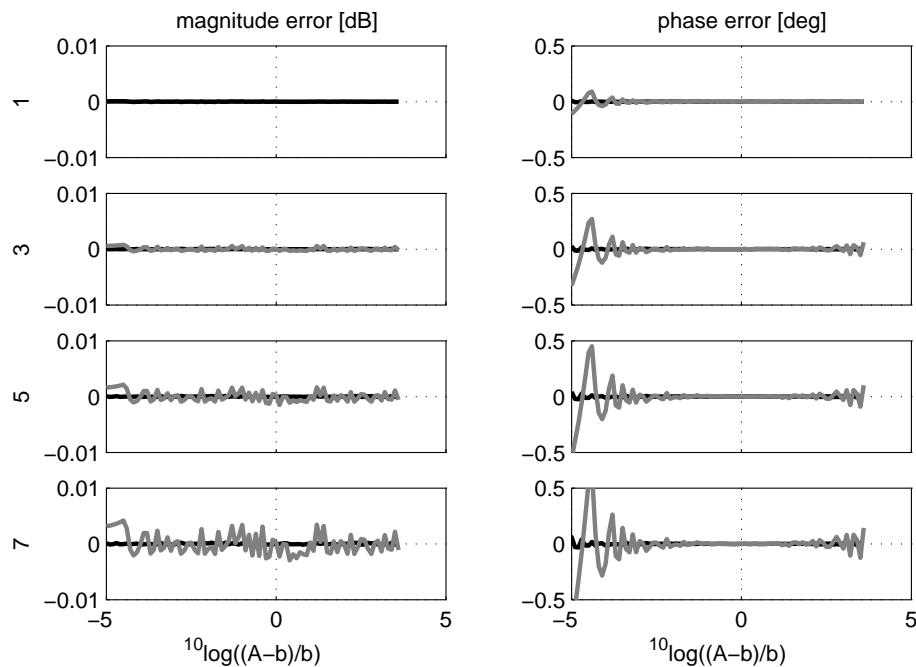
Figure 4.9 / Magnitude and phase errors of the odd HOSIDF derived with the FFT methode for two values of f_s during simulation. Legend: black $f_s = 2048f_0$, grey $f_s = 512f_0$.

4.2.2   IQ based method

When analyzing the time series with the IQ method, special attention has to be payed to the settling behavior of the lowpass filters, especially when the measurements have a large dynamic range. Since the time-series consist of stepped amplitude time sequences, each excitation level was kept constant for 12 periods of the excitation sinusoid to allow the lowpass filters to settle. Although both time-series with $f_s = 2048 f_0$ and $f_s = 512 f_0$ have been processed with the FFT method, only time-series with $f_s = 512 f_0$ have been processed with the IQ based method because of the memory allocation limitations induced by the simulation software. In Fig. 4.10 the results after settling of the filters are shown. A major difference with the FFT based results as displayed in Fig. 4.8 can be found in the even orders. Because the non-linearity is odd, the even order HOSIDF should be zero. This is not the case in the even order results here. Also the dynamic range of the third order HOSIDF is limited to approximately -55dB for high excitation levels.
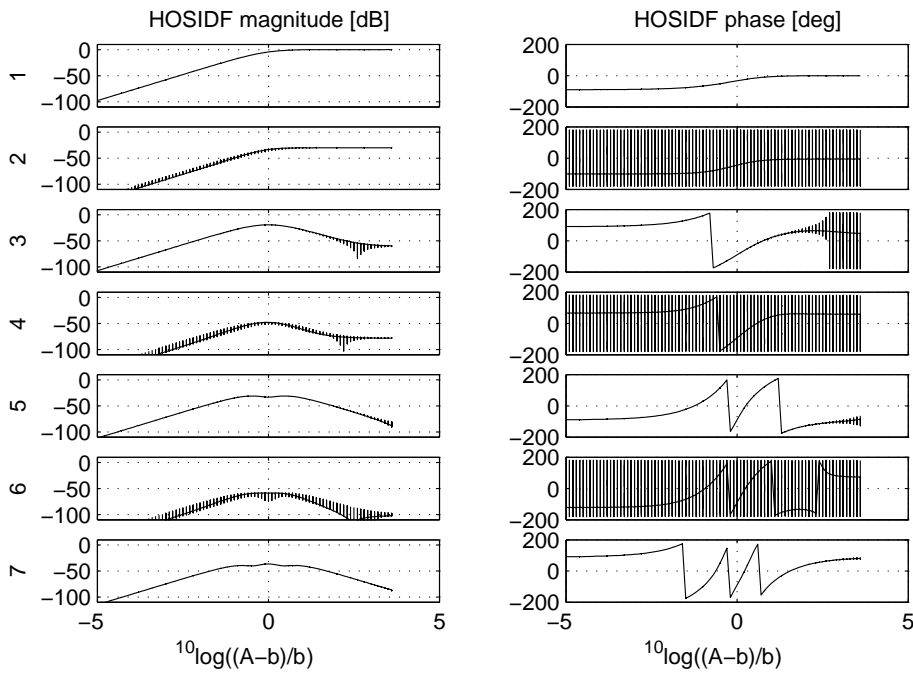
Figure 4.10 / Simulation results using IQ with $f_s = 512 f_0$, LP filter 5th order Butterworth $f_{-3dB} = f_0/2$.

Fig. 4.11, 4.12 show the differences between the theoretical results and the results for the odd orders generated by the IQ method for a 4th order and a 5th order lowpass filter. The results show an excitation amplitude dependent error which decreases with the filter order number. The source of the errors in both the even and the odd orders is the non ideal low-pass filtering of the I_k and Q_k signals (Fig. 3.2). The implemented digital filters have finite attenuation at the harmonics of the excitation frequency. Power from the sum and
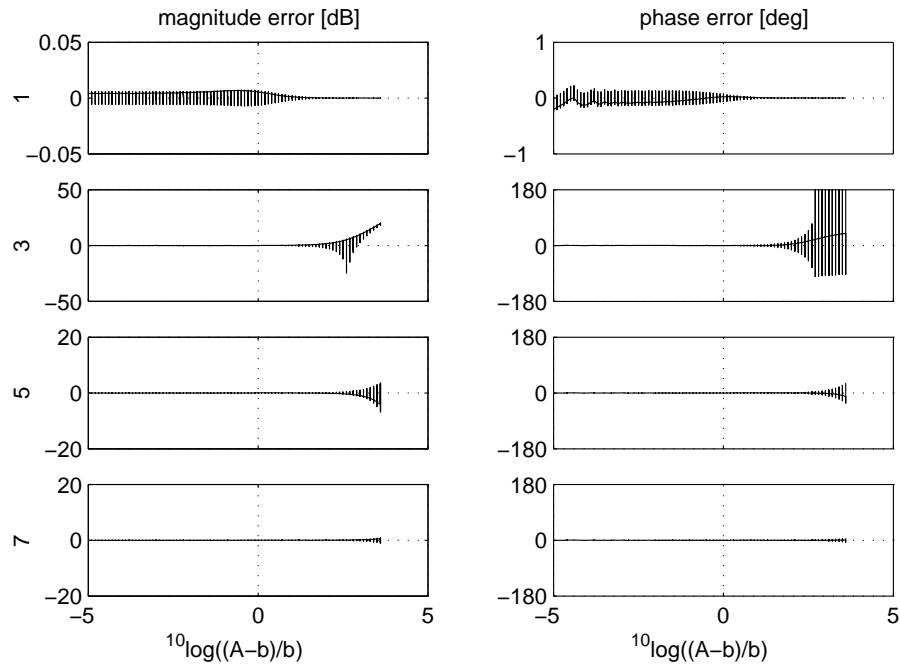
Figure 4.11 / Magnitude and phase errors in the odd HOSIDF generated with the IQ method. $f_s = 512f_0$ LP filter 5th order Butterworth $f_{-3dB} = f_0/2$.
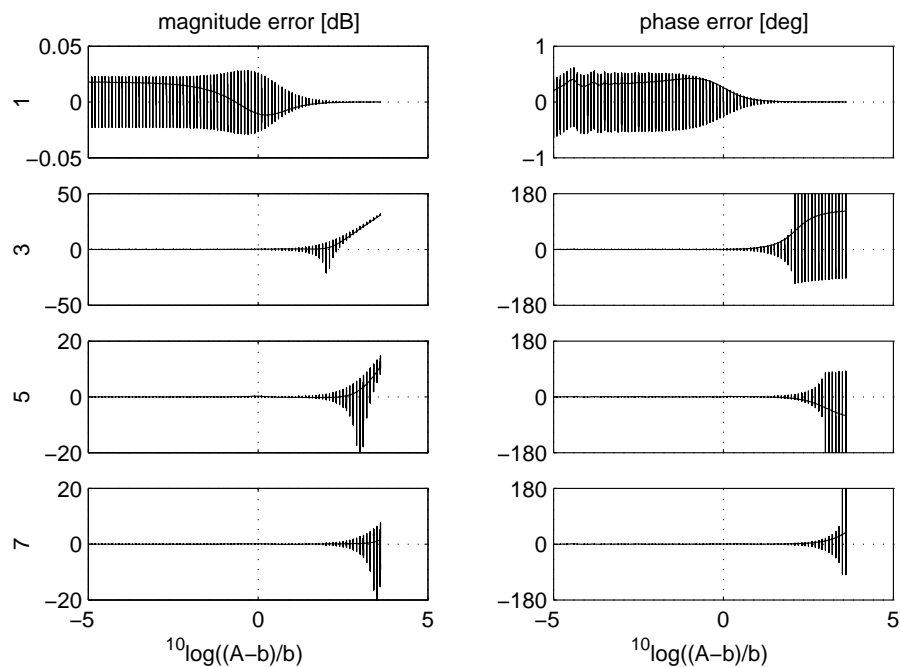
Figure 4.12 / Magnitude and phase errors in the odd HOSIDF generated with the IQ method. $f_s = 512f_0$ LP filter 4th order Butterworth $f_{-3dB} = f_0/2$.

difference signals with frequencies $\omega = (n \pm k)\omega_0$ for $n \neq k$ adds onto the power of the difference signal with frequency $\omega = (n \pm k)\omega_0$ for $n = k$.

4.3 Discussion

The simulation shows that the FFT based method yields nearly perfect results. Both the selectivity and the dynamic range are in line with the analytically derived results. The reason for this near perfect behavior is the perfect selectivity of the FFT based filters, due to the specific location of its zeros. If the window length $l_{window} = 1/\Delta f = k/f$ for $k \in \mathbb{N}$ where Δf is the FFT resolution, the frequency f to be analyzed coincides with an FFT line. The zeros in the filter characteristic of this FFT line will provide infinite attenuation of all the harmonics of f. Unlike the rectangular weighting function, for weighting functions like Hanning and Hamming the first zero in their Frequency Response Function has a frequency of $2\Delta f$. If the excitation frequency $f = \Delta f$, its harmonic $2f$ will not be suppressed. To prevent this, the minimum length of the Hanning weighting function must be $2/f$ (Fig. 4.13). The selectivity of the digital filters used in the IQ method is not
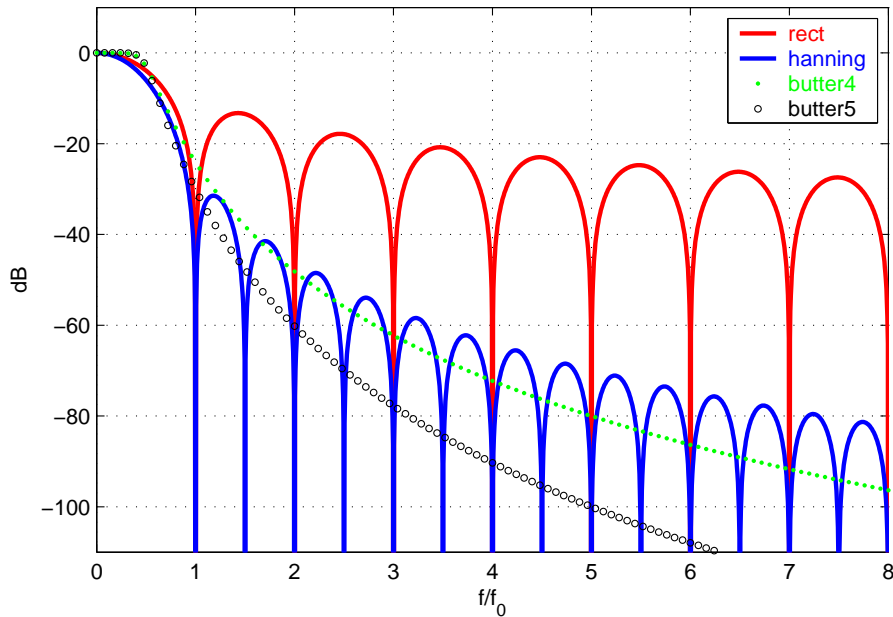
Figure 4.13 / Frequency selectivity of the applied filters. FFT method: Rectangular $l_{window} = 1/f_0$, Hanning $l_{window} = 2/f_0$. IQ method: 4th and 5th order Butterworth $f_{-3dB} = f_0/2$.

perfect for the harmonics of the excitation frequency as can be seen in Fig. 4.13 also. This results in a complicated error mechanism because the errors in the individual HOSIDF depend on the combination of filter selectivity and the power distribution of the harmonic

components in the response signal. The dynamic range of all HOSIDF will be limited by the remaining power outside the passband of the lowpass filter after filtering the sum and difference signals. An increased selectivity requires steeper filters, thus a higher filter order and/or a different filter type, but always at the expense of extra settling-time. In this research no special attention is payed to the optimal tradeoff between the digital filter characteristics, required settling time and the resulting selectivity. The simulations described in Section 4.2 do not take the influences of noise into account. From Fig. 4.13 can be concluded that, depending on the filter shape, the IQ method can be less susceptible to broadband noise than the FFT method. In the FFT methode however, the influence of noise can be reduced significantly by time domain averaging since the excitation signal and the part of the output signal caused by the excitation signal are both deterministic. From these results we conclude that the FFT based technique is superior due to its ideal selectivity. If, however, real time implementation is required, additional arguments have to be taken into consideration. These aspects are not evaluated in this thesis and can be an interesting field for future research.

Application of the proposed identification techniques in practice

Abstract / After the validation of both methods with respect to selectivity and dynamic range under simulated extreme conditions, some practical aspects of a HOSIDF measurement like design of the excitation signal and numerical compensation of the bias caused by harmonic distortion will be presented on the basis of an experiment on a real system.

In Section 4.2 both measurement techniques were validated under extreme conditions: noise free pure sinusoidal excitation over a very wide range of amplitudes. These hypothetical conditions allowed the investigation of the dynamic range and selectivity of both techniques. In this section some subjects will be discussed which become relevant in a realistic measurement: design of the excitation signal, settling time in the IQ filters, noise as limiting factor for the dynamic range of the measurements and a reduction of the bias in HOSIDF estimates caused by the harmonic power distribution in the excitation signal. In this case study a mechanical system with real friction is tested in physical reality.

5.1 Design of the excitation signal

The theoretical background for the HOSIDF as explained in Section 2.3 presumes a single sinusoid excitation and thus a constant amplitude. In practice it is not possible to completely realize this condition. The limitations are dictated by the hardware of the signal generator, the linearity of the actuator, sensor noise and the measurement time available.

Hardware restrictions

Hardware restriction are dictated by the signal generating hardware and the actuators used. Key elements determining the spectral purity of a digital signal generator are the phase noise in its master oscillator, the dynamic range and linearity of the DA convertor and the quality of the analog smoothing filters required to eliminate the impact of the zero order hold reconstruction. The output subsystem of the SigLab analyzer which is used for the experiments consists of an 18 bits DAC with analog reconstruction filter. This limits the magnitude difference between the sine component in the output signal and all other components to $90dB$. In practice however the non-linear distortion caused by the power amplifier and the actuator dominates the generation of harmonics in the excitation signal. As examples one can think of crossover distortion in a push-pull amplifier and the inability of an electromagnetic shaker to deliver a sinusoidal force to a load with a non-linear impedance. Apart from harmonic distortion, the measured excitation signal which serves as the input for the HOSIDF calculations can also contain noise generated by the sensor. Especially under low excitation signal condition this noise contribution has to be taken into consideration because it will negatively influence the dynamic range of the measurements.

Amplitude-time relation

The required amplitude-time relation can be implemented as a phase continuous stepped amplitude signal (Fig. 4.7). This garanties the required spectral purity but at the expense of increased measurement time. One has to wait for the system to settle after every step in the amplitude. Also the settling time of the digital filters used in the IQ methode has to be respected. If the requirements for the spectral purity are reduced, different amplitude-time relations can be used and the required total settling time can be decreased. Fig. 5.1 shows the results of this trade off. In this example two signals are analyzed, $Gen_1(t)$ with a phase continuous stepped amplitude with 5 levels and $Gen_2(t)$ with a linear amplitude time relation:

$$Gen_1(t) = \frac{1}{5}\Big\{floor(t) + \frac{1}{2}\Big\}cos(2\pi f_0 t) \qquad\qquad 0 \leq t \leq 5 \qquad\qquad (5.1)$$

$$Gen_2(t) = \frac{t}{5}cos(2\pi f_0 t) \qquad\qquad 0 \leq t \leq 5 \qquad\qquad (5.2)$$

with $f_0 = 320 Hz$ and both sampled at $12.8kHz$. Fig. 5.1 shows the spectral lines containing the fundamental frequency and its harmonics as function of time for both signals. In the left hand column the analysis is done with a 1600 lines FFT and Hanning weighting, resulting in 40 data-blocks and a frequency resolution $\Delta f = 8Hz$. In the analysis of $Gen_1(t)$, the data-blocks are chosen such that they contain constant amplitude levels. The 40 data-blocks in the analysis of $Gen_2(t)$ have an equal position in time as the corresponding data-blocks of $Gen_1(t)$. Within any data-block of $Gen_2(t)$ the absolute increase in the

amplitude is $C_G \Delta f$ with $C_G = 1/5$ the amplitude gradient used in this example. Due to the phase continuous stepped amplitude, $Gen_1(t)$ consists of the fundamental frequency component f_0 only. Apart from the fundamental frequency f_0, the FFT representation of $Gen_2(t)$ also contains frequency components with a periode equal to integer fractions of the FFT block length. Since f_0 is chosen to fit an integer number of periodes in the data block, $Gen_2(t)$ will contain low level harmonics of f_0 which only depend on the amplitude gradient of the signal and the frequency resolution of the measurement. The right hand
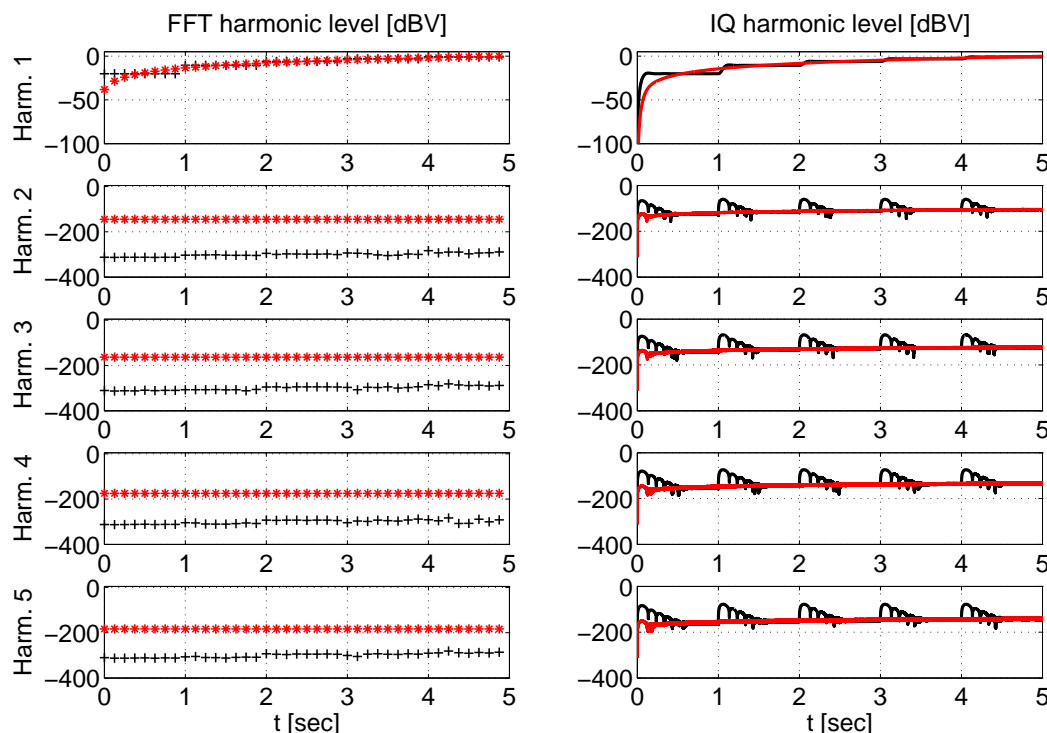
Figure 5.1 / Staircase vs. ramp. Left column: FFT based results, + staircase, * ramp. Right column: IQ based results, black staircase, red ramp.

column of Fig. 5.1 shows the corresponding harmonics determined with the IQ methode. The 3rd order Butterworth lowpass filters have a slope of $-60dB/dec$, equal to the slope of the Hanning filter characteristic. The cutoff frequency $f_{-3dB} = 5.75Hz$ and is calculated from the requirement that the Effective Noise Bandwidth (ENBW) of the IQ filters and the FFT filters are equal. The ENWB is defined as the width of an ideal rectangular filter of the same reference transmission level which transmits the same power from a white noise source. The ENWB of a Hanning window is $1.5 \cdot \Delta f$ (Oppenheim and Schafer, 1999), the ENWB of a 3rd order Butterworth filter is $1.047 \cdot f_{-3dB}$, (Shelton and Adkins, 1970). The response to the staircase signal clearly shows the settling behavior of the filters. Also the limited selectivity of the filters, as discussed in Section 4.2.2, is visible in

the harmonic levels of the staircase signal: where the FFT technique shows harmonic levels down to $-300dB$, the corresponding levels measured with the IQ methode are limited to approximately $-150dB$. Because of this limited selectivity it is not possible to detect the differences in harmonic levels between the two excitation signals with the chosen filter characteristics. A major difference between the signals in this example is the total settling time required by the filters in the measurement. For the ramp signal the settling time is approximately $0.3sec$ where the stepped sine signal requires approximately 8 times longer. It is important to stipulate that these results only describe the difference in settling time of the digital filters when measuring a stepped amplitude change versus a ramped amplitude change. In the response signals of the non-linear system these conditions will not be met and on top of a probably different settling behavior of the filters, one also has to take the settling time of the system into account. However it is to expected that this difference in overall settling time between both excitation signals will increase with the amount of measured amplitude levels. No attempt is done to optimize the trade-off between selectivity and settling time. This aspect can be a challenging subject for future work.

5.1.1   Numerical compensation of harmonic excitation

As a result of hardware restriction and/or the implemented amplitude-time relation of the excitation signal, harmonics of the excitation sinusoid will be present at the input of the system under test. This conflicts with the sinusoidal excitation condition required (Slotine and Li, 1991; Atherton, 1975; Nuij et al., 2006). This harmonic input signal $u(t)$ causes several non-linear phenomena in the output signal $y(t)$ (Bussgang et al., 1974; Wiener and Spina, 1980; Billings and Tsang, 1989a; Solomou et al., 2002; Yue et al., 2005a) like:

Gain compression/expansion. The input amplitude dependent relation between an input frequency component ω_0 and the output signal at frequency ω_0. This mechanism is completely described by the first order SIDF.

Generation of harmonics. The generation of harmonics as function of frequency and input amplitude which is described by the higher order SIDF.

Desensitization. Desensitization describes the influence an input frequency component ω_1 has on a not harmonically related output component with frequency ω_2.

Intermodulation. As the result of intermodulation, two input frequency components of for example $5\omega_0$ and $3\omega_0$ will cause an output frequency component $2\omega_0$.

Neglecting the non-linear effects of desensitization and intermodulation, a numerical compensation of the presence of harmonics at the input for the system under test is

(a) Biased n^{th} HOSIDF, n is a prime number.   (b) Biased n^{th} HOSIDF, n is not a prime number.
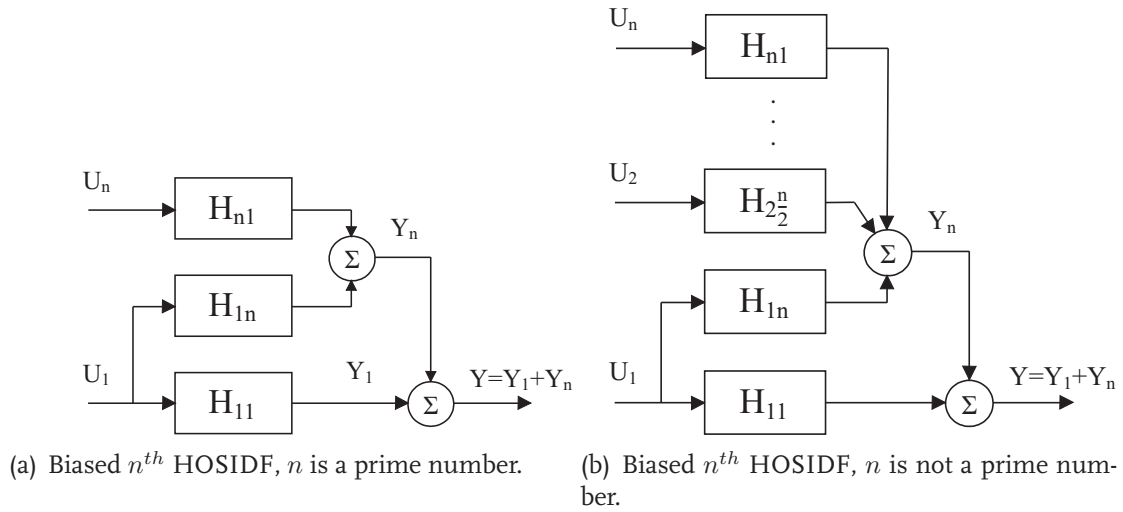
Figure 5.2 / Bias in the estimate of the nth order SIDF due to harmonic components in the excitation signal.

possible. Consider the class of time-invariant, stable, non-linear systems with a harmonic response to a sinusoidal excitation. Suppose the input signal $u(t)$ can be decomposed into its harmonic components $U(\omega) = \sum_{n=0}^{\infty} U_n$ with $n \in \mathbb{N}$. Likewise the output $y(t)$ of the system can be expressed as $Y(\omega) = \sum_{n=0}^{\infty} Y_n$. Let us consider the signal equations relating the excitation signal components U_1 and U_n with n a prime number to the first harmonic component Y_1 and the nth harmonic component Y_n of $Y(\omega)$ (Fig. 5.2(a)), hereby neglecting the non-linear effects of desensitization and intermodulation. Under these conditions the output component Y_n only consists of the responses to U_1 and U_n:

$$Y_1 = U_1 \cdot H_{11} \tag{5.3}$$
$$Y_n = U_1 \cdot H_{1n} + U_n \cdot H_{n1} \tag{5.4}$$

with H_{11} the approximated first order SIDF at ω relating U_1 and Y_1. H_{n1} represents the relation between the nth order harmonic U_n in the excitation signal and its contribution to the total content of Y_n. H_{n1} can be estimated by evaluating the approximated first order SIDF H_{11} at the frequencies $n\omega$. H_{1n} is the nth order SIDF and models the contribution of the first harmonic U_1 in the excitation signal to the output signal Y_n. This term models the generation of the nth harmonic as function of the first harmonic. Without taking the contribution of U_n into account the estimate for H_{1n} will be:

$$\hat{H}_{1n} = \frac{Y_n}{U_1} \tag{5.5}$$

A better estimate can be made by incorporating the contribution of U_n:

$$\hat{H}_{1n} = \frac{Y_n}{U_1} - \frac{U_n}{U_1} H_{n1} \tag{5.6}$$

If n is not a prime number, the output component Y_n will consist of more than 2 signal contributions (Fig. 5.2(b)). In this situation the output component Y_n consists of the responses of at least 2 harmonics summed with the response to the main sinusoidal component U_1:

$$Y_n = \sum_{k=1}^{n} U_k \cdot H_{k\frac{n}{k}} \;\; with \;\; k, n \in \mathbb{N} \;\; and \;\; \forall_k |\frac{n}{k} \in \mathbb{N} \tag{5.7}$$

From Eq. 5.7 again an estimate of H_{1n} can be derived, this time for the case that n is not a prime number:

$$\hat{H}_{1n} = \frac{Y_n}{U_1} - \sum_{k=2}^{n} U_k \cdot H_{k\frac{n}{k}} \;\; with \;\; k, n \in \mathbb{N} \;\; and \;\; \forall_k |\frac{n}{k} \in \mathbb{N} \tag{5.8}$$

For non-prime number high order SIDF, it will prove necessary to first calculate the estimates of the lower order SIDF before the estimate of the high order SIDF can be determined.

5.2 Description of the system under test

The test object is a system, which consists of a $20W$ electric DC collector motor. The motor is powered by a voltage-to-current converter (Fig. 5.3). The input to the system,
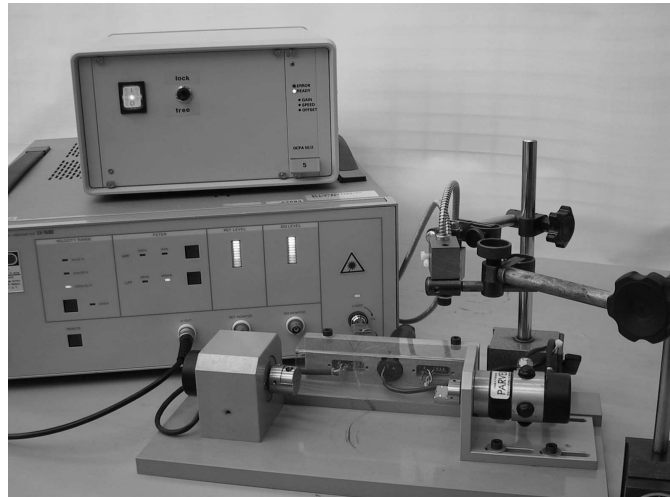

Figure 5.3 / Case study on a small DC motor.

i.e. the motor current I_m, is measured with a current probe with a sensitivity of $2A/V$. The response signal is angular velocity ω_{out}. J represents the inertia of the motor and T is the driving torque. A block diagram of the measurement set-up is given in Fig. 5.4.
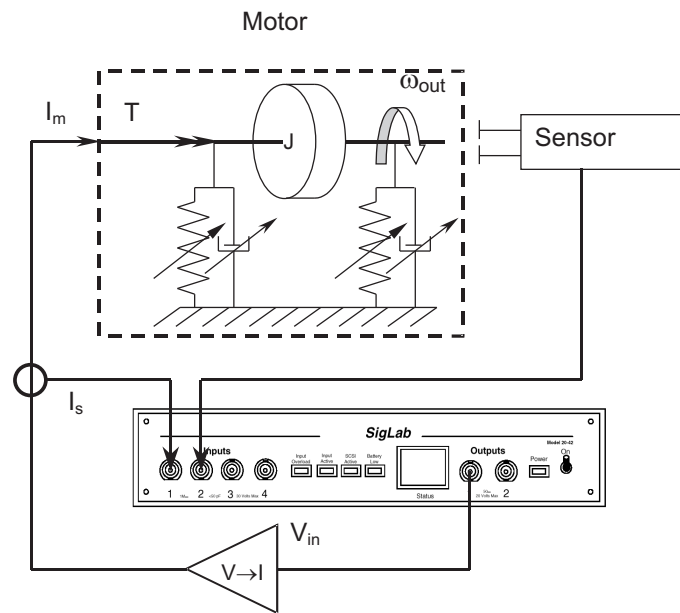
Figure 5.4 / Block diagram of measurement set-up.

For small rotations the angular velocity is measured with a dual fibre laser vibrometer. The angular velocity ω_{out} is approximated by the linear velocity difference between two points spaced 180^0 on the circumference of the shaft divided by the spacing of the points. The resulting sensitivity is $0.588 rad/s/V$. Friction in the bearings and seals will cause a friction-induced resonance (Symens et al., 2002; Nuij, 2002; Hensen et al., 2002a) the frequency of which will depend upon the excitation level.

5.3 Measurement of the FRF using white noise excitation

The H_1 Frequency Response Function ω_{out}/I_s was measured with a SigLab 20-42 dynamic signal analyzer providing $90dB$ aliasing protection. The resolution was $\Delta f = 0.313Hz$ in the frequency range of $0Hz$ to $1kHz$. A Hanning weighting function was applied. The excitation signal was band-limited random noise in the same frequency range. The crest factor of the noise was 3. The excitation levels were $1.5mA_{RMS}$, $6mA_{RMS}$ and $36mA_{RMS}$. These levels are not high enough to force the system from the stick phase into the slip phase so the system-behavior will be non-linear due to the dominant influence of friction. This situation occurs frequently in accurate point-to-point motion tasks. Fig. 5.5 shows the results after 20 averages per measurement. The FRFs in the upper two graph clearly show excitation amplitude dependent system behavior. In the frequency range up to approximately $400Hz$ the magnitude plot of the $1.5mA$ measurement shows a +1 slope which is consistent with the phase of $90deg$ and indicates stiffness dominated behavior. In the plots a resonance is visible with a frequency varying between $540Hz$
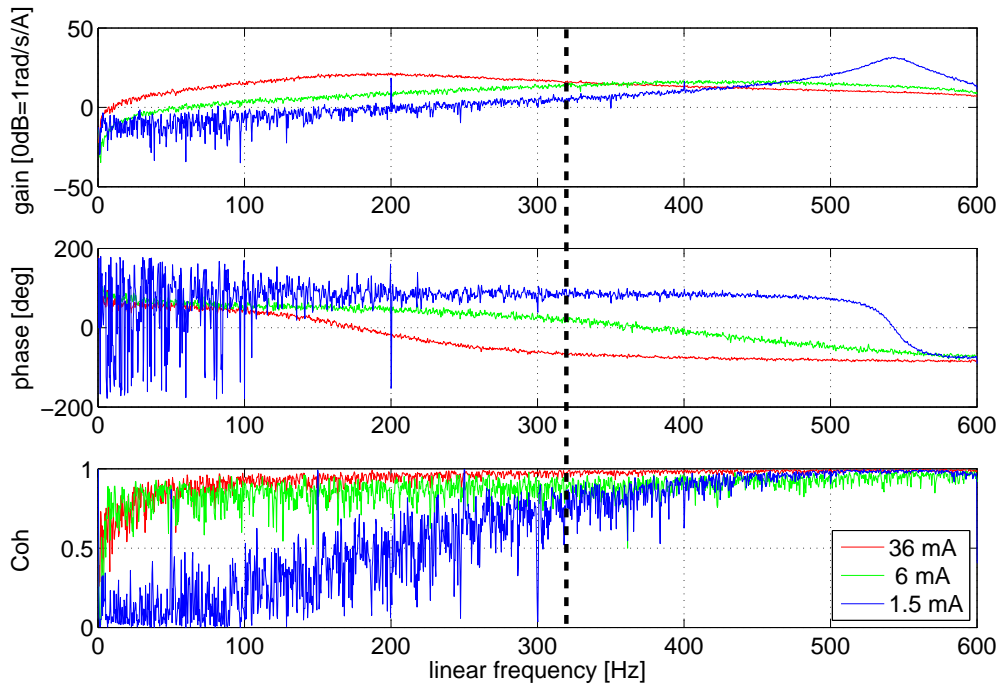
Figure 5.5 / H_1 estimate of the FRF as function of excitation level.

and $200Hz$. It is caused by the friction induced stiffness in combination with the motor inertia J. Its damping varies significantly as can be seen from the differences in phase gradients. The noisy behavior in these plots and the low value of the coherence plots can be caused by the non-linear system behavior and/or by poor signal to noise ratios of the measurement. Although the multisine excitation techniques (Schoukens et al., 1998; Weiss et al., 1998; Evans and Rees, 2000a; Pintelon and Schoukens, 2001; Dedene et al., 2002; Solomou et al., 2004; Schoukens et al., 2005) as discussed in Section 1.4.1 can be used to distinguish between linear, odd and even non-linear components and noise, in the next section the HOSIDF techniques described in Chapter 3 will be used to further investigate the non-linear system behavior.

5.4 Measurements of the HOSIDF

In this case study, without any loss of generality, the HOSIDF will be determined for only one excitation frequency. Subsequent measurements at different frequencies are required to gather information over a frequency range. An excitation frequency of $320Hz$ is chosen. This frequency excites the system both above and below its friction induced resonance frequency depending upon the instantaneous amplitude of the excitation signal, see the vertical dashed line in Fig. 5.5. Other considerations for the choice of this specific

frequency are that $320Hz$ is not a multiple of the $50Hz$ mains frequency and that the signal can be generated with an integer number of $12.8kHz$ samples per period, being one of the sampling frequencies of the SigLab 20-42 dynamic signal analyzer. This assures leakage free results when being processed with the FFT method. In this example measurement, the linear amplitude-time relation (Eq. 5.2) is chosen as discussed in Section 5.1 in order to reduce the measurement time. Fig. 5.6 shows the generator signal, the input current signal and the system response. The maximum angular displacements of the sys-
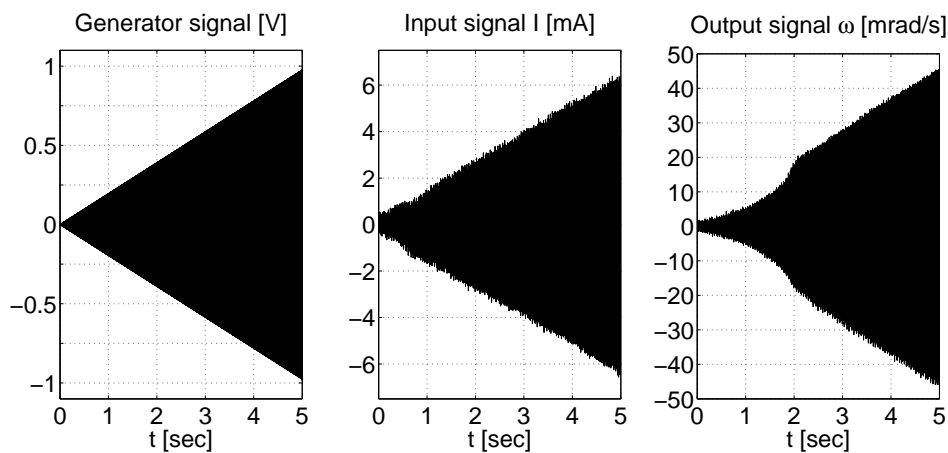
Figure 5.6 / Generator signal, input and output measurement signals.

tem can be calculated from the system response and is approximately 25μrad. The main parameters used for the FFT method are a block-size of 1600 samples and a sampling frequency of $12.8kHz$ so $\Delta f = 8Hz$, Hanning window, no overlap processing. Within one data-block the absolute variation of the amplitude is 0.025. The 3rd order low-pass filters used in the IQ method have a Butterworth characteristic with a cut-off frequency $f_{-3dB} = 5.75Hz$ which guarantees an equal ENBW as is realized with the FFT based measurement. This lowpass characteristic offers at least $105dB$ suppression of all harmonics outside the pass-band. This value exceeds the spectral purity which can be achieved by the hardware of the signal generator by $15dB$. In Fig. 5.7 the left column shows the magnitudes of the harmonics as function of time present in the measured input signal. The solid line shows the results from the IQ method, the dots indicate the measurements from the block based FFT method. The setting behavior of the Butterworth filter is clearly visible in the magnitude of the first harmonic. In the right column, the level of the main component in the input signal relative to the level of the other harmonics is show. A comparison with Figs. 5.1 shows that the signal contains a high level of noise, as this relative strength is never less than approximately $100dB$ in the noise free situation. Since the harmonics are noise dominated, as successful reduction of the bias in the estimates of the HOSIDF is not possible. Fig. 5.8 shows the amplitude dependency of the HOSIDF measured at the fixed frequency of $320Hz$. Again, the solid line shows the results from
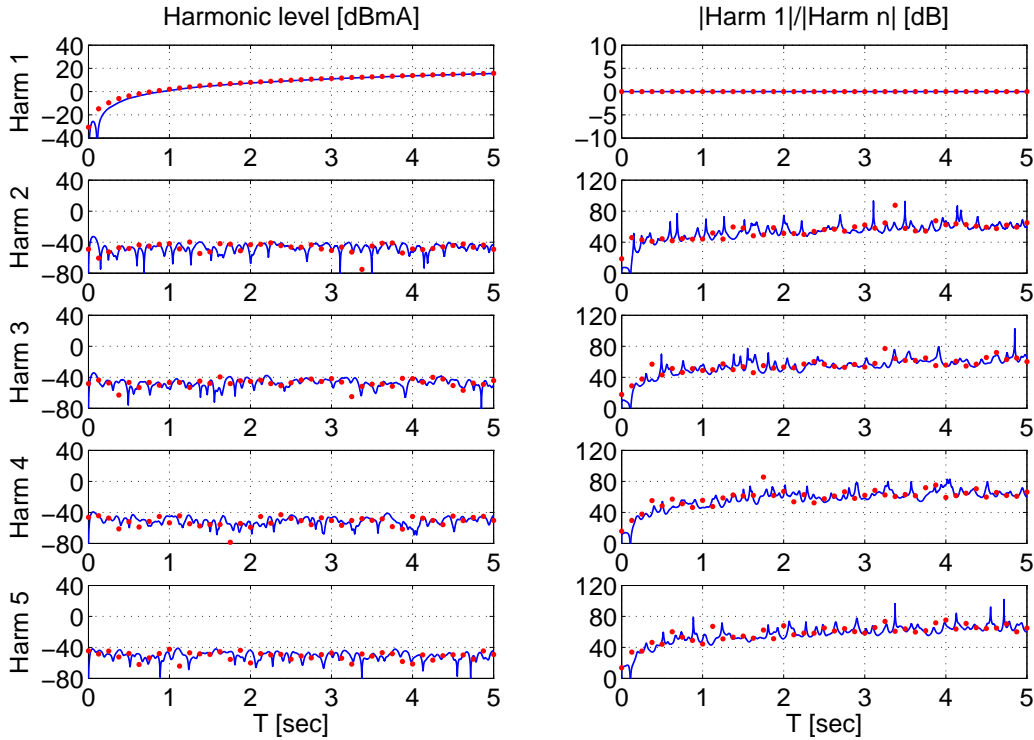
Figure 5.7 / Harmonic content (left column) and relative harmonic level (right column) of the input signal measured with IQ (solid line) and FFT method (dotted line) at a fixed frequency of $320Hz$.

the IQ method, the dots indicate the measurements from the block based FFT method. The results of the two measurement techniques do not show the discrepancies as described in Section 4.2. This is not due to a high suppression of the harmonics outside the pass-band of the filters used in the IQ methode. In this case study, the estimates of the HOSIDF will not have a high dynamic range due to the high noise levels. The limited selectivity of the digital filters will not be noticed in this example, consequently the limited harmonic selectivity is sufficient. In the left column of Fig. 5.8, the magnitude plots are presented for the HOSIDF. The right hand column gives the corresponding phase relations. In the magnitude plot of the first order SIDF we can distinguish three regions. From $0mA$ to approximately $0.4mA$ the system gain is strongly excitation dependent. In this range the digital filters of the IQ methode settle and the signal to noise ratio is very poor. This range can be typified as a poor measurement. Between $0.4mA$ and approximately $2.5mA$ an increasingly strong excitation level dependency is visible. Above $2.5mA$ the gain is independent of the excitation level at a stable $18dB$ but the system remains non-linear as can be concluded from the plots of the HOSIDF. The gain of the third order SIDF decreases initially. Again, this is due to the settling behavior of the filters and the low signal to noise ratios in this region which results in large uncertainties in the calculations. For increasing excitation its magnitude increases and reaches a maximum
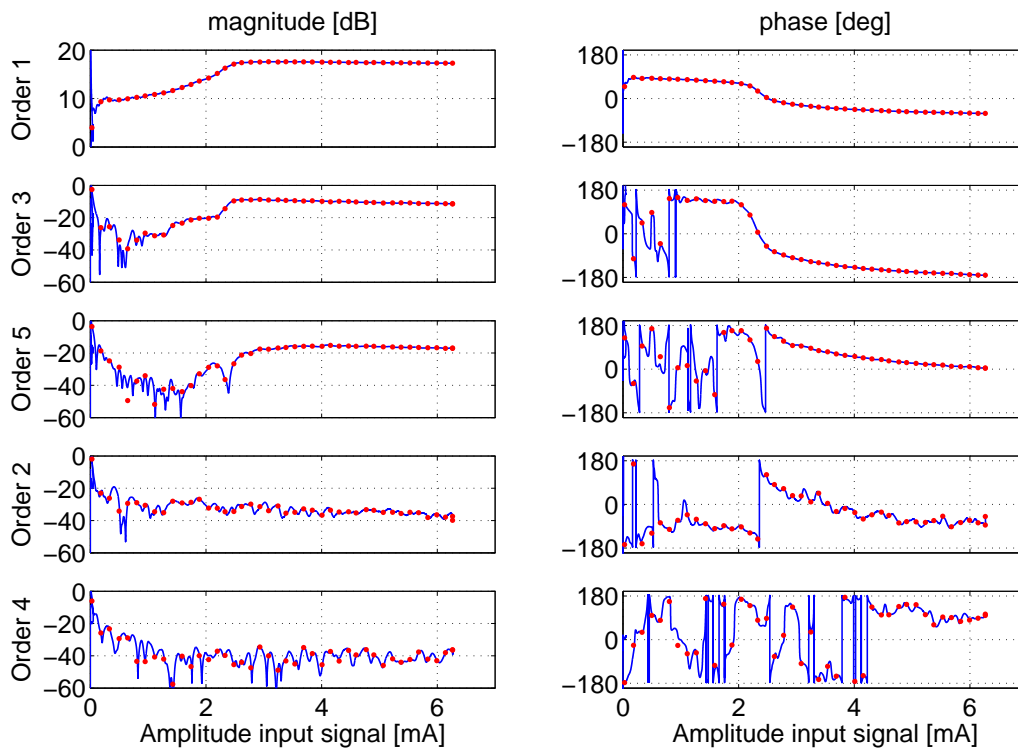
Figure 5.8 / HOSIDF measured with IQ (solid line) and FFT method (dotted line) at a fixed frequency of $320Hz$.

of $-8dB$ at approximately $2.5mA$. Above that excitation level the gain decreases again slightly. The same pattern is visible for the fifth order SIDF, however its maximum of $-15dB$ is reached at an excitation level of $4.5mA$. The magnitude characteristics of the even orders have a lower value compared to the odd orders. The amplitude dependency is small too. In Fig. 5.8 first row, right column, the phase relation of the first order FRF must not be mistaken for the phase graph of the bode-plot of a standard linear second order system relating input torque and output angular velocity, since the x-axis does not indicate frequency but input signal magnitude here. This plot however does contain information about the resonance frequency of the system as function of excitation level. In the phase plot of Fig. 5.5 we see for low excitation levels at 320 Hz a phase of approximately 90° and a resonance frequency above $320Hz$. For high excitation levels the phase has decreased to -90°, and the resonance frequency is shifted below $320Hz$. At the actual resonance frequency the phase will be 0°. From the phase plot in Fig. 5.8, the excitation level required for the system to resonate at $320Hz$ can be determined to be approximate $2.5mA$. The higher order phase plots have similar characteristics. In these plots the difference $\Delta\varphi$ between the phase values at $2mA$ and $6mA$ is approximately $\Delta\varphi(n) = (n+1)90^o$ with n the order number. Based on these measured HOSIDF results, the phase values at approximately $2.5mA$, which correspond with the resonance condition of the first order

SIDF, can be expressed as $\varphi(n)_{res} = (n+1)45^o - 2^{(\frac{n-1}{2})}90^o$. Because of this measured increase in steepness of the phase gradient as function of the order number the use of this higher order phase information can be beneficial in the detection of this sliding resonance. Although this example only describes a measurement at one frequency the results clearly show that the concept of HOSIDF is suitable for analyzing amplitude dependent non-linear system behavior.

5.5 Discussion

In this example some practical aspects of the HOSIDF measurement techniques were discussed on the basis of a real measurement on a real system with friction. We showed that a non-stationary excitation signal can be beneficial with respect to the required measuring time of that excitation signal if some harmonic contamination of the excitation signal is tolerated. The results indicate that under noise free conditions and with a given selectivity of the IQ filters, the stepped amplitude excitation signal requires a longer total measurement time for an equal amount of information compared to the ramped amplitude excitation signal. This observation motivates the search for an excitation signal with an optimal amplitude-time relation with respect to harmonic contamination and required overall measurement time under realistic (=not noise free) conditions. The optimal amplitude-time relation will probably depend on the parameters determining the filter characteristics of the applied measurement technique (FFT or IQ) and the noise distribution in the measurements. Another aspect for additional research is the impact of the assumption that non-linear phenomena like desensitization and intermodulation can be ignored in the compensation of the bias in the HOSIDF estimations due to harmonic excitation. This assumption raises some questions about the influence of these phenomena on the true non-linear behavior and about a possible quantification of the estimation errors caused by this assumption. We noticed that the measured input signal contained a significant amount of noise. This noise will influence the system behavior and noise in the measurement signals has influence on the estimation results. Is it possible to quantify the influence of the noise in the excitation signal on the system behavior? And finally, are both measurement techniques equally sensitive to noise in the measurement signals? The FFT methode has ideal harmonics selectivity and signal averaging capabilities but suffers from leakage. The IQ method, although with perhaps only sufficient harmonics selectivity, can have better wide-band selectivity depending on the filter type and order. Finding answers to these questions will be a challenging and rewarding task for those scientists and engineers who really lost their heart to practical measuring techniques.

Analysis of the stick to sliding transition in a bearing with friction.

Abstract / In contrast to the classical FRF, HOSIDF reveal information about non-linear system behavior. In this chapter the odd order HOSIDF will be used to determine the stick to sliding transition of a linear bearing with friction. From this information the maximum tangential force in the stick phase will be determined without the need of a separate force measurement.

In the previous chapters the concept of the HOSIDF was presented, two non-parametric measurement techniques were proposed and validated. In this chapter we will give an answer to the question about practical use. Are we really able to generate useful, additional information from a non-linear system with this new technique? Again we will focus on a system with friction. In this chapter the stick to sliding transition present in many positioning systems with friction will be studied with the HOSIDF method.

6.1 System under test

To study the applicability of the HOSIDF method with respect to characterizing stick to sliding transitions, a small test set-up is designed. In this set-up, an electromechanical shaker is excited with a sinusoidal current. The resulting force drives a sledge, which is subjected to dry friction, through its stick/sliding transition. This happens in a well controlled and reproducible way. Both the electrical stimulus to the shaker and the acceleration of the mass are measured. From these data the HOSIDF are determined. The excitation force is also measured for validation purposes. The system consists of a supported mass with one translational degree of freedom. Although air bearings and hydrostatic bearings have very low and reproducible friction behavior, low friction linear ball bearings were chosen because of their low complexity and similarity with numerous

drive systems in industry. The dry friction in the system is realized with a separate friction finger mounted onto the sledge. This finger slides over a very smooth and wear-resistent stationary surface to ensure reproducible and position independent friction behavior. The normal force in the contact point can be changed to adjust the friction force. This additional friction force is made significantly larger than the friction in the ball bearings. The overall system dimensions allow the use of commonly available piezo sensors for measuring force and acceleration. The light-weight and stiff design results in clean dynamic behavior in the frequency range of interest. In Figs. 6.1, 6.2 a picture and a functional drawing of the measurement setup are shown. In Appendix 11.2 the details of the measurement setup are presented.
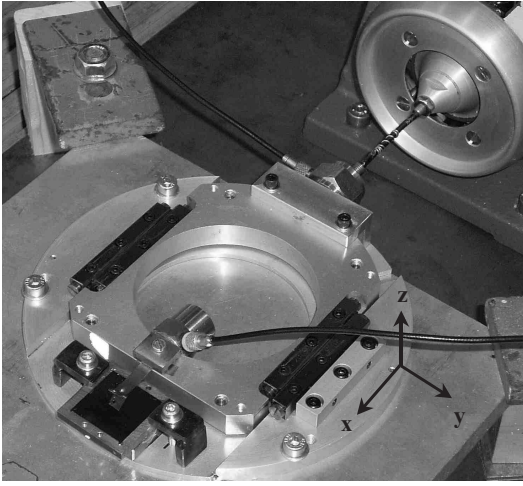
Figure 6.1 / Picture of the system under test.
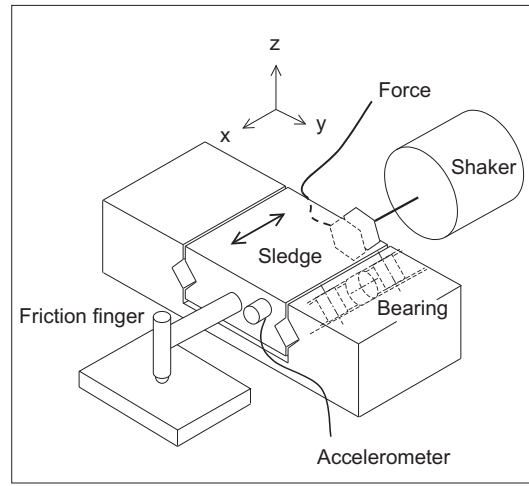
Figure 6.2 / Layout of system under test.

Fig. 6.3 shows a model of the system. The various system components and their interconnections are modeled in order to explain the behavior of the system. The model has only one translational degree of freedom. The linear bearings are assumed frictionless. In the model the shaker, stinger (connection rod), sledge and friction finger can be recognized. The sledge has an acceleration of $\ddot{x}$. The shaker has an elastically suspended moving mass m_1 and is driven with a current i_m. The axial stiffness and damping of the suspension are $b_1 = 1.6 Ns/m, k_1 = 2.8e3 N/m$. The magnetic force F_1 generated in the shaker is proportional with the drive current i_m. The shaker is coupled with the sledge m_2 through a mass-less stinger. The axial stiffness k_2 of the stinger is approximately $1.5e6 N/m$. The effective excitation force of the shaker is F_2. For validation purposes this force is measured with a force sensor which mass must be taken into consideration. The mass between the sensor's seismic plane and its connection to the sledge is added to m_2. The remaining mass of the sensor and the mass of the stinger are added to the moving mass m_1 of the shaker. As a result of this mass distribution, $m_1 = 0.045 kg$ and
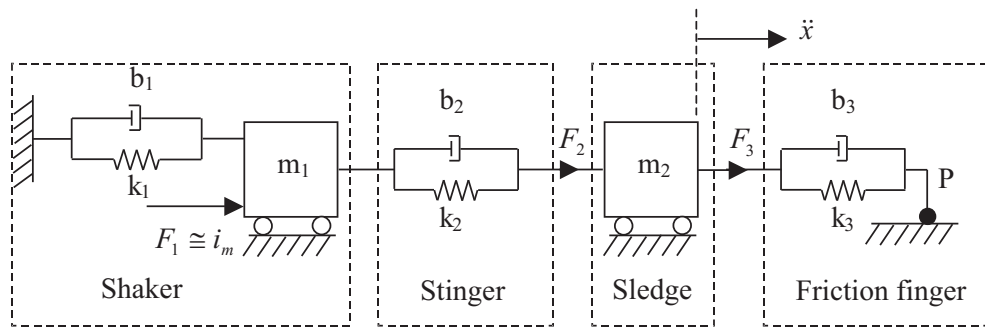
Figure 6.3 / Block diagram of the system under test.

$m_2 = 0.133kg$. In the friction finger, P is a generalized contact point representing the sum of all the asperities of the friction finger between the static base of the set-up and the sledge. In P the friction force is assumed to be generated. In the stick-phase, the friction contact point P has a tangential stiffness k_3 and a damping b_3 because the tangential force is less than the breakaway force (Armstrong-Hélouvry et al., 1994). In the gross sliding phase, when the applied force exceeds the breakaway force, the stiffness k_3 can be neglected. By imposing a high normal force in P, the friction force in P is high compared to the real friction force in the linear bearing. Consequently, the pre-sliding displacement of the system will be determined by k_3, b_3 and the tangential force in P. The transition from stick to gross sliding depends on the breakaway force in P.

6.2 Measurements

The mechanical system will be analyzed using two different approaches. The first technique is the classical FRF measurement with band limited white noise excitation. The results will approximate the linear behavior of the system. The alternative technique is the newly developed HOSIDF technique able to investigate its non-linear behavior. For both the FRF and HOSIDF measurements the shaker current i_m will serve as the reference signal. Firstly, because in many motion systems, for example equipped with a linear motor, a measurement of the actual driving force is often impossible or is very difficult to instrument. Secondly, sinusoidal excitation is a prerequisite for the HOSIDF technique. This is assured by taking the shaker current, generated in a highly linear voltage to current converter, as reference signal.

6.2.1 Measurement of H_1 FRF using band limited white noise

In the first set of measurements the classical Frequency Response Function (FRF) between the shaker current i_m as the input signal and the acceleration $\ddot{x}$ of the system as

output signal is determined, using the H_1 estimator (Randall, 1987):

$$H_1 = \frac{G_{ab}}{G_{aa}} \tag{6.1}$$

with G_{aa} the estimate of the single sided spectrum of the input signal i_m and G_{ab} the cross spectrum between system input i_m and measured output $\ddot{x}$ based on 5 averages. The excitation signal is band limited random noise in a frequency range from $0Hz$ to $1kHz$. The RMS value of the signal is varied exponentially over 3.4 decades from $1mV$ to $2.5V$. Figs. 6.4-6.6 show the magnitude, phase and coherence of the FRF as function of the excitation frequency and the generator voltage. The dynamic behavior of the system exhibits strong excitation level dependency. For low excitation levels, the system is in the stick-phase and its Bode plot shows the friction-induced resonance (Nuij, 2002) at approximately $200Hz$, see the $-50dBV_{rms}$ traces in Figs. 6.4(b), 6.5(b). Knowing the value of the friction-induced resonance frequency, and using the model as depicted in Fig. 6.3, and assuming the friction-induced stiffness k_3 independent of frequency, its value can be calculated from:

$$k_1 + k_3 = (2\pi f_{res})^2 \cdot (m_1 + m_2) \tag{6.2}$$

with $k_1 = 2.8e3N/m$ the axial shaker stiffness. This results in a friction-induced stiffness value for of approximately $2.8e5N/m$. For high excitation values, the system is in the sliding-phase and the value of the friction induces stiffness approaches $0N/m$. Again, the system can be characterized as a second order system with additional dynamics, see the $+8dBV_{rms}$ trace in Figs. 6.4(b) and 6.5(b). The low frequency resonance of approximately $20Hz$ is caused by the axial stiffness of the shaker $k_1 = 2.8e3N/m$ and the combination of the moving mass of the shaker and the sledge $m_1 + m_2 = 0.178kg$. The coherence plot, Fig 6.6(a) indicates two regions with a low value. In the region with low excitation values the frequency independent low coherence is a result of a poor signal to noise ratio of the acceleration signal. The second region, centered around an excitation level of $-25dBV$ ranging from $0Hz$ to approximately $300Hz$ also has a low coherence value. But here the drop in coherence indicates non-linear system behavior. An interesting aspect is the variation in damping in the system. For excitation levels both below and above approximately $-25dBV$, the damping is less than the value at $-25dBV$. Specific information about the stick to sliding transition can not be derived from these FRF measurements due to the implicit assumption of linearity of the system to be described with the FRF technique.

(a) Excitation amplitude dependency   (b) For 3 excitation levels
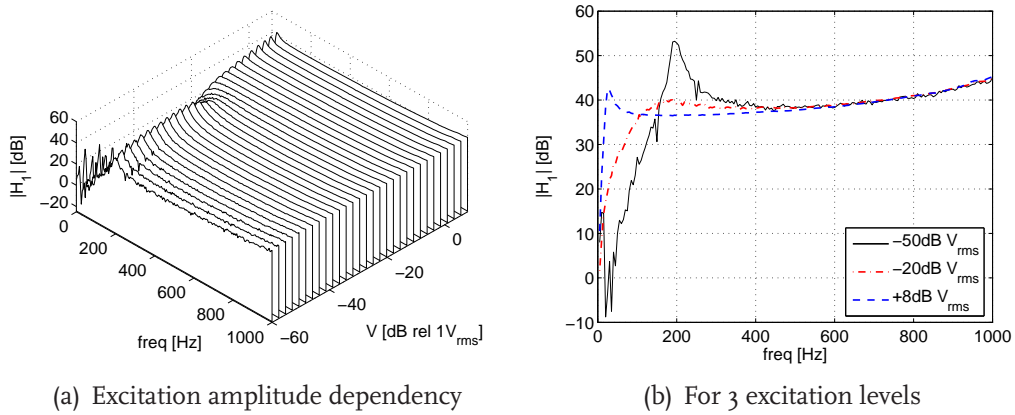
Figure 6.4 / Magnitude of the H_1 FRF of the system.

(a) Excitation amplitude dependency   (b) For 3 excitation levels
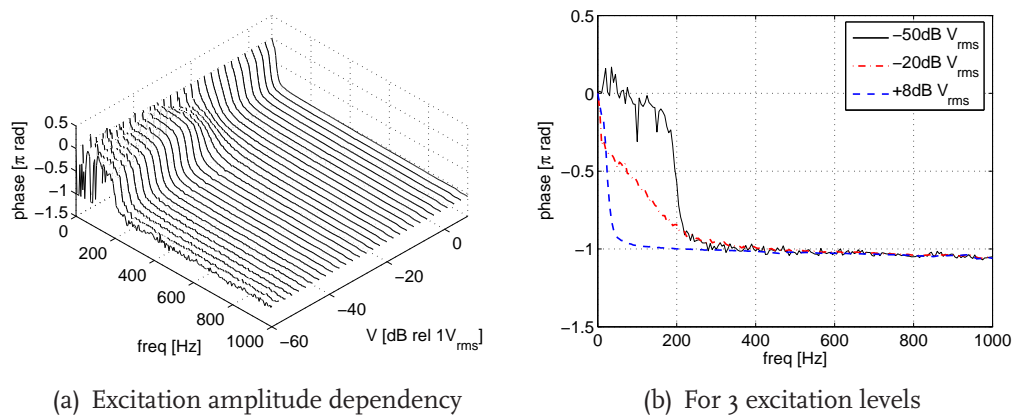
Figure 6.5 / Phase of the H_1 FRF of the system.

(a) Excitation amplitude dependency   (b) For 3 excitation levels

Figure 6.6 / Coherence of the H_1 FRF of the system.

6.2.2   Measurement of the HOSIDF

In order to get a better understanding of the friction-induced non-linear behavior of this system, a HOSIDF analysis is done. The measurement setup remains unchanged.

Measurement setup

The system is excited with a single sinusoid, which frequency is varied with $5Hz$ increments from $10Hz$ to $1kHz$ resulting in a grid of 199 frequency point. In every point of the frequency grid, the excitation amplitude is decreased exponentially in 50 discrete steps from $2.5V_{rms}(8dBV)$ to $1mV_{rms}(-60dBV)$. During every measurement the excitation level is kept constant. Between consecutive measurements a fixed waiting time of $500msec$ is programmed to allow the system to settle. Time averaging over 5 time records of $400msec$ is applied to reduce the influence of non-synchronous disturbance signals. With the sampling frequency of $5120Hz$, the maximum frequency of the nth order SIDF is $5120/(2n)Hz$. Using these measurement parameters, a complete measurement takes approximately 8 hours.

Validation of the excitation condition

Since the measurement technique is based upon the assumption of single frequency sinusoidal excitation, the harmonic distortion of the excitation signal must be low. This is assured by taking the shaker current, generated in a highly linear voltage to current converter, as reference. In Fig. 6.7 the harmonic distortion magnitudes of the shaker current i_m are shown. The values are calculated as the quotients of the power in the individual harmonics and the power of the base component. Values of $-90dB$ indicate measurement points with a harmonic power less 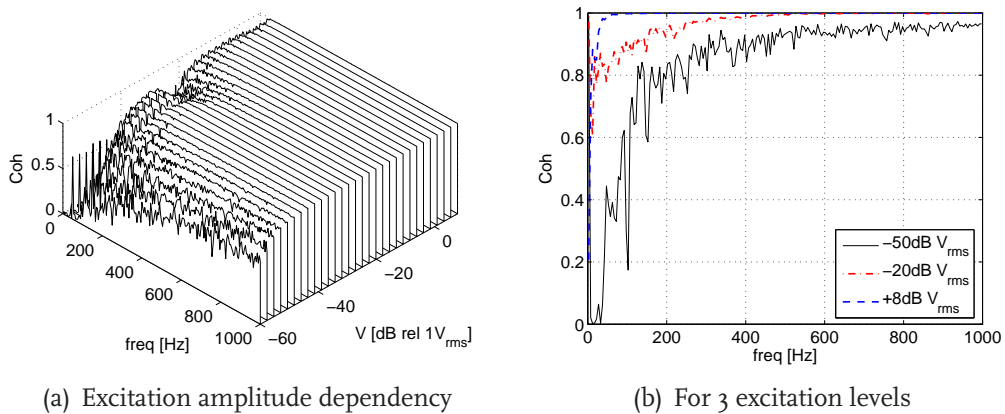than the quantization noise of the instrumentation. The largest distortion component is the second order component at maximum drive level. Its magnitude is less than $-55dB$ with respect to the base component. From these measurements it is decided that the shaker current can serve as input signal although some bias due to harmonic excitation can not be ruled out. This bias is most like to occur when a harmonic component of the excitation signal coincides with a resonance frequency in the first order SIDF, creating the contribution $U_n \cdot H_{n1}$ as described in Eq. 5.3 in Section 5.1.1. In all subsequent HOSIDF measurements in this chapter the shaker current i_m will be the excitation signal and acceleration $\ddot{x}$ the response (Fig. 6.3).

Results

In Figs. 6.8- 6.18 the magnitude plots and the phase plots of the first order up to the fifth order SIDF are shown. The frequency axes have an upper limit depending on the order
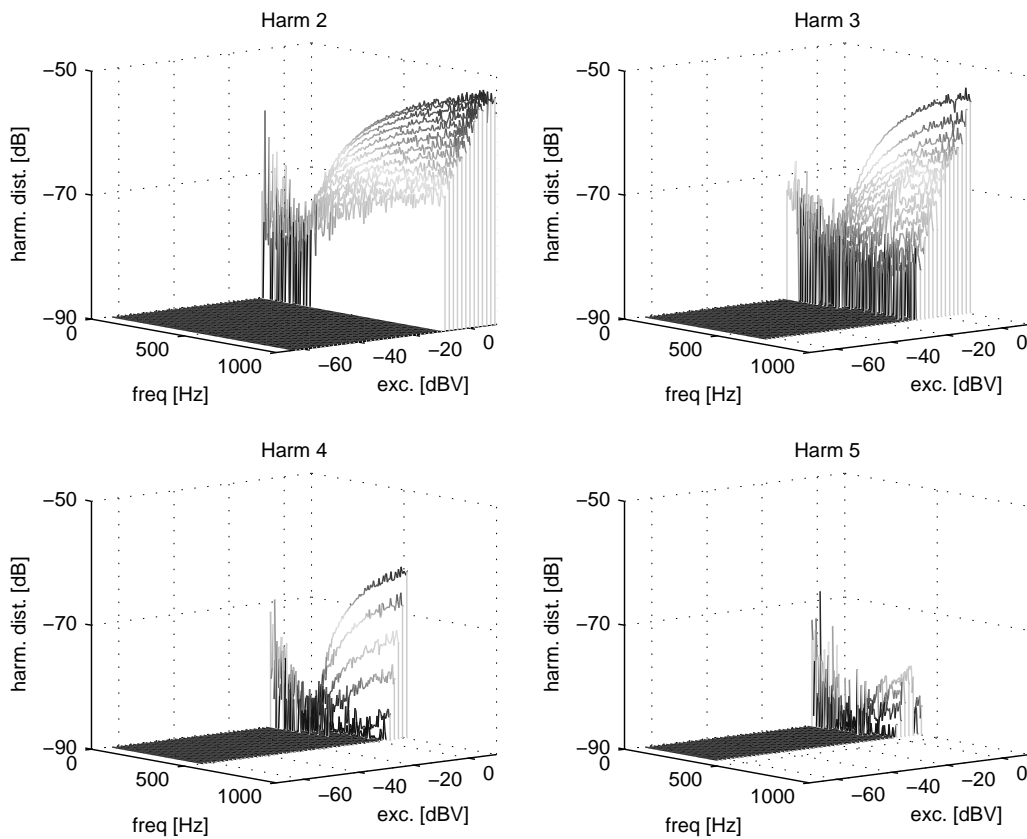
Figure 6.7 / Magnitudes of the harmonic distortion components of the shaker current signal relative to the magnitude of the base component [dB] as function of frequency [Hz] and excitation amplitude $[dBrel1V_{rms}]$.

number. The excitation magnitude axes indicating the generator voltages are equal for all 3D plots. All 2D plots except Fig. 6.10 show cuts along the frequency axis for constant excitation levels of $-50dBV$, $-20dBV$ and $+8dBV$. The measurement results show two groups of HOSIDF with distinctly different characteristics. The odd orders, (Figs. 6.8-6.14), and the even order, (Figs. 6.15-6.18). The odd orders show features with a strong excitation amplitude dependency. The first order SIDF, Figs. 6.8(a), 6.8(b) bears resemblance with the H$_1$ FFT method measurements Figs. 6.4(a), 6.5(a). The differences are mainly concentrated in the frequency region from $0Hz$ to $250Hz$ centered around an excitation level of $-25dBV_{rms}$ as can also be seen in Figs. 6.10(a), 6.10(b). This region coincides with the region of low coherence in the FFT measurements (Fig. 6.6(a)). The first order SIDF (Fig. 6.9) displays the friction induced resonance at approximately $180Hz$ for an excitation levels of $-50dBV$. This value is $20Hz$ lower than the corresponding value determined in the FFT measurement with equal excitation RMS level but obtained with a random noise excitation signal (Fig. 6.4(b)). A possible explanation for this shift is the

(a) First order SIDF mag

(b) First order SIDF phase
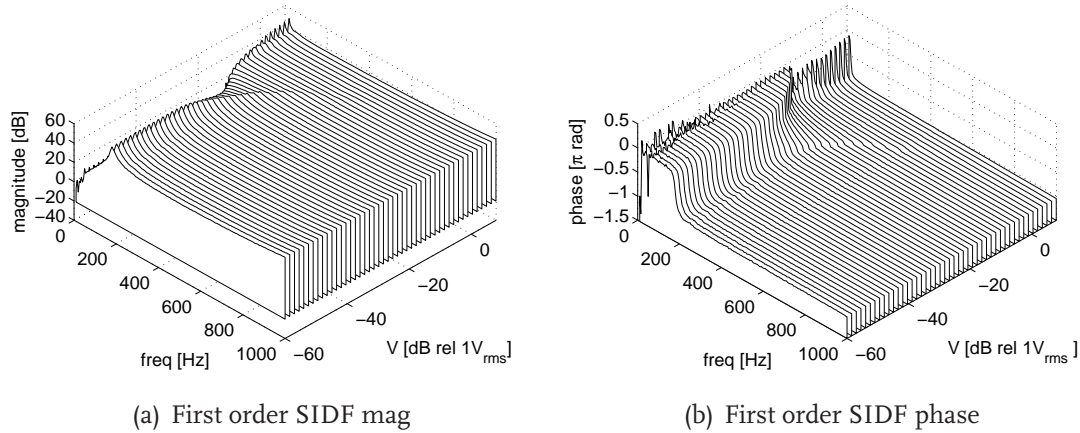
Figure 6.8 / Magnitude and phase of the first order SIDF.
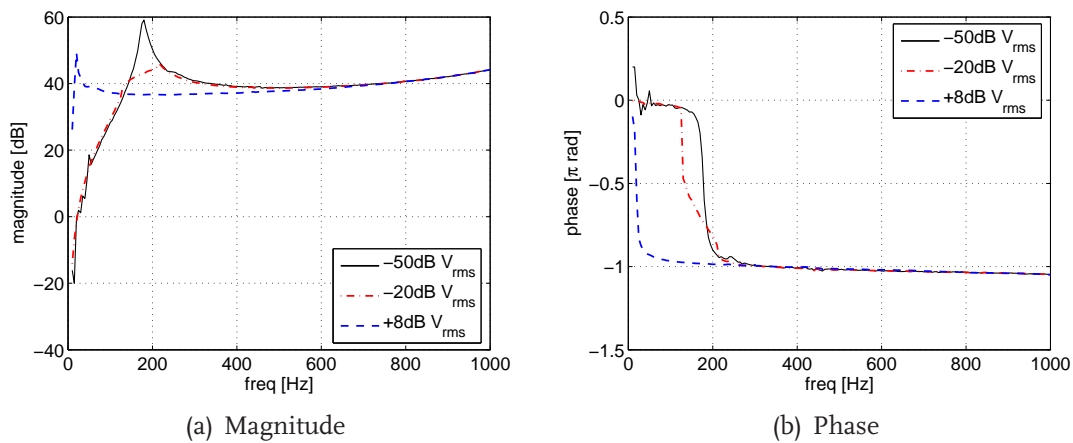
(a) Magnitude

(b) Phase

Figure 6.9 / Magnitude and phase of the first order SIDF for 3 excitation levels.

difference in the probability density functions of the excitation signals which for the sine signal is more concentrated towards the extreme values. This might result in a lower value of the friction induced stiffness in comparison with the FRF measurement with the noise excitation signal with equal RMS value. An overview of the magnitude plot of the third order SIDF (Fig. 6.11(a)) and fifth order SIDF (Fig. 6.13(a)) clearly reveals the development of odd order non-linear system behavior. Two regions can be distinguished as function of the excitation level. For low excitation levels when the friction contact P (Fig. 6.3) is in the stick phase, the magnitude of the third order and fifth order SIDF is low. For high excitation levels, so P is in the sliding phase, the magnitude increases by more than $20dB$. The transition between the two regions is both dependent on excitation level and frequency. For increasing excitation levels in the sliding region, the magnitude of the third order and fifth order SIDF decreases again (Fig. 6.10(a)). This can be explained by the fact that for increasing excitation levels, the influence of the stick/sliding

(a) Magnitude at 105Hz

(b) Phase at 105Hz

(c) Magnitude at 220Hz
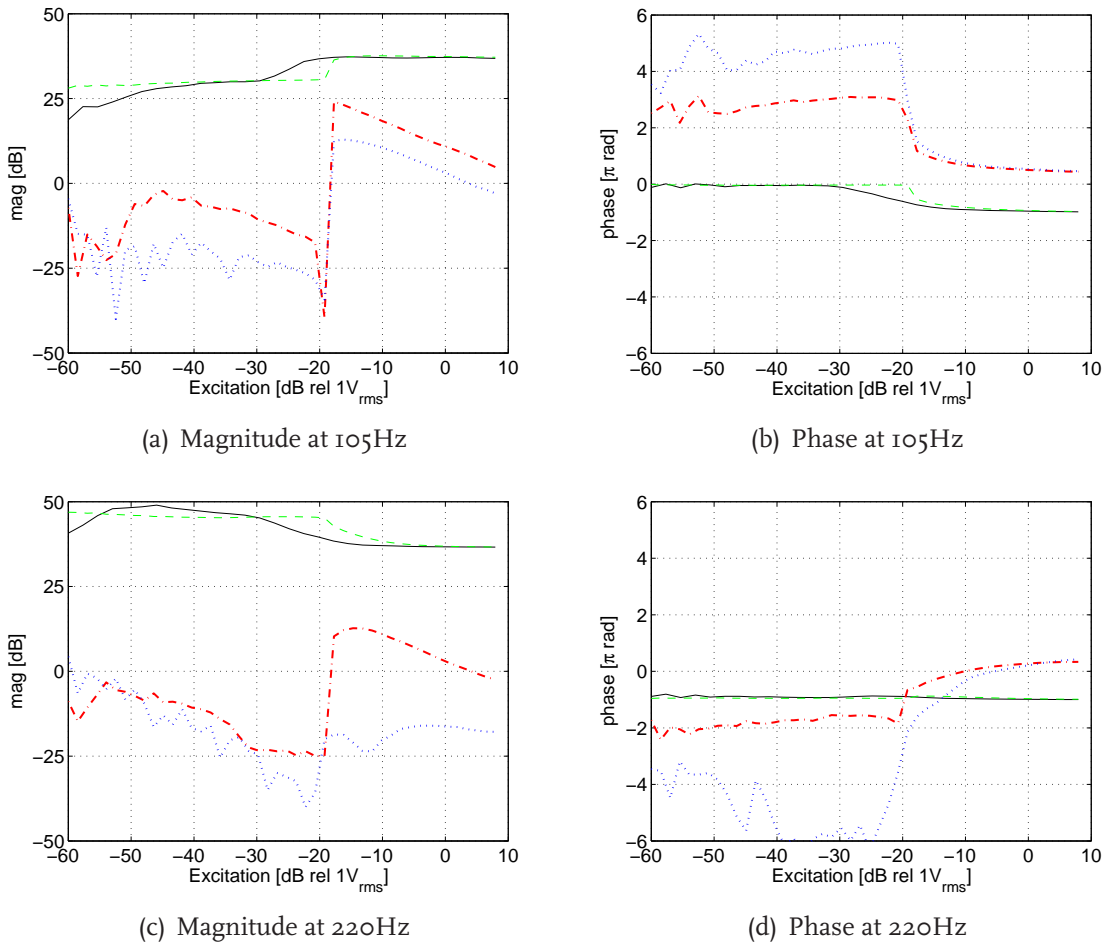
(d) Phase at 220Hz

Figure 6.10 / Magnitude and phase as function of excitation level for constant frequency of 105Hz and 220Hz. Legend: Solid line black H_1 FRF, Dashed line green HOSIDF$_1$, Dash-dot red HOSIDF$_3$, dotted blue HOSIDF$_5$.

transition of P on a full periode of movement will decrease and the system tends to linear behavior for large excitation forces compared to the friction force. This decrease is also visible in the theoretical HOSIDF plots (Fig. 4.4) of the system with backlash as presented in Sec. 4.1. An interesting phenomenon in the third and fifth order SIDF measured at $105Hz$ is the sudden drop in magnitude at an excitation level of approximately $-19dBV$ before the steep increase until an excitation level of approximately $-17dBV$ (Fig. 6.10(a)). This drop is absent in the magnitude plots of the third and fifth order SIDF measured at $220Hz$ (Fig. 6.10(c)). This local decrease in magnitude occurs in the same excitation band in which the phase difference between the third order and fifth order HOSIDF at $105Hz$ changes from $2\pi rad$ to $0rad$ (Fig. 6.10(b)). In the transition from $2\pi rad$ to $0rad$, this phase difference will reach πrad which apparently leads to destructive interference in the third and fifth order components in the output signal, causing the drop in magnitude. In the fixed frequency plot measured at $220Hz$ (Fig. 6.10(c)), so a frequency above the fric-

(a) Third order SIDF mag

(b) Third order SIDF phase
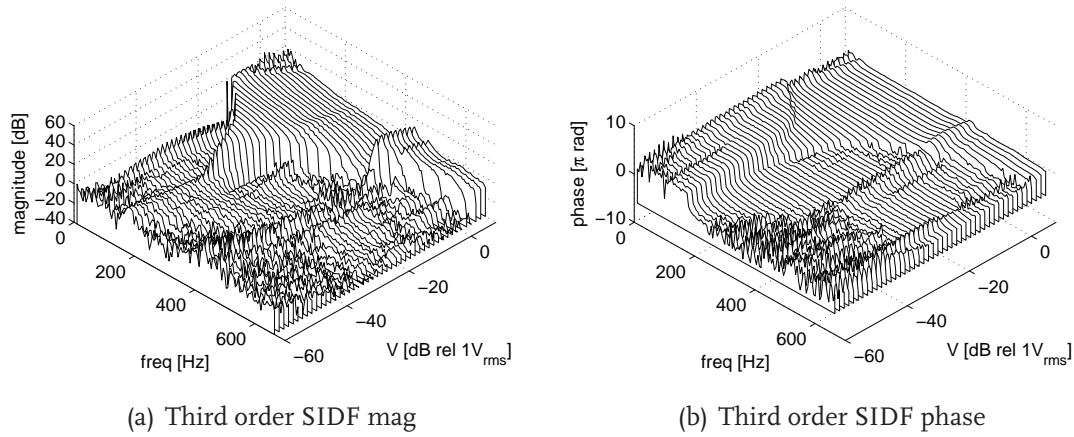
Figure 6.11 / Magnitude and phase of the third order SIDF.
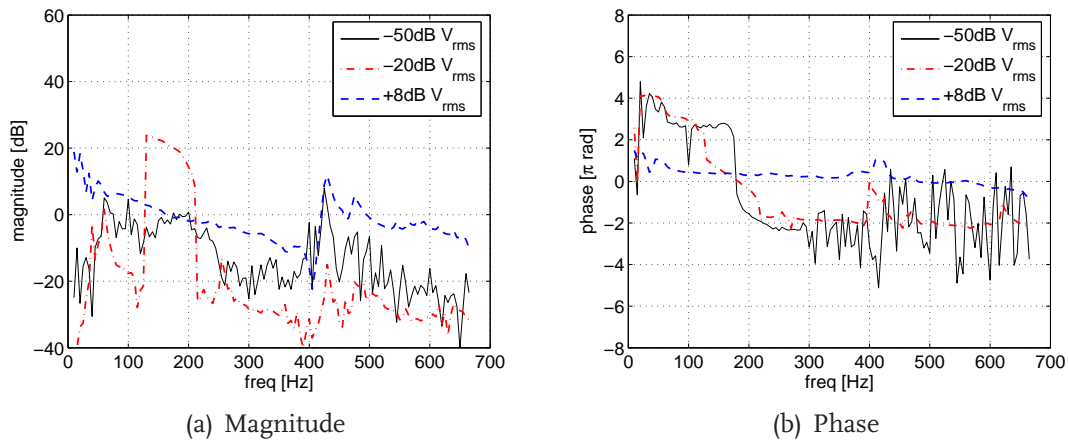
(a) Magnitude

(b) Phase

Figure 6.12 / Magnitude and phase of the third order SIDF for 3 excitation levels.

tion induced resonance frequency of $180Hz$, this drop is not visible in the the third and fifth order SIDF. A closer inspection of the phase plot measured at $220Hz$ (Fig. 6.10(d)) shows that the phase difference between the third and fifth order components is close to πrad in the excitation band from $-17dBV$ to $-12dBV$. In this excitation region both the third and fifth order magnitude plots measured at $220Hz$ (Fig. 6.10(c)) are more flattened off by comparison with the corresponding values in the magnitude plot measured at $105Hz$ (Fig. 6.10(a)). This difference also can be explained by the assumption of destructive interference reducing the magnitudes of the third and fifth order components in the output signal. Additional research is necessary to prove this assumption. In the HOSIDF phase plots, phase unwrapping is necessary. The unwrapping is done in such a way that the phase values for the highest excitation levels are set closest to zero and the derivatives of the phase to frequency and excitation magnitude are minimized over the stick/sliding boundary. In the third and fifth order magnitude plots (Figs. 6.11(a)-6.14(a))

(a) Fifth order SIDF mag

(b) Fifth order SIDF phase
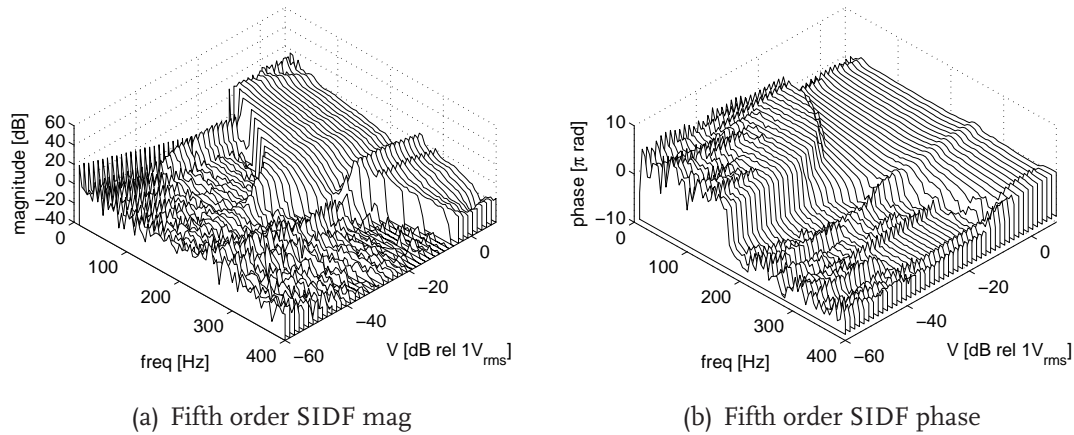
Figure 6.13 / Magnitude and phase of the fifth order SIDF.
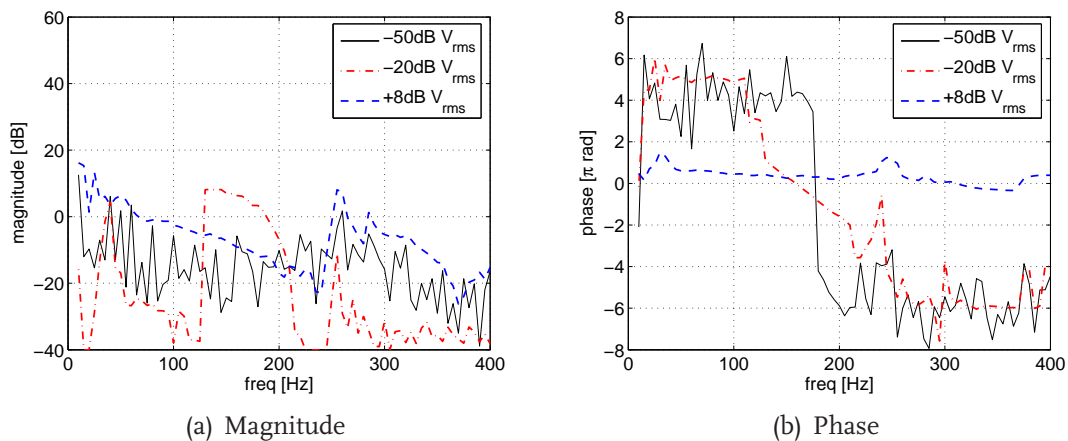
(a) Magnitude

(b) Phase

Figure 6.14 / Magnitude and phase of the fifth order SIDF for 3 excitation levels.

the friction induced resonance is not clearly visible because this resonance occurs in the linear region of the HOSIDF, so the magnitudes are low. In the corresponding phase plots (Figs. 6.11(b)-6.14(b)) the phase shift due to the friction-induced resonance is clearly visible. The magnitudes of the even HOSIDF (Figs. 6.15(a), 6.17(a)) are approximately 30dB lower than the odd HOSIDF magnitudes indicating dominant odd order non-linear behavior. The transition between stick and sliding is less pronounced and the magnitudes do not decrease for high excitation levels. The even HOSIDF show a stronger frequency dependent behavior than the odd order SIDF. The second order SIDF shows two strong resonance like phenomena at approximately $640Hz$ and $700Hz$. In a lesser extent these resonances are also visible in the fourth order SIDF at $320Hz$ and $350Hz$ (Figs. 6.16(a), 6.18(a)). At twice, respectively four times these frequencies i.e. $1280Hz$ and $1420Hz$ the FRF of the measured excitation force F_2 as function of the shaker current i_m has two resonances (Fig. 6.19). These resonances are identified as bending modes in the

(a) Second order SIDF mag

(b) Second order SIDF phase
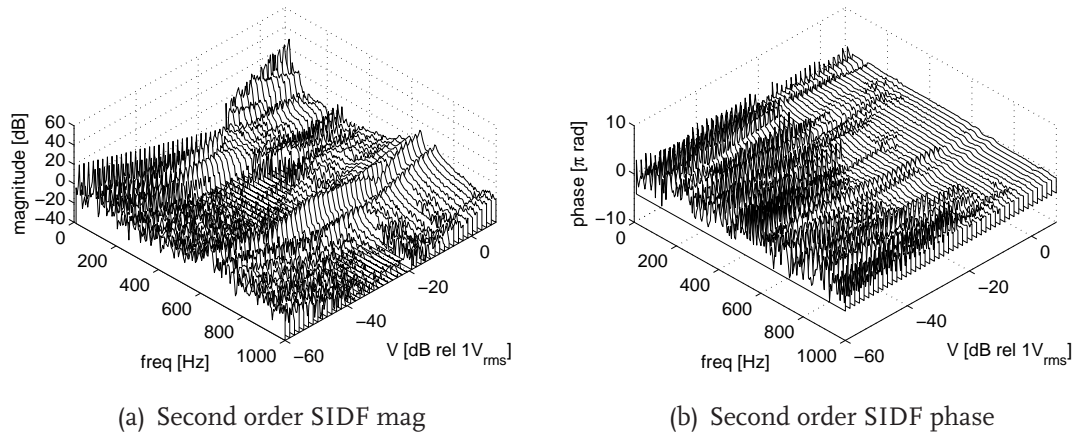
Figure 6.15 / Magnitude and phase of the second order SIDF.
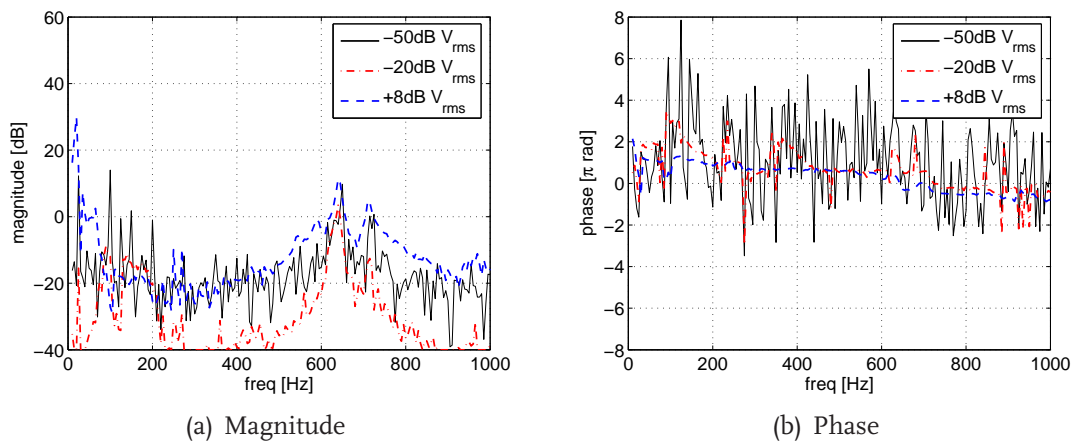
(a) Magnitude

(b) Phase

Figure 6.16 / Magnitude and phase of the second order SIDF for 3 excitation levels.

stinger, the flexible element coupling the shaker and the test object. These resonances are also visible in the odd HOSIDF but at frequencies of $1/n \cdot 1280 Hz$ and $1/n \cdot 1420 Hz$ with n the order number. The mechanism behind the appearance of these structural dynamic phenomena in the HOSIDF is not investigated. It is unlikely that it is solely caused by harmonic pollution of the excitation signal i_m (Fig. 6.3). The strength of each harmonic component in the shaker current is an exponential function of the excitation voltage with the exponent linked to the harmonic number (Fig. 6.7). For low excitation levels, with very low harmonic pollution, these structural dynamic phenomena are still visible in the HOSIDF plots. A more likely explanation is a combination of harmonic distortion in the shaker which generates harmonics in the force signal F_2 and strong resonances in the frequency dependent relation between the shaker current and the true excitation force F_2 (Fig. 6.19).

(a) Fourth order SIDF mag

(b) Fourth order SIDF phase
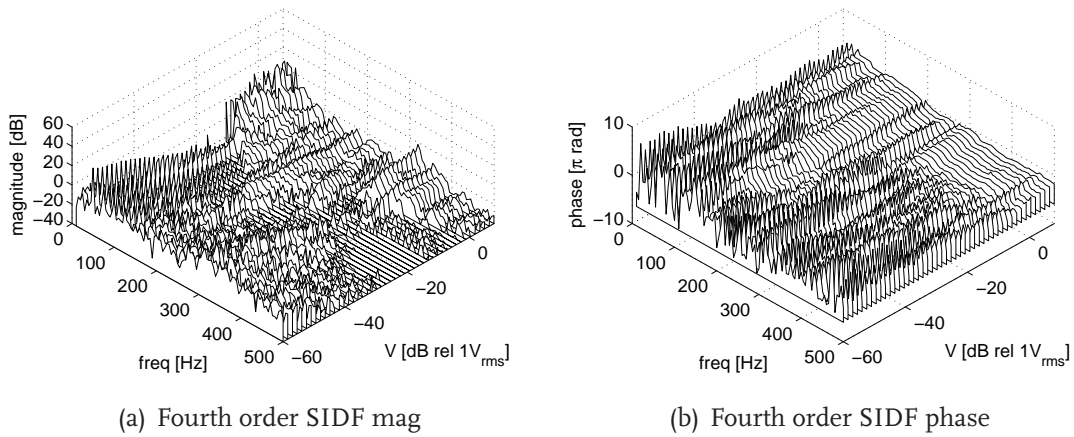
Figure 6.17 / Magnitude and phase of the fourth order SIDF.
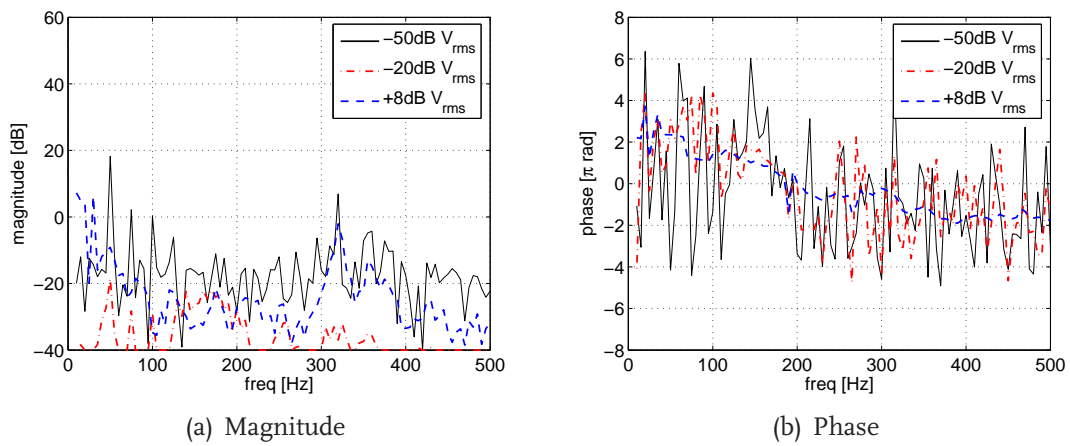
(a) Magnitude

(b) Phase

Figure 6.18 / Magnitude and phase of the fourth order SIDF for 3 excitation levels.

(a) Magnitude

(b) Phase
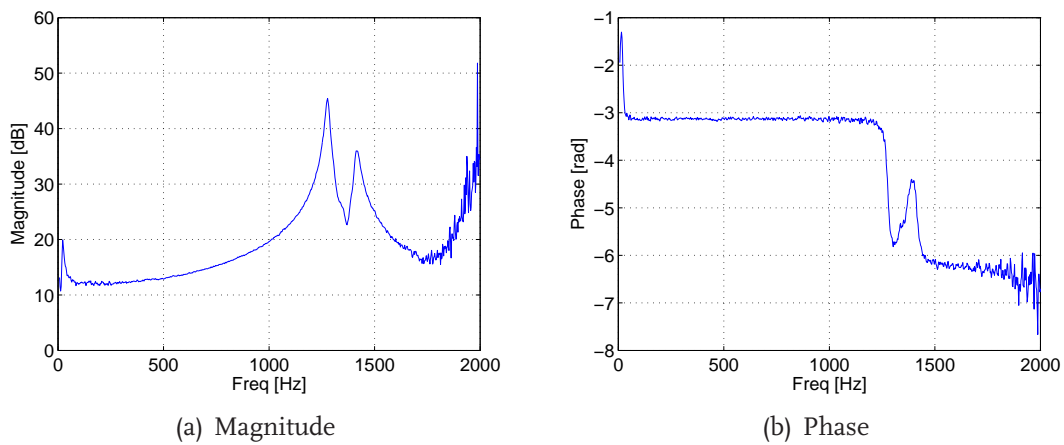
Figure 6.19 / H_1 FRF of excitation force F_2 as function of shaker current i_m measured with high level random noise excitation.

6.3 Determination of the stick to sliding transition

From the *third order* SIDF magnitude characteristics, the stick/sliding transition is determined as function of the measured amplitude/frequency grid. Fig. 6.11(a) shows that for a fixed frequency, the stick/sliding transition is a continuous, monotonous function of the excitation amplitude. Consider such a constant excitation frequency with increasing excitation amplitude. The transition is assumed to coincide with the positive extreme value of the partial derivative of the magnitude of the third order SIDF with respect to the excitation magnitude, being the maximum in the transition from linear to non-linear system behavior. Fig. 6.20 shows this partial derivative in the measured amplitude/frequency grid-points. The stick/sliding transition is clearly visible as a Λ-shape, dividing the two regimes. Because of the discrete steps in excitation magnitude, the true transition will only be approximated. The partial derivative of the *first order* SIDF is not discriminative for the stick/sliding transition as is shown in Fig. 6.21. The extreme values are not strictly positive and the extreme values do not separate between the stick/sliding transition and influence of the excitation magnitude on the frequency of the friction-induced resonance. The measurements show that this influence is caused by the decrease of the tangential stiffness k_3 in the friction contact P (Fig. 6.3) as a result of an increase in elastic displacement in the stick phase. For frequencies close to the friction induced resonance frequency, an extreme value of the partial derivative of the first order SIDF is therefore not an indication for the stick/sliding transition. Based on the information provided by
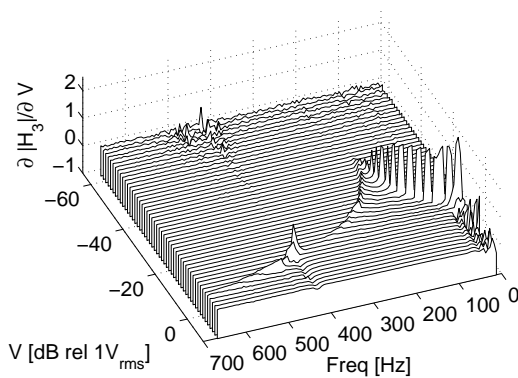
Figure 6.20 / Partial derivative $\frac{\partial |H_3|}{\partial V}$.
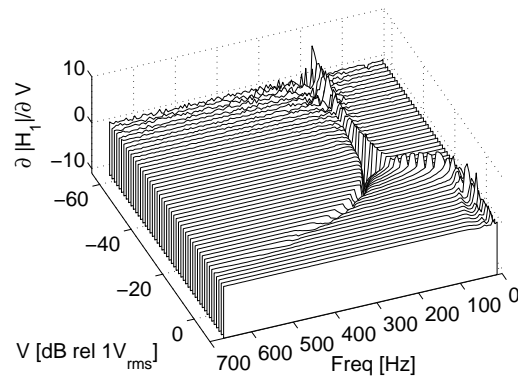
Figure 6.21 / Partial derivative $\frac{\partial |H_1|}{\partial V}$.

the partial derivative of the third order SIDF (Fig. 6.20), the amplitude/frequency grid-points approximating the stick/sliding transition are displayed in Fig. 6.22 together with curves of constant displacement amplitude of the sledge (solid lines). The displacement x of the sledge is calculated by double integration of the measured acceleration signal $\ddot{x}$ (Fig. 6.3). Between the curve indicating $100nm$ displacement amplitude and the curve

of $1\mu m$ displacement amplitude, curves representing a multiple of $100nm$ displacement amplitude are shown. The plot shows that the stick/sliding transition approximately coincides with the $200nm$ displacement curve. For frequencies below the friction-induced resonance the stick/sliding transition is steep, $\frac{\delta x}{\delta V}$ is large. Here a small variation in excitation magnitude will result in a large variation in displacement. For frequencies above the
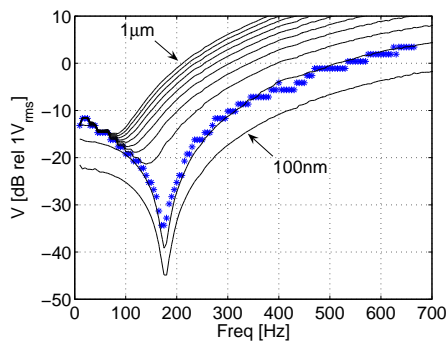
Figure 6.22 / Excitation/frequency grid-points for stick/sliding transition.
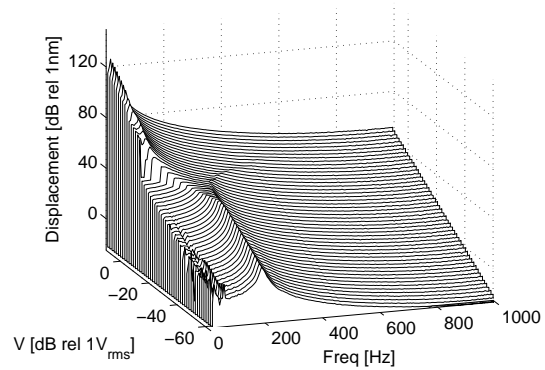
Figure 6.23 / Displacement of sledge.

friction-induced resonance $\frac{\delta x}{\delta V}$ is significantly smaller. At the friction-induced resonance, the displacement due to the excitation force reaches a maximum. For equal magnitude excitation signals with a different frequency, the resulting displacement will be less. Consequently, the excitation signal with the lowest magnitude causing a stick/sliding transition has a frequency equal to the actual friction-induced resonance frequency. Both the friction-induced resonance at approximately $180Hz$ and the steep stick/sliding transition region between $10Hz..100Hz$ and $-20dBV..-10dBV$ are also clearly visible in Fig. 6.23 which shows the displacement of the sledge in the measured amplitude/frequency grid-points. From the identified stick/sliding transition grid-points, the maximum displacement of the system in the stick regime can be calculated by double integrating the acceleration values in these grid-points. Fig. 6.24 shows that the maximum pre-sliding displacement of the system is approximately $200nm$ with a slight tendency to decrease with increasing frequency. Also indicated are the error bars on these displacement values. Due to the discrete excitation levels, the real stick/sliding transition per frequency is likely to occur between two excitation grid points V_n and $V_{n\pm1}$. For every identified stick/sliding transition grid-point (f_k, V_n), the real transition is certain to occur between V_{n-1} and V_{n+1}. The very wide error bars for the frequencies below the friction-induced resonance are caused by the very high sensitivity of the magnitude of the third order SIDF to the excitation magnitude when the system is close to the stick/sliding transition. This is clearly visible in Fig. 6.10(a) for excitation levels between $-20dBV$ and $-15dBV$. This uncertainty can be reduced by decreasing the amplitude steps between consecutive
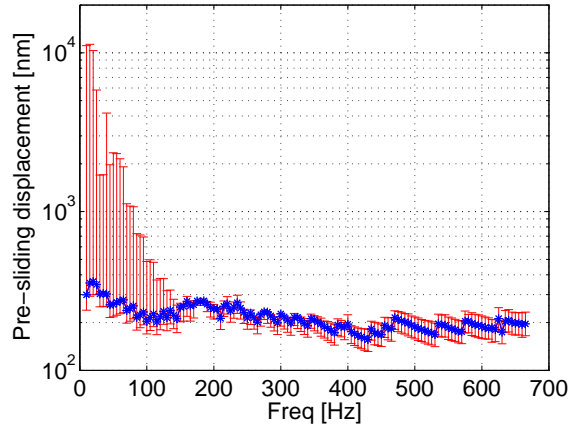
Figure 6.24 / Pre-sliding displacement

measurements of equal excitation frequency when the system is close to the stick/sliding transition, so when the partial derivative $\frac{\partial |H_3|}{\partial V}$ of the third order SIDF is high.

6.4 Calculation of the maximum tangential force

Because the friction-induced resonance frequency just before the stick/sliding transition is known from the results of the first order SIDF, one is able to calculate the related stiffness to yield this resonance if the moving mass is assumed to be known. Using (6.2), k_3 is approximately $2.2e5 N/m$, again assuming k_3 independent of frequency. Since this stiffness is realized in the stick-phase, the required tangential force $F_t(\omega)$ in contact point P can be calculated with:

$$F_t(\omega) = -F_3(\omega) = k_3 \cdot x_{ps}(\omega) \tag{6.3}$$

where $x_{ps}(\omega)$ is the pre-sliding displacement of the system. In Fig. 6.25(a) the calculated tangential force $F_t(\omega)$ in P is shown together with the uncertainty intervals due to the final resolution of the excitation grid. The uncertainty in the stick/sliding results propagates linearly in the calculation of the tangential force. Increasing the density of the excitation grid when the partial derivative $\frac{\partial |H_3|}{\partial V}$ of the third order SIDF is high will also reduce the uncertainty intervals in the calculation of the tangential force.

In order to validate the values of the calculated tangential force, the measured force signals F_2 (Fig. 6.3) are used:

$$F_3(\omega) = F_2(\omega) - m_2 \cdot \ddot{x}_{ps}(\omega) \tag{6.4}$$

where $\ddot{x}_{ps}(\omega)$ is the maximum pre-sliding acceleration. The results are displayed in Fig. 6.25(b) together with the uncertainty intervals. The data from the acceleration

(a) Based on acceleration measurements.

(b) Based on force measurements.
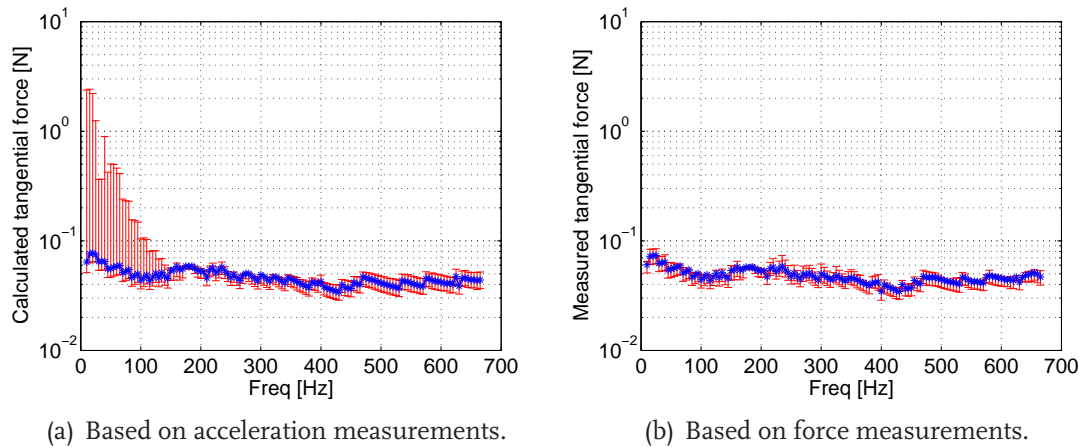
Figure 6.25 / Reconstructed maximum tangential force in P in the stick-phase.

based method correspond very well with the results from the force measurements based method. The main difference is the width of the uncertainty intervals up to $150Hz$. It should be noticed however, that in many real positioning systems, a true measurement of the actual friction force under operating conditions is impossible.

6.5 Discussion

The purpose of this chapter was to show that the HOSIDF reveal information about a non-linear system that otherwise would have been hidden using linear analysis methods. Where both the FRF technique and the HOSIDF technique are conclusive about the existence and value of the friction induced resonance, the transition from stick phase to sliding phase is not visible in the H_1 FRF. The first order SIDF is not discriminative for the stick/sliding transition because this order is also sensitive for the influence of the excitation level on the frequency of the friction induced resonance. The odd HOSIDF however clearly depict this transition. Merging information about the friction induced resonance frequency from the first order SIDF and the stick/sliding transition from the third order SIDF results in both qualitative and quantitative information about the friction force without the need of a force sensor. From these results it is obvious that the HOSIDF method generates additional information about non-linear behavior. These results however also raise some important questions which will not be answered in this thesis: how does the HOSIDF technique relate to other non-linear methods like bifurcation diagrams and Poincaré sections and how does a bifurcation manifest itself in a HOSIDF? These questions are guides for direction of future research.

Measuring the HOSIDF of a non-linear plant operating in feedback

Abstract / In this chapter two measuring techniques are presented for measuring the HOSIDF of a non-linear plant operating in feedback. In a controlled system the harmonics generated by the non-linear system will be fed back to the input of the plant, changing the sinusoidal excitation into a harmonic excitation. The first method applies linear techniques to compensate the bias caused by the harmonic components in the excitation signal. The second method uses a modified repetitive control scheme to suppress the harmonic components in the excitation signal. The effectiveness of both methods is tested in simulation experiments of a mass subjected to Coulomb friction, Stribeck-effect and hysteresis in the pre-sliding regime. The friction forces are modeled with the modified Leuven friction model. The results are compared with the HOSIDF measured under open loop condition. Both methods prove able to produce reliable results.

In this chapter we will expand the realm of the HOSIDF technique to non-linear systems operating in feedback. This greatly expands the applicability because it allows the HOSIDF technique to be used in a class of non-linear systems which require feedback for their stable operation, as is the case for most motion systems.

7.1 HOSIDF of a non-linear plant in a controlled system

Let us consider the class of systems consisting of a causal, time invariant, controlled, stable non-linear plant with a harmonic response to sinusoidal excitation. As stated in Section 2.3, sinusoidal excitation is a necessary condition in the concept of HOSIDF. Fig. 7.1 shows the non-linear plant H with feedback controller C. This system is subjected to sinusoidal excitation $p(t)$ and generates an output $y(t)$. Due to the non-linear behavior of the plant the output of H will also contain harmonics of the excitation frequency. As

$$p(t) = \hat{a}\cos(\omega t + \varphi) \quad u(t) = \sum_{n=0}^{\infty} E_n \cos(n\omega t + \theta_n)$$

$$y(t) = \sum_{n=0}^{\infty} G_n \cos(n\omega t + \vartheta_n)$$
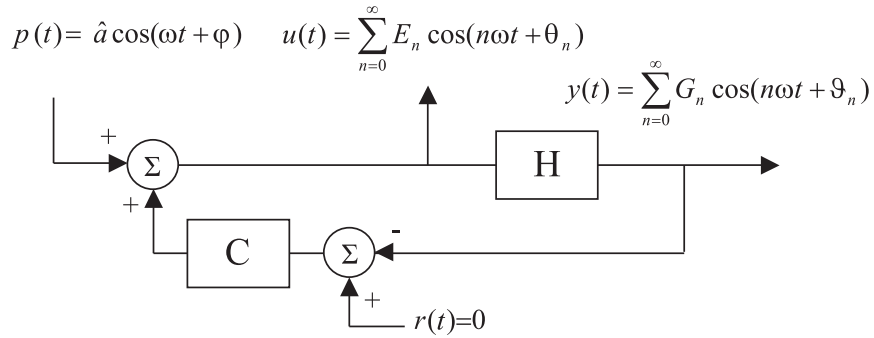
Figure 7.1 / Feedback system.

a result of the feedback, these harmonics will appear at the input of the plant H. This conflicts with the sinusoidal excitation condition required (Taylor, 1999; Slotine and Li, 1991; Atherton, 1975; Nuij et al., 2006). This harmonic input signal $u(t)$ causes several non-linear phenomena in the output signal $y(t)$ like gain compression/expansion, generation of harmonics, desensitization and intermodulation (Bussgang et al., 1974; Wiener and Spina, 1980; Billings and Tsang, 1989a; Solomou et al., 2002; Yue et al., 2005a) as described in Section 5.1.1.

In Section 7.1.1 a numerical compensation method will be presented to reduce the bias in the HOSIDF caused by gain compression/expansion. This compensation technique is based on the methode presented in Section 5.1.1. An alternative approach is presented in Section 7.1.2. In this section is described that, since the harmonics in the input signal can be treated as periodic disturbances and since their period-time is exactly known, significant rejection is possible using repetitive control (Hara et al., 1988; Tomizuka et al., 1988; Yau and Tsai, 1999). Both approaches will be demonstrated with a simulation in order to objectively evaluate their effectiveness under well controlled circumstances.

7.1.1 Numerical compensation

Consider the class of causal, time-invariant, controlled, stable non-linear systems with a harmonic response to a sinusoidal excitation. Due to the feedback a sinusoidal excitation signal $p(t)$ results in a harmonic excitation $u(t)$ of the non-linear plant H, (Fig. 7.1). In the frequency domain the input signal of the plant $u(t)$ can be decomposed into its harmonic components $U(\omega) = \sum_{n=0}^{\infty} U_n$ with $n \in \mathbb{N}$. Likewise the output $y(t)$ of the plant can be expressed as $Y(\omega) = \sum_{n=0}^{\infty} Y_n$, (Fig. 7.2). Let us consider the signal equations relating the excitation signal $P(\omega)$ to the first harmonic component U_1 and the nth harmonic component U_n of $U(\omega)$, hereby neglecting the non-linear effects of desensitization and
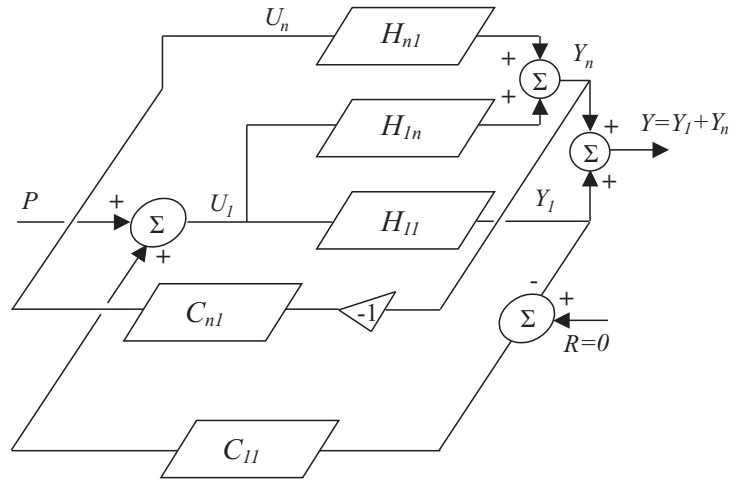
Figure 7.2 / Compensation of the linear bias in the nth order HOSIDF due to harmonic excitation.

intermodulation (Billings and Tsang, 1989a).

$$\frac{U_1}{P} = \frac{1}{1 + H_{11}C_{11}} \tag{7.1}$$

$$\frac{U_n}{P} = -\frac{1}{1 + H_{11}C_{11}} \cdot \frac{H_{1n}C_{n1}}{1 + H_{n1}C_{n1}} \tag{7.2}$$

with C_{11} and C_{n1} the complex values of the (linear) controller for respectively ω and $n\omega$. H_{11} is the approximated first order SIDF at ω relating U_1 and Y_1. H_{n1} represent the relation between the nth order harmonic U_n in the excitation signal and its contribution to the total content of Y_n. H_{n1} can be estimated by evaluating the approximated first order SIDF H_{11} at the frequencies $n\omega$. H_{1n} is the nth order SIDF and models the generation of the nth harmonic as function of the first harmonic. H_{11} and H_{1n} can be determined from the excitation signal P, which can serve as the instrumental variable, and the input signal U of the plant:

$$\left| H_{11} \right| = \left| \frac{1}{C_{11}} \left(\frac{P}{U_1} - 1 \right) \right| \tag{7.3}$$

$$\angle H_{11} = \angle \left\{ \frac{1}{C_{11}} \left(\frac{P}{U_1} - 1 \right) \right\} \tag{7.4}$$

$$\left| H_{1n} \right| = \left| \frac{U_n}{P} \frac{(1 + H_{n1}C_{n1})(1 + H_{11}C_{11})}{C_{n1}} \right| \tag{7.5}$$

$$\angle H_{1n} = \angle \left\{ -U_n \frac{(1 + H_{n1}C_{n1})}{C_{n1}} \right\} + n\angle \left\{ \frac{1 + H_{11}C_{11}}{P} \right\} \tag{7.6}$$

In Eq.7.3, 7.4 the first order SIDF H_{11} will be biased because this model does not take the influences of intermodulation into account. This non-linear process can generate a

signal with frequency ω in Y_1 which is not modeled. Its influence however is considered small with respect to the signal generated by $U_1 H_{11}$. Subsequently H_{n1} will be biased too because it is derived from H_{11} by evaluating H_{11} at frequency $n\omega$. The term $(1 + H_{n1}C_{n1})$ in Eq.7.5, 7.6 is the compensation of the bias in the nth order SIDF which results from the linear effects of the nth harmonic present in the excitation signal. The bias in H_{1n} caused by intermodulation however can not be removed because the contributions of this phenomenon to Y_n has not been modeled.

7.1.2 Repetitive control

Consider the ideal repetitive control system shown in Fig.7.3. The repetitive controller M is an add-on device which generates infinite amplification at the harmonics of the excitation frequency ω_0 (Steinbuch, 2002). The function relating the input signal $e(t)$ of the memory loop to the excitation signal $p(t)$ is given by:

$$T = -\frac{CH}{1 + CH + M} \tag{7.7}$$

Since $|M(n\omega_0)| = \infty \; \forall n \in \mathbb{N}$, the input $e(t)$ of the memory loop will be zero for DC and all the harmonics of the sinusoidal excitation signal $p(t)$. Consequently the input of the plant $u(t)$ will be equal to the excitation signal $p(t)$. The system is in an open loop condition for the excitation frequency and its harmonics and so the HOSIDF can be determined without bias from $u(t)$ and $y(t)$.
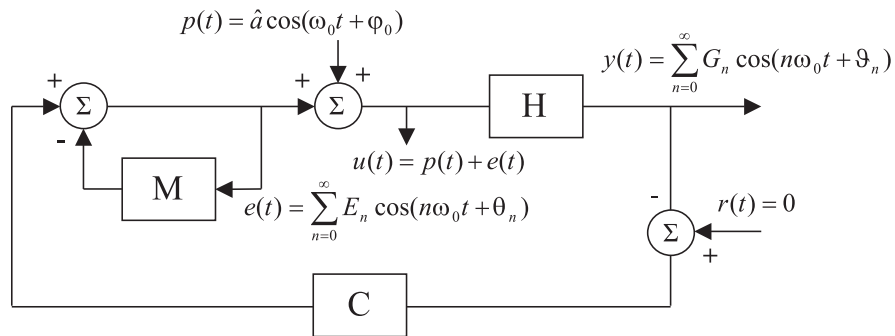
Figure 7.3 / Feedback system including repetitive control memory loop M.

Repetitive controller

In its basic layout, the repetitive controller M consists of a delay of length $T_0 = 2\pi/\omega_0$ and positive feedback. In Fig. 7.4 a block diagram of the applied repetitive controller is shown. The controller consists of two delays, a robustness filter $Q(z)$, constant gain blocks γ, γ^{-1},
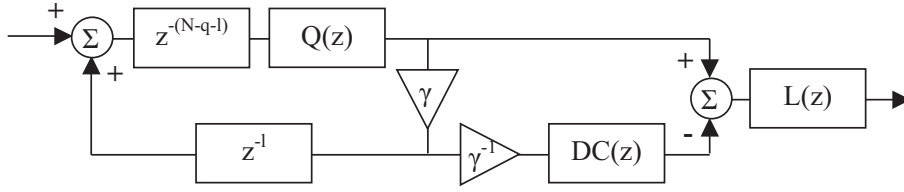
Figure 7.4 / Memory loop with positive feedback and DC reconstruction filter.

DC reconstruction filter $DC(z)$ and learning filter $L(z)$. The delays are implemented as discrete time FIFO shift registers. Their total length is $N - q - l$ and l respectively with $N = T_0 \cdot f_s$, f_s being the sampling frequency of the memory loop. The constants q and l are the delays caused by the linear phase lowpass filter $Q(z)$ and the learning filter $L(z)$ required for stability. The DC reconstruction filter is required for canceling the gain at $0Hz$ in the memory loop. Without this filter, the DC amplification in the memory loop will be infinite so there will be no feedback at $0Hz$ in a repetitive control system. This is undesirable in applications where DC feedback is required for the system to function like positioning systems subjected to gravity. The output of the DC reconstruction filter, which equals the DC level of the memory loop, is subtracted from the memory loop signal (Fig. 7.4). The transfer function of the DC reconstruction filter is given by the following comb-filter:

$$DC(z) = \frac{1}{N} \frac{z^{N-1} + z^{N-2} + ... + z^0}{z^N} \tag{7.8}$$

The upper trace of Fig. 7.5 shows the magnitude of the Frequency Respons Function (FRF) of the ideal memory loop without DC reconstruction. The FRF of the memory loop with DC reconstruction filter is shown in the lower trace of Fig. 7.5.

Stability

In order to successfully apply the memory loop as an add-on device under measurement conditions, overall system stability must be preserved (Tomizuka et al., 1988; Hillerström, 1996; Chew and Tomizuka, 1990). The transfer function of the memory loop M is given by:

$$M(z) = \frac{Q\gamma z^{-(N-q-l)}}{1 - Q\gamma z^{-(N-q)}}(1 - DC)L \tag{7.9}$$

Assuming linearity of H, Eq. 7.7 can be rewritten as:

$$T = -\frac{CH}{1 + CH + M} = -\frac{CH}{1 + CH}M_s \tag{7.10}$$

M_s is the modifying complementary sensitivity function and describes the modification of the complementary sensitivity function of the original system without repetitive con-
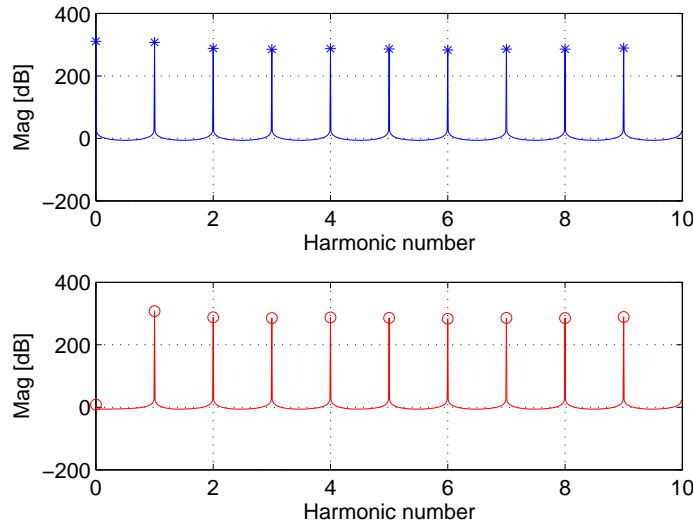
Figure 7.5 / Magnitude of the FRF of the memory loop, without (upper trace) and with DC reconstruction filter (lower trace).

trol. Substituting Eq. 7.9 in Eq. 7.10 yields:

$$M_s(z) = \frac{1 - Q\gamma z^{-(N-q)}}{1 - Qz^{-(N-q)}\{\gamma - SLz^l(1 - DC)\}} \tag{7.11}$$

where S is the sensitivity:

$$S = \frac{1}{1 + CH} \tag{7.12}$$

From Eq. 7.11 a sufficient condition for stability based upon small gain assumptions can be derived:

$$|Qz^{-(N-q)}\{\gamma - SLz^l(1 - DC)\}| < 1 \tag{7.13}$$

for all z with $|z| = 1$. Since $|Q| \leq 1$, the stability criterion (Eq. 7.13) can be reduced to

$$|\gamma - SLz^l(1 - DC)| < 1 \tag{7.14}$$

At $0Hz$ $|1 - DC| = 1$, for all other frequencies $|1 - DC| < 1$. So stability is guaranteed if $|\gamma| = 1 - \epsilon$ and $L = S^{-1}$. The learning filter L can be designed with the ZPETC algorithm (Tomizuka, 1987) and the resulting phase delay of l samples is absorbed in the two delay blocks. Depending upon the characteristics of S, an additional notch-filter may be required to reduce the DC gain of the L filter in order to maintain DC feedback in the main system. The notch should not be positioned inside the memory loop since it does not exhibit a linear phase characteristic like the robustness filter Q. As a result its delay can not be compensated resulting in a significant reduction of the gain at the harmonics of the excitation frequency. Since the gain block γ does not exhibit phase shift, its influence on the memory loop gain is significantly less.

7.2 Simulation experiment

The effectiveness of both methods is tested with well controlled simulations instead of measurements on a real system in order to focus on effects truly related to the individual methods. The plant under test consists of a single degree of freedom mass M subjected to friction (Fig. 7.6). The mass is excited with a driving force F and experiences a friction force F_f. Its position x is subtracted from the reference signal $r = 0$. The error signal is amplified by the PD controller. With S_1 open, the plant operates in open loop. With S_1 closed and S_2 open, the plant operates in feedback, with S_2 closed the repetitive control action is added . The actual friction force F_f is calculated with the modified Leuven model which incorporates Coulomb friction, Stribeck-effect and hysteresis in the pre-sliding regime (Swevers et al., 2000; Lampaert et al., 2002). The friction model parameters are chosen such to generate odd (point symmetric) friction behavior. In Ap-
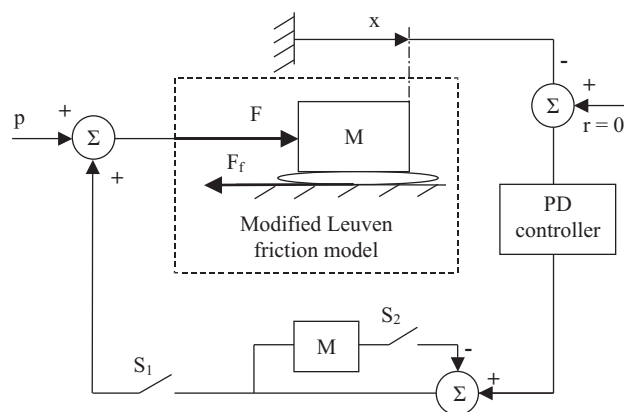
Figure 7.6 / System under test.

pendix 11.3 the modified Leuven friction model is described in more detail. The excitation range covers both the pre-sliding and the gross-sliding regime. Since the system has odd behavior, it will not require feedback to remain at a constant position when being excited sinusoidally in the gross-sliding regime. This allows the HOSIDF to be determined under open loop conditions. These open loop results will be used as a reference for the HOSIDF determined under closed loop conditions. All presented HOSIDF give the relation between force input F and position output x. The time-series $F(t)$ and $x(t)$ are the simulation results and serve as the input data for the calculations of the HOSIDF. These time-series have a length of 8 times the period length of the actual excitation frequency f_{exc}. This results in a frequency resolution $\Delta f = 1/8 f_{exc}$. In the first simulation the odd order SIDF of the plant are determined. These results will serve as a reference for a second simulation under closed loop conditions and a third simulation under closed loop conditions with additional repetitive control.

7.2.1 Open loop simulation

The results of the open loop experiment are presented in Fig. 7.7. The left column shows the magnitude plots. The right column shows the phase information. For excitation levels
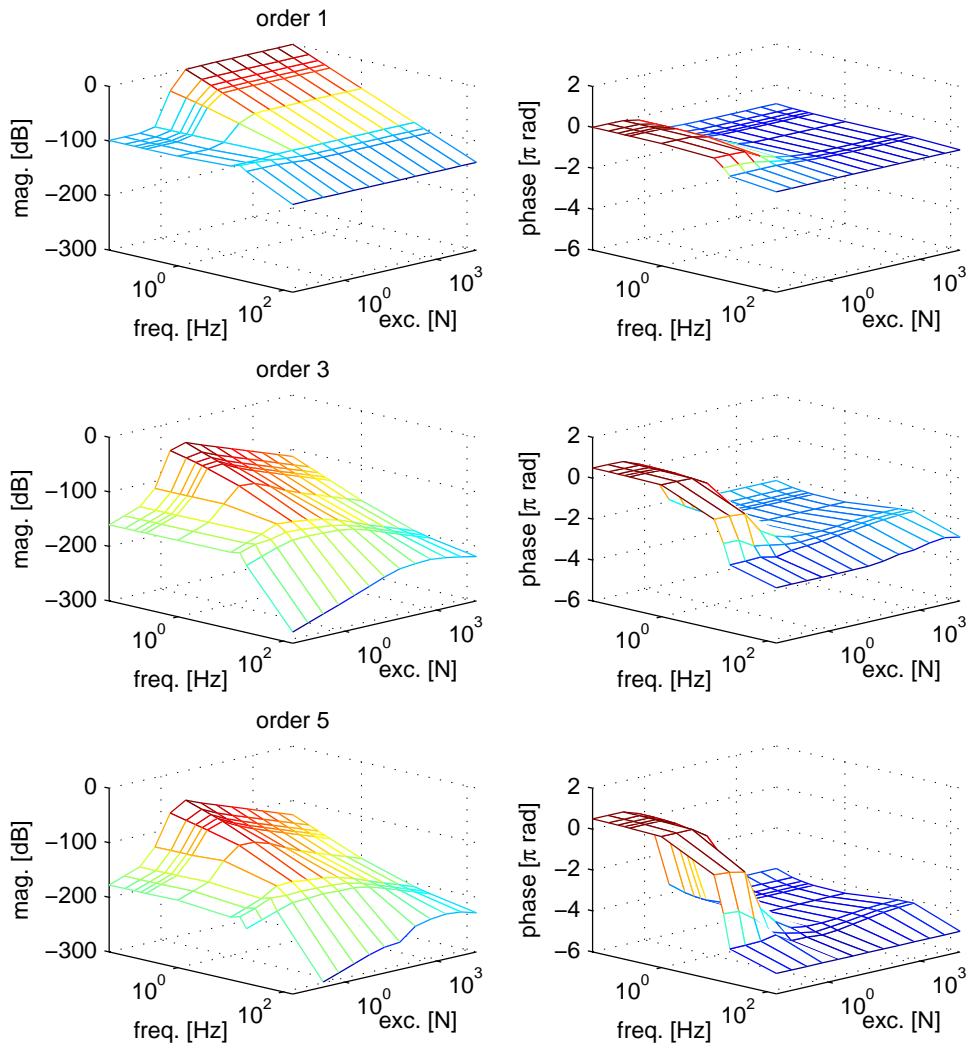
Figure 7.7 / Odd order SIDFs of the open loop system.

less than 1N, the system is in the pre-sliding regime and the first order SIDF resembles the frequency response function of a damped second order system. For frequencies below approximately $15Hz$ the system is dominated by the friction induced stiffness. This stiffness equals the sum of the stiffnesses k_i of the individual Maxwell slip elements used for modeling the hysteresis (Appendix II.3). The maximum friction induced stiffness of

$9e4N/m$ results in a level of $-99dB$ in the magnitude of the first order SIDF. Since the mass is $10kg$ this combination yields a friction induced resonance frequency of $15Hz$ which is visible in both the magnitude curve and the phase curve of the first order SIDF. Above $15Hz$ the mass behavior becomes dominant. For low frequencies the border between the pre-sliding regime and the gross sliding regime is clearly visible. An excitation with a magnitude less than $1N$ and a frequency below $15Hz$ will not lead to gross sliding. Excitations above $1N$ will cause gross sliding and the first order SIDF becomes independent of the excitation amplitude. This can mistakenly be interpreted as a linear regime of this non-linear system. The high values of the third and fifth order SIDF however indicate non-linear system behavior present also in the gross sliding regime. For increasing excitation levels, the magnitudes of the third and fifth order SIDF decrease which indicates that the system tends to linear behavior for very high excitation levels. Both the third order and fifth order magnitude plots show a maximum value as function of excitation for every frequency. Fig. 7.8 displays these amplitude/frequency combinations and shows that these maxima do not occur at a fixed excitation level.
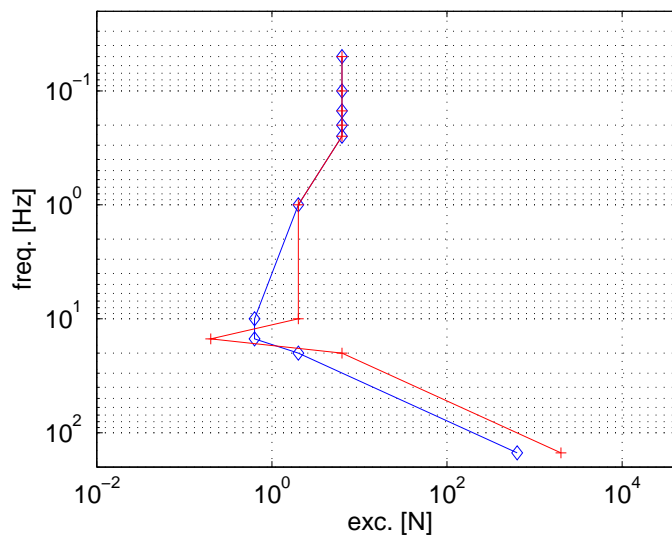
Figure 7.8 / Frequency and magnitude dependency of the maximum value of the third ($\diamond$) and fifth ($+$) order SIDF.

7.2.2 Numerical compensation validation

In the second simulation the feedback loop is closed (S_1 closed, S_2 open in Fig. 7.6). The level of the excitation signal P is changed to equalize the magnitude values of the first harmonic U_1 and the magnitude values of the sinusoidal excitation signal in the open loop experiment within 0.5%. Fig. 7.9 shows the errors in the closed loop results relative

to the open loop results. These errors are calculated as:

$$magnitude\ error\ [dB] = 20 \log \frac{|HOSIDF_{cl}|}{|HOSIDF_{ol}|} \qquad (7.15)$$

$$phase\ error\ [rad] = \angle(HOSIDF_{cl}) - \angle(HOSIDF_{ol}) \qquad (7.16)$$

with $HOSIDF_{cl}$, $HOSIDF_{ol}$ the HOSIDF measured under closed loop conditions and open loop conditions respectively. To increase the visibility of the results, the magnitude
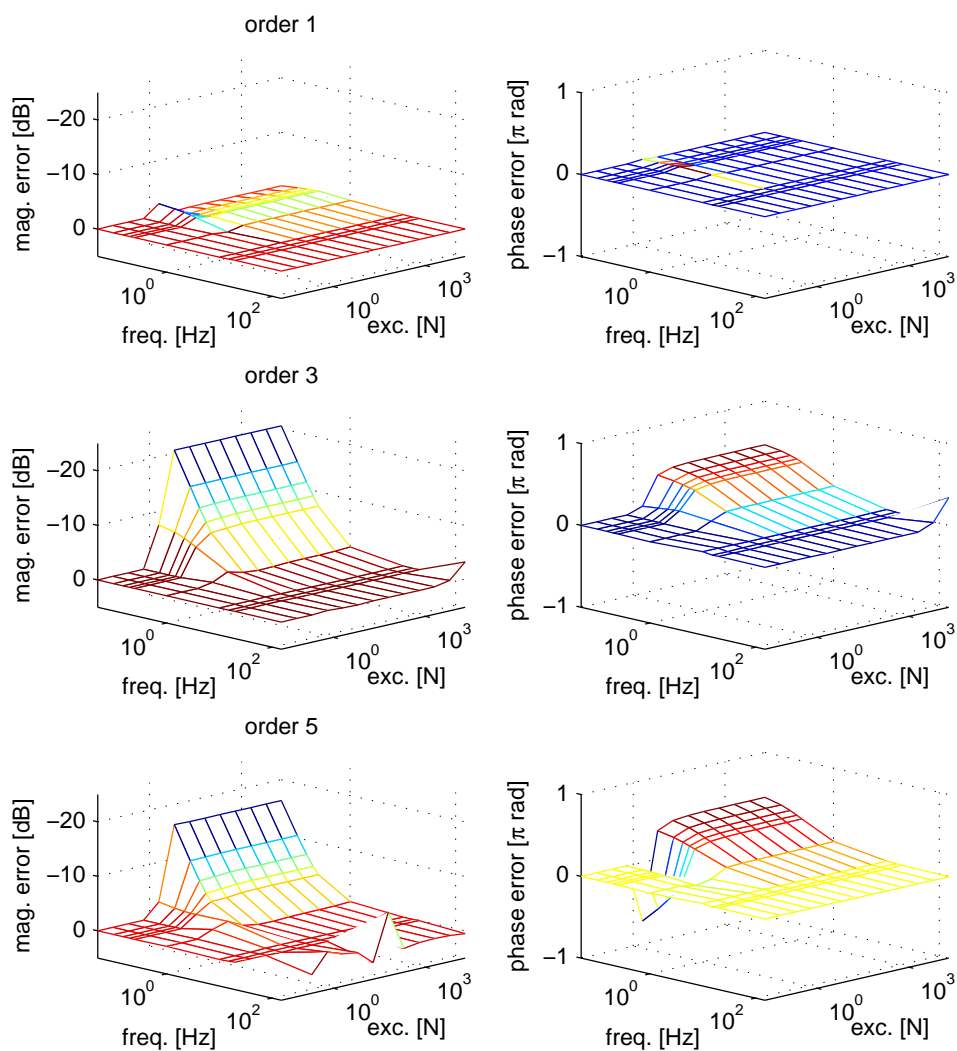
Figure 7.9 / Magnitude and phase errors in odd order HOSIDF measured under closed loop conditions.

errors in the left column of Fig. 7.9 are plotted along a reversed z-axis. The closed loop measurement condition has only little influence on the estimate of the first order SIDF as can be seen in the first row of Fig. 7.9. The third and fifth order SIDF however show significant bias errors, see rows 2 and 3. For the lowest frequency of $0.05Hz$ the magnitude errors of the third order SIDF exceed $-20dB$ (so an underestimation of more than $20dB$) and for both the third order and the fifth order the phase errors are nearly $\pi/2$ rad. To test the effectiveness of the numerical compensation techniques presented in Section 7.1.1, the fifth order SIDF at $0.05Hz$ and $0.2Hz$ are recalculated using Eq. 7.5, 7.6. In the first
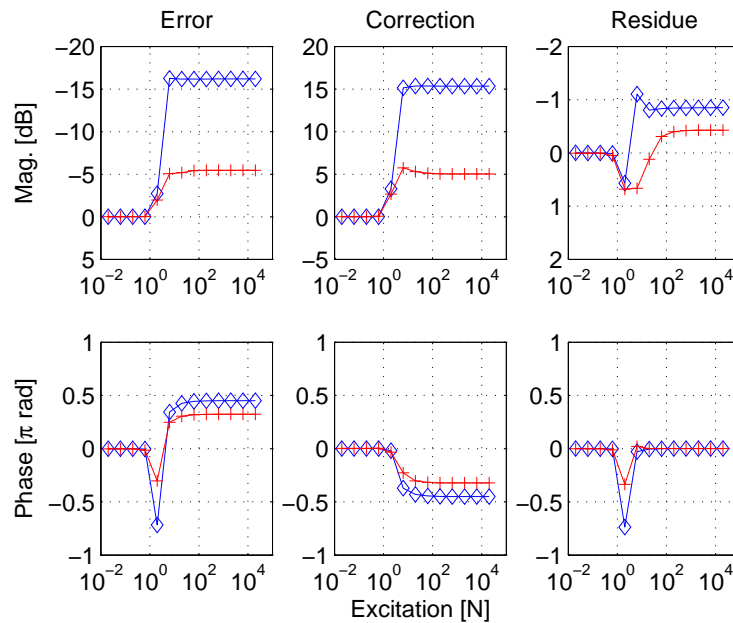
Figure 7.10 / Compensation of fifth order SIDF at 0.05Hz ($\diamond$) and 0.25Hz ($+$).

column of Fig. 7.10 the magnitude errors and phase errors are shown, calculated as the difference between the fifth order data from the closed loop simulation and the open loop simulation. The second column shows the correction values derived from the first order SIDF at $0.25Hz$ respectively $1Hz$ derived from the closed loop simulation. The third column shows the remaining errors after compensation. The magnitude residue has extreme values on the steep flanks of the HOSIDF, when the system leaves the pre-sliding regime and enters the gross sliding regime. Due to this steepness an excitation error of 0.5% will cause a variation of approximately $0.25dB$ in the magnitude estimates of the first and fifth order SIDF. The steady error in the excitation range above $100N$ can not be explained by this excitation tolerance. Likely causes are non-modeled phenomena like intermodulation and desensitization. No further research is done into these errors mechanisms. The stick/sliding transition is also visible in the residual phase error. Outside this border region the residual phase error is very small. From the results can be concluded that measuring HOSIDF in a closed loop situation is prone to large errors if the

influence of the existence of higher harmonic components in the excitation signal is ig-
nored. Applying a compensation method based upon purely linear assumptions reduces
the errors significantly. The main drawback of the compensation method is the require-
ment to do additional measurements at multiples of the frequency of interest thereby
increasing the throughput time of the measurement session.

7.2.3   Repetitive control validation

In the repetitive control simulation the feedback loop is closed and the system is equipped
with an additional repetitive controller (S_1 closed, S_2 closed in Fig. 7.6). The plant has
odd behavior so it will not drift from its position under sinusoidal excitation. Therefore
no DC feedback is required and the DC reconstruction filter (Fig. 7.4) is omitted for sim-
plicity and speed of simulation. The learning filter L (Fig. 7.4) is designed as the inverse
of the sensitivity function (Eq. 7.12). The plant data are derived from the first order SIDF
data simulated under closed loop conditions. Since the plant data depend strongly upon
the excitation level, both the pre-sliding and the sliding regime require tailored L filters.
In practice this might prove difficult because the design of the L filter is based upon a
linearized model. In those situations the stability of the repetitive control loop has to
be further increased by reducing the learning rate of the memory loop at the expense of
speed of convergence. This is realized by incorporating an additional gain of $1 - \varepsilon$ in
series with the L filter. A well tuned memory loop effectively suppresses the excitation
frequency component ω_0 in the controller signal so the input of the plant is equal to the
excitation signal $P(\omega_0)$. Subsequently no amplitude matching is required to assure equal
excitation levels in both the open loop simulation and the repetitive control simulation.
The magnitude and phase differences between the repetitive control data and the open
loop data are presented in Fig. 7.11. The magnitude errors shown in the first column for
all three HOSIDF are less than $1dB$ (12%) over the entire excitation/frequency grid. This
is a reduction of up to $20dB$ in comparison with the results without repetitive control. The
maximum errors are located in the gross sliding regime (excitation force $> 1N$) at exci-
tation frequencies around $1Hz$. The dominant phase errors of approximately $0.025rad$
depicted in the second column are located at the stick to sliding transition. Here the phase
gradient $\frac{\delta\varphi}{\delta\hat{a}}$, in the direction of the excitation axis is the steepest (Fig. 7.7). Closer inspec-
tion of the remaining small magnitude errors in the third order SIDF and fifth order SIDF
reveal a correlation between these errors and the excitation frequency/magnitude combi-
nations used in the simulation. The first row in Fig. 7.12 indicates these excitation fre-
quency/magnitude combinations which resulted in magnitude errors exceeding -0.1dB
(1%) in the third order SIDF and fifth order SIDF. The second row shows the excitation
frequency/magnitude grid points in which the excitation signal $u(t)$ still has noticeable
third and fifth harmonic components. In these excitation grid points, the third and fifth
order harmonics are more than 90dB above the noise floor of the excitation signal $p(t)$.
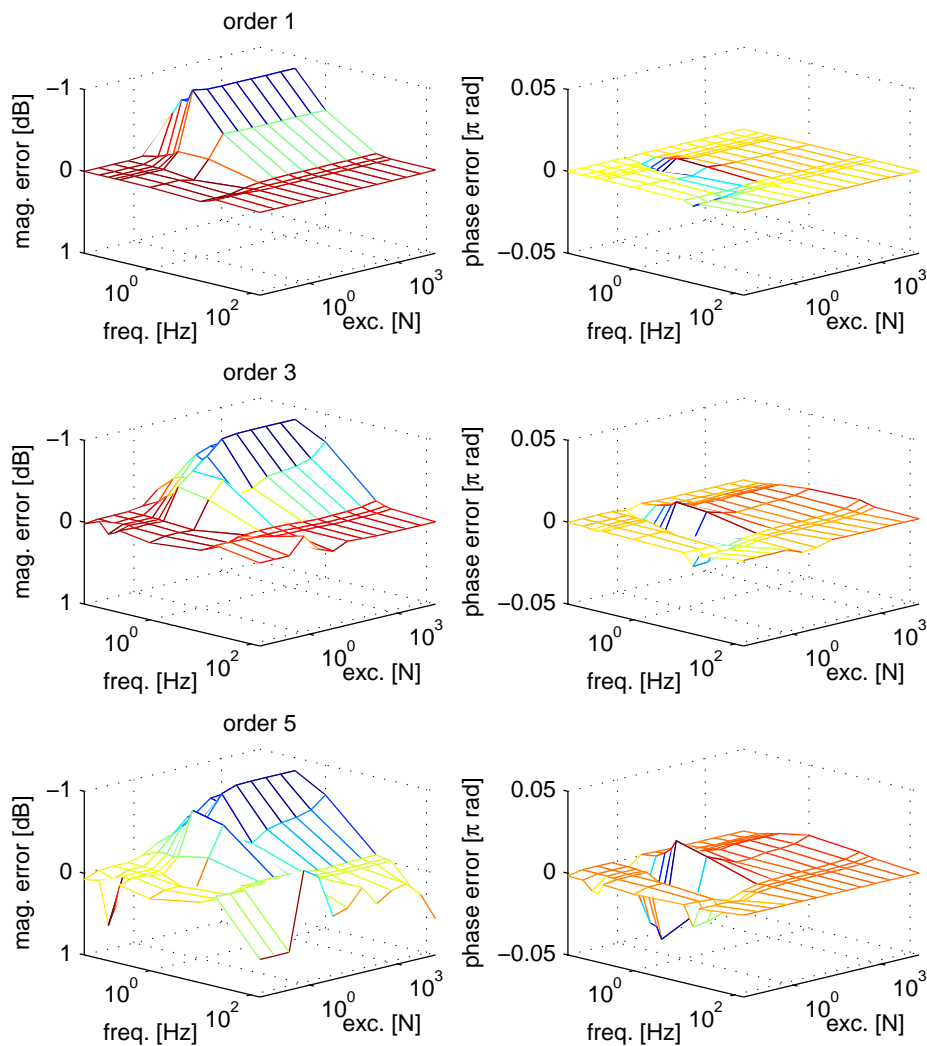
Figure 7.11 / Magnitude and phase errors in odd order HOSIDF measured under closed loop conditions with additional repetitive control suppressing harmonics in the input signal.

The similarities between both rows indicate that the small remaining errors depicted in Fig. 7.11 can be explained by non-perfect suppression of the harmonic components in the input signal $u(t)$ to the plant. No further research is done into the relation between the amount of harmonic suppression and the simulation parameters like step size, type of solver and sampling frequency in the repetitive loop. The results show that the HOSIDF of a non-linear plant in a closed loop system can be determined reliably if the harmonic components in the excitation signal are sufficiently suppressed using repetitive control.
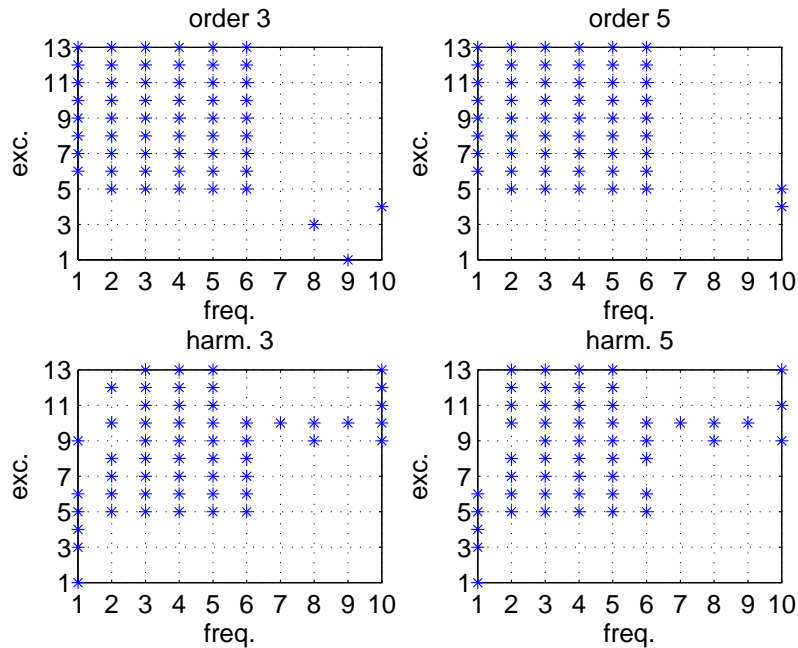
Figure 7.12 / Amplitude/frequency grid point with a HOSIDF magnitude error larger than $-0.1dB$ (upper row) and grid points with harmonic excitation signal components more than $90dB$ above noise level (lower row).

7.3 Discussion

Measuring HOSIDF in a closed loop situation is prone to large errors if the influence of the existence of higher harmonic components in the input signal to the plant is ignored. Applying the proposed compensation method based upon purely linear assumptions reduces the errors significantly. The main drawback of this compensation method is the requirement to do additional measurements at multiples of the frequency of interest, thereby increasing the throughput time of the measurement session. The alternative, being repetitive control, proves to be a viable technique to suppress the harmonic components in the excitation signal. Since this technique influences the stability of the control loop, a learning filter must be incorporated. Also for this solution additional measurements are required since the characteristics of the learning filter are derived from the first order SIDF which can be biased. From a theoretical point of view, the repetitive control technique may be the preferred one because it does right to the assumption of sinusoidal excitation. In practice however, designing the learning filter, implementing the repetitive loop and effectively suppressing the harmonic energy in the input signal to the system may prove difficult.

Applicability in machine condition monitoring

Abstract / Small changes in the friction behavior of a mechanical system are clearly visible in its HOSIDF. This fact can be exploited in the application of HOSIDF in machine condition monitoring.

In many machines, changes in dynamic behavior over time are indicative for wear. Detecting these changes is a prerequisite for efficient preventive maintenance. Both linear (Zattoni, 2005) and nonlinear techniques (Wong and Barhorst, 2006; Neto et al., 2006) are used for detection. Since the HOSIDF reveal valuable additional information about non-linear behavior, monitoring HOSIDF can generate additional information about the wear status of a machine. As presented in Chapter 7, measuring the HOSIDF of a real machine is viable, also when operating in feedback. The required sinusoidal test signals are well defined and have a low crest factor which make them suitable for testing sensitive systems. The increasing flexibility of digital controllers allow repetitive controllers to be implemented as add on devices. Combined with additional self-diagnosis software, the machine can be programmed to compare its actual HOSIDF data with the data from its virgin state. For the comparison to be reliable, the test conditions should be close to the reference situation, both with respect to the operating point chosen and with respect to the average external disturbances acting on the machine. Establishing the allowable tolerances on operating conditions might prove difficult in practice. To demonstrate an application in machine condition monitoring, consider the system presented in Section 7.2. In the stick phase, the system behavior is dominated by its friction induced (hysteretic) spring stiffness and its mass. In the simulation, the total spring stiffness $\sum k_i = 9e4N/m$, (Appendix 11.3). With a mass of $10kg$ this yields a friction induced resonance frequency f_{res} of $15Hz$. In Fig. 8.1, the HOSIDF are shown for an excitation amplitude of $0.2N$. The first order SIDF clearly reflects the dynamics of a second or-
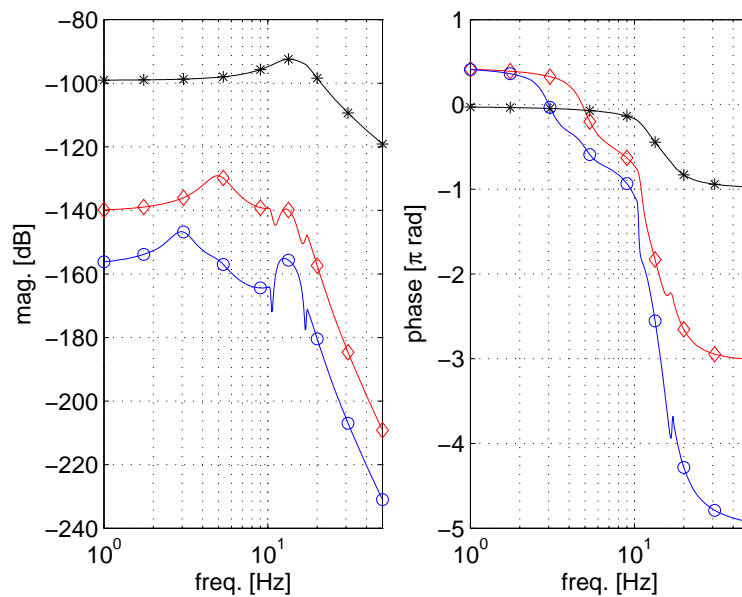
Figure 8.1 / Magnitude (left) and phase (right) of HOSIDF 1($*$), 3($\diamond$) and 5($\circ$), for a total friction induced stiffness of 9e4N/m in the stick phase.

der system with a resonance frequency of $15Hz$. The HOSIDF of order three and five indicate non-linear system behavior. The maxima in their magnitude plots are located at $f_{res}/3$ and $f_{res}/5$ respectively. Their phase plots show steep gradients around $15Hz$. These HOSIDF serve as the reference situation in a comparison simulation. In subsequent simulations, the spring stiffnesses k_i are multiplied with 0.99 and 1.01. Fig. 8.2 shows the HOSIDF relative to the HOSIDF of the reference system for k_i multiplied with 0.99 and 1.01 respectively. Differences between the corresponding HOSIDF indicate changes in the behavior of the system. The magnitude and phase differences of the first order SIDF are only small which makes it difficult to detect the small changes in system behavior from these data. The differences clearly increase as the order of the SIDF increases. The differences for the fifth order are approximately 20 times larger than the corresponding data for the first order, which makes them much easier to detect.
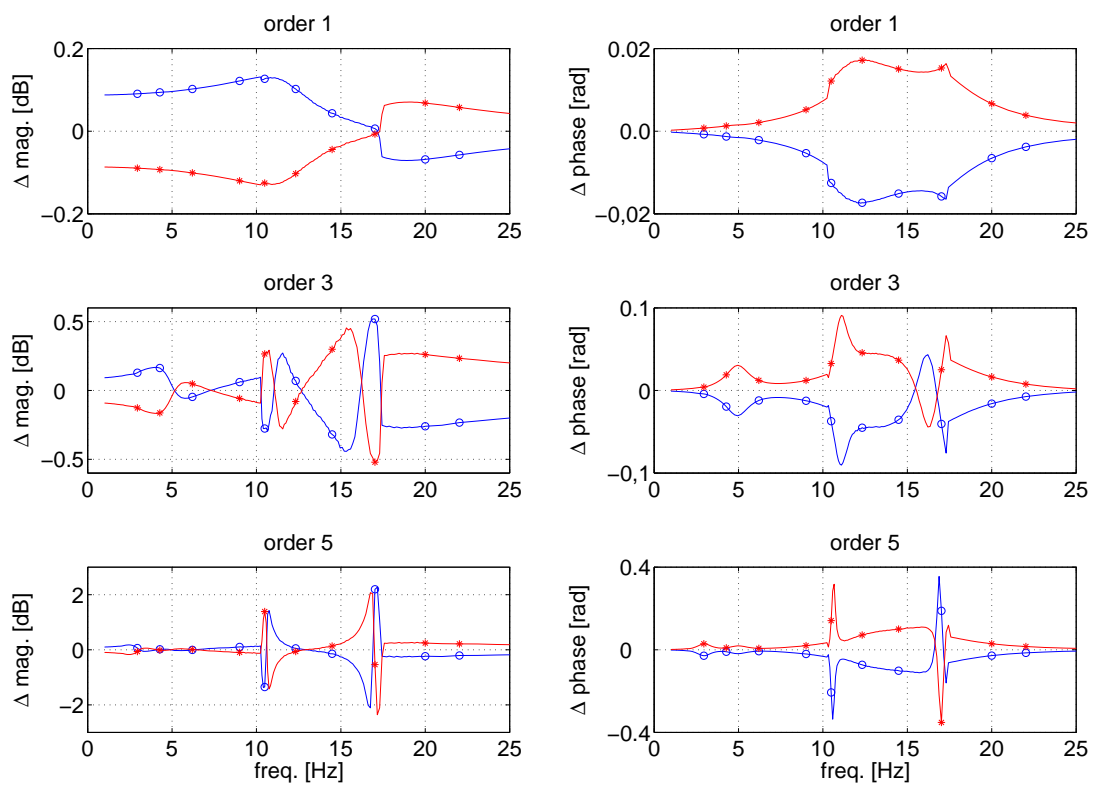
Figure 8.2 / HOSIDF of a system with friction induced stiffnesses $0.99k_i(\circ)$ and $1.01k_i(\star)$ relative to the HOSIDF of the reference system with k_i.

Higher Order Sinusoidal Output Describing Functions

Abstract / In Chapter 2 the Virtual Harmonics Expander was defined as a concept to extend the Sinusoidal Input Describing Function to the Higher Order Sinusoidal Input Functions (HOSIDF). The dual of this concept is presented as the Virtual Harmonics Compressor. Analogous to the definition of the HOSIDF, its dual is defined as the Higher Order Sinusoidal Output Describing Functions (HOSODF). For the identification of the HOSODF of a system it is necessary to control the state of that system to generate a sinusoidal output as a response to a harmonic excitation. A feedback loop is presented incorporating a repetitive controller able to force a sinusoidal output from that system.

In Chapter 2, the HOSIDF concept was presented for the class of causal, stable, time-invariant, non-linear systems with a harmonic response to a sinusoidal excitation. The HOSIDF relate the magnitude and phase of individual harmonics in the output signal to the sinusoidal input signal causing this harmonic response. Without further proof of existence, let us presume a stable, time-invariant non-linear system which has a sinusoidal response to a specific harmonic excitation. From these excitation and response signals higher order describing functions can be calculated. These higher order describing functions differ from the higher order sinusoidal input describing functions in the sense that they are based on a sinusoidal output situation. Subsequently these describing functions will be referred to as Higher Order Sinusoidal Output Describing Functions (HOSODF). In this chapter the concept of the HOSODF will be presented. The sequel of this chapter will have great similarity with Chapter 2 because the HOSODF can be considered the dual of the HOSIDF. To derive this duality in a consistent way, a Virtual Harmonics Compressor (VHC) is defined as the dual of the Virtual Harmonics Expander.

9.1 Definition of the class of systems under consideration

Not all systems belonging to class I will belong to the class we are aiming at. As an example one can think of a system with output saturation. To define the class of systems we will discuss, a new class definition is given.

Definition 2. (Class of non-linear systems under consideration): The class O of causal, stable, time invariant non-linear systems which have a sinusoidal response to a harmonic excitation.

When we mention non-linear systems in the sequel of this thesis, we assume these systems to belong to O, unless mentioned otherwise.

9.2 Virtual Harmonics Compressor

In this chapter we will consider the class O of systems which outputs have a sinusoidal response to a harmonic excitation. Consider a stable, non-linear time invariant system belonging to class O as defined in Def. 2. Let $y(t) = \hat{a}cos(\omega_0 + \varphi_0)$ be the output signal. The system excitation $u(t)$ is considered to consist exclusively of harmonics of the fundamental frequency ω_0 of the output signal $y(t)$, i.e. we assume that the transient behavior has vanished. The input signal $u(t)$ can be written as a summation of harmonics of the output signal $y(t)$, each with an amplitude and phase, which depend on the amplitude $\hat{a}$, phase φ_0 and frequency ω_0 of the output signal (Fig. 9.1). This system can be modeled

$$u(t) = \sum_{n=0}^{\infty} A_n(\hat{a},\omega)\cos(n\omega t + \varphi_n(\hat{a},\omega)) \quad\boxed{\begin{array}{c}\text{Non-linear}\\ \text{system}\end{array}}\quad y(t) = \hat{a}\cos(\omega t + \varphi)$$
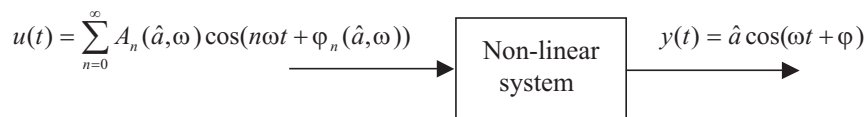
Figure 9.1 / General sinusoidal output-input relation.

as a cascade of a (non)linear system and a harmonics compressor (Fig. 9.2). The Virtual Harmonics Compressor is defined as a non-linear component which transforms a harmonic input signal $\breve{y}(t)$ into a sinusoidal output signal $y(t)$ with frequency ω, amplitude $\hat{a}$ and phase φ, (Eq. 9.1). This input signal $\breve{y}(t)$ consists of an infinite amount of harmonics of the output signal $y(t)$ with frequency $n\omega$, amplitude $\hat{a}$ and phase $n\varphi$ with $n \in \mathbb{N}$:

$$y(t) = \hat{a}\cos(\omega t + \varphi) \tag{9.1}$$

$$\breve{y}(t) = \sum_{n=0}^{\infty} \hat{a}\cos(n(\omega t + \varphi)) \tag{9.2}$$

$$u(t) = \sum_{n=0}^{\infty} A_n(\hat{a},\omega)\cos(n\omega t + \varphi_n(\hat{a},\omega))$$

Non-linear system

$$y(t) = \hat{a}\cos(\omega t + \varphi)$$

$u(t)$

$$\sum_{n=0}^{\infty} A_n(\hat{a},\omega)\cos(n\omega t + \varphi_n(\hat{a},\omega))$$

(Non)linear system

$$\breve{y}(t)$$

$$\sum_{n=0}^{\infty} \hat{a}\cos(n(\omega t + \varphi))$$

Virtual harmonics compressor

$y(t)$

$$\hat{a}\cos(\omega t + \varphi)$$
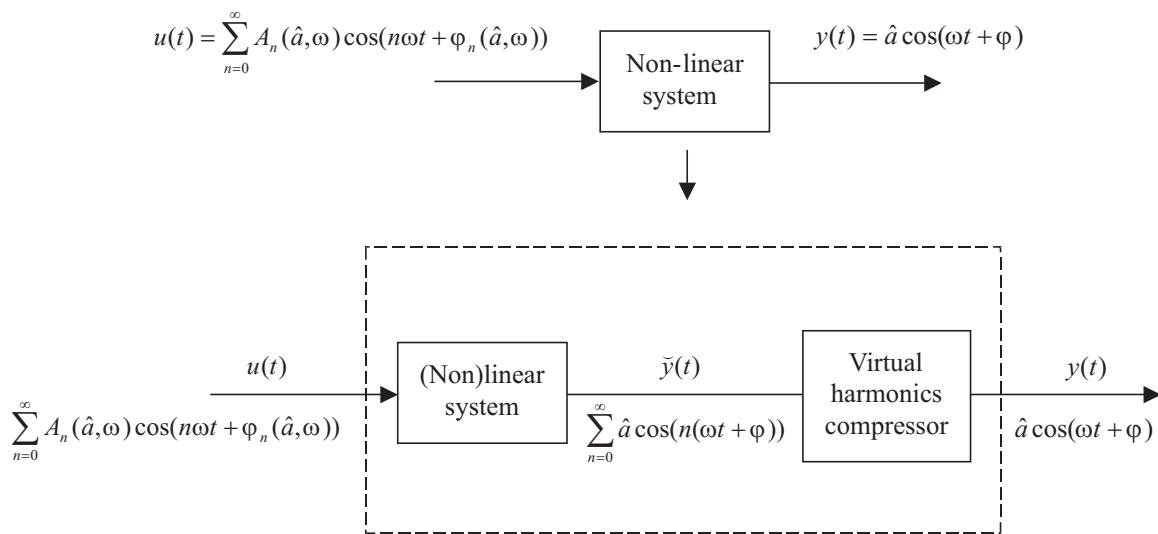
Figure 9.2 / Virtual Harmonics Compressor as separate block in the model of a non-linear system with sinusoidal response.

By defining a separate block for the compression of harmonics in modeling this class of non-linear systems, the complexity of the preceding (non)linear block will be significantly less and linear approaches may become feasible depending upon the remaining non-linear behavior. The resulting model structure has strong similarities with a Wiener model. This structure however is not a Wiener model since the first block is not necessarily linear (Narendra and Gallman, 1966).

9.3 Higher Order Sinusoidal Output Describing Functions

Consider a non-linear system belonging to class **O** as defined in Definition 9.1 with $u(t)$ the input signal and $y(t)$ the system response after the transient behavior has vanished (Fig. 9.1). The sinusoidal output describing function $R(\hat{a}, \omega)$ of the system is defined as the complex ratio of the output sinusoid $y(t)$ and the fundamental component of the system excitation $\tilde{u}(t)$ (Fig. 9.3).

$$\tilde{u}(t) = A_1(\hat{a},\omega)\cos(\omega t + \varphi + \varphi_1(\hat{a},\omega))$$

$$R(\hat{a},\omega)$$

$$y(t) = \hat{a}\cos(\omega t + \varphi)$$
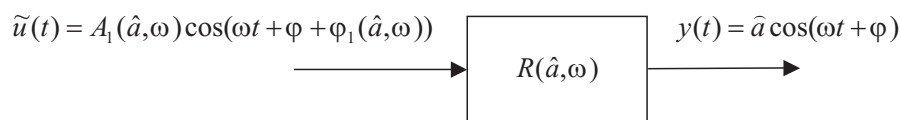
Figure 9.3 / Sinusoidal output describing function representation.

The sinusoidal output describing function $R(\hat{a}, \omega)$ can be calculated as:

$$R(\hat{a}, \omega) = \frac{\hat{a}e^{j\omega t + \varphi}}{A_1(\hat{a}, \omega)e^{j(\omega t + \varphi + \varphi_1(\hat{a}, \omega))}} = \frac{\hat{a}}{b_1(\hat{a}, \omega) + ja_1(\hat{a}, \omega)} \tag{9.3}$$

The Fourier coefficients a_1 and b_1 are calculated as in Eq.9.4, 9.5 with $T = 2\pi/\omega$:

$$a_1 = \frac{2}{T} \int_{t_0}^{t_0+T} \tilde{u}(t) \cos(\omega t) dt \tag{9.4}$$

$$b_1 = \frac{2}{T} \int_{t_0}^{t_0+T} \tilde{u}(t) \sin(\omega t) dt \tag{9.5}$$

In Fig. 9.4 the block representation of the non-linear system with sinusoidal response is redrawn by separating the Virtual Harmonics Compressor from the system. The remaining system can be represented as a parallel connection of subsystems, each relating a harmonic component of the non-linear system input to the corresponding harmonic component of the Virtual Harmonics Compressor. The subsystem $R_1(\hat{a}, \omega)$ is the sinusoidal

Figure 9.4 / Higher order sinusoidal output describing function representation.

output describing function of the system. This describing function can be interpreted as the first element of a set of higher order sinusoidal output describing functions $R_n(\hat{a}, \omega)$.

These functions can be defined as the complex ratio of the virtual k^{th} harmonic signal derived from the response signal to the kth harmonic component in the input signal. This virtual harmonic has equal amplitude as the fundamental sinusoid but its starting-phase is n times the starting phase of the response signal. Like the first order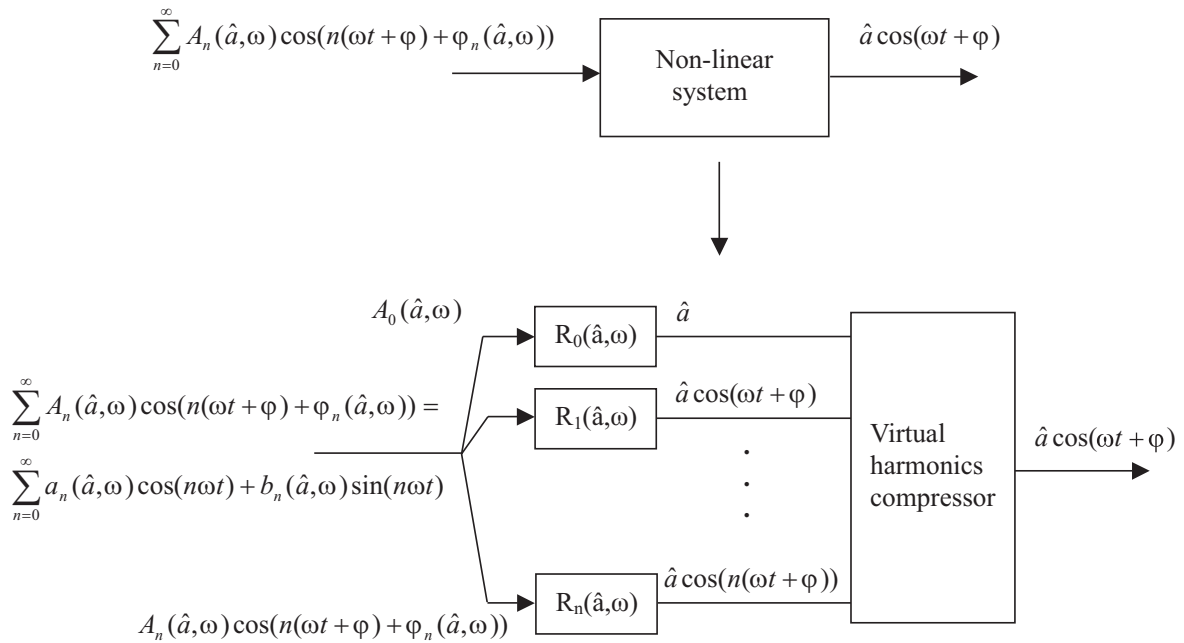 sinusoidal output describing function (Eq. 9.3), the higher order sinusoidal output describing functions are calculated from the corresponding Fourier coefficients (Eq. 9.6).

$$
\begin{aligned}
R_k(\hat{a}, \omega) &= \frac{\hat{a}e^{jk(\omega t + \varphi)}}{A_k(\hat{a}, \omega)e^{j(k(\omega t + \varphi) + \varphi_k(\hat{a}, \omega))}} \\
&= \frac{\hat{a}}{A_k(\hat{a}, \omega)e^{j(\varphi_k(\hat{a}, \omega))}} = \frac{\hat{a}}{b_k(\hat{a}, \omega) + ja_k(\hat{a}, \omega)}
\end{aligned}
\tag{9.6}
$$

$R_k(\hat{a}, \omega)$ can be interpreted as a descriptor of the individual harmonic distortion components at the input of a time invariant non-linear system required for the system to generate a sinusoidal response, as function of the amplitude and frequency of that sinusoidal response. The functions $R_k(\hat{a}, \omega)$ will be referred to as the Higher Order Sinusoidal Output Describing Functions (HOSODF).

9.4 Non-parametric identification of HOSODF

The HOSODF describe the system behavior of a non-linear system with a sinusoidal output due to harmonic excitation. Identification of HOSODF requires control of the sinusoidal output of the system within its domain of possible sinusoidal output signals. This specific state of the non-linear system can be reached by incorporating the system under test in a feedback loop and defining the desired sinusoidal output as the control objective of a dedicated controller. As in Section 7.1.2 we can make use of the concept of repetitive control. The positive feedback in the memory loop generates infinite gain at the harmonics of the operating frequency. The time period of this operating frequency is equal to the total internal delay in the memory loop. By incorporating the memory loop in the feedback system, the signal at the input of the memory loop will be free of the harmonics of its operating frequency. This property is used to suppress the harmonics of the excitation signal at the input of the non-linear system H (Fig. 7.3). In Fig. 9.5 the control loop is rearranged by positioning the repetitive controller at the output of the non-linear system H. Again in this configuration the input signal $e(t)$ to the repetitive controller block M will be free of harmonics of the operating frequency of the memory loop. If the excitation signal $p(t)$ is chosen a sinusoid with a frequency equal to the operating frequency of the memory loop, the output signal $e(t)$ of the summing node will be zero for this frequency and all its harmonics since the loop gain will be infinite at these frequencies. As a result of this, the output $y(t)$ of the non-linear system must be equal to the excitation signal $p(t)$. The stability considerations presented in Section 7.1.2

$$u(t) = \sum_{n=0}^{\infty} R_n \cos(n\omega_0 t + \vartheta_n) \qquad\qquad p(t) = \hat{a} \cos(\omega_0 t + \varphi_0)$$
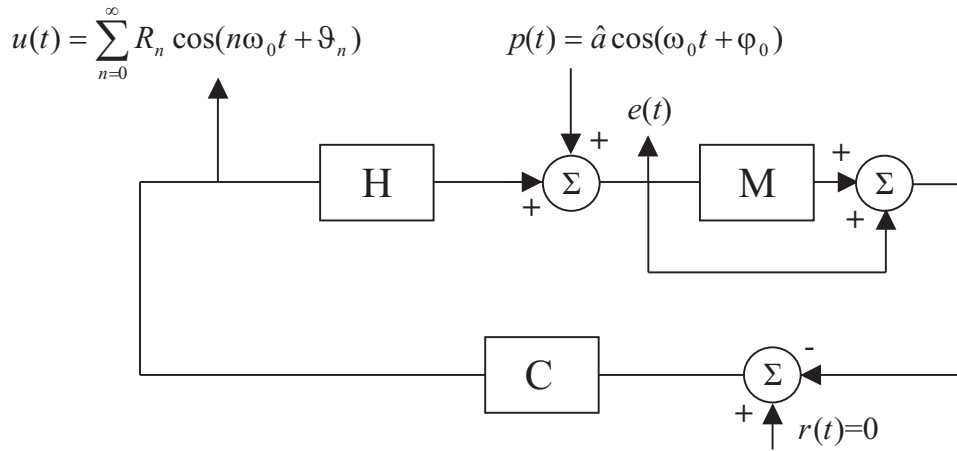
Figure 9.5 / Layout of the feedback system for the identification of HOSODF.

also hold for this arrangement of feedback system. This means that Eq. 7.9-7.14 also apply. From these equations the required learning filter can be designed.

9.5 Discussion

From Sections 2.2 and 9.2 it is evident that the Virtual Harmonics Expander and the Virtual Harmonics Compressor are duals. This is also the case for the HOSIDF and HOSODF. It is however not evident that a system belonging to class *I* automatically belongs to class *O*. In other words, it is not true that every system belonging to *I* can be controlled, even theoretically, in such a way that the conditions required for measuring the HOSODF can be achieved. This subject has interesting parallels with the mathematics behind the representation of non-linear systems with Volterra functional series (Brockett, 1976; Lesiak and Krener, 1978; Sandberg, 1982, 1983a,b) or the approximation with (truncated) Volterra series (Rugh, 1981; Boyd and Chua, 1985; Sandberg, 1985, 1992). In this thesis this subject is not further explored.

The method of using repetitive control for the nonparametric identification of HOSODF as proposed in Section 9.4 possibly has an interesting mechanical application. In particular mechanical testing situations, like normal mode testing (Gabri and Matthews, 1980), a sinusoidal excitation force is required. Conventional sine testing instrumentation employs linear feedback techniques to compensate for the influence of the linear dynamics of the system under test on the shake system. The actual shaker force signal is fed back to a controller which is implemented as a linearized, inverse model of the system under test. This allows the magnitude of the required excitation frequency component to be controlled. However, the true system under test is non-linear, and its non-linear mechanical

impedance will force the sinusoidal excitation signal to become harmonic. By employing the HOSODF approach, a data-based inverse representation of the non-linear system H is incorporated in the control loop. If the shaker force is considered the output $y(t)$ of a non-linear system H (Fig. 9.5), implementing the repetitive control loop M will result in a sinusoidal output of the shaker if the non-linear system H belongs to class $\boldsymbol{O}$. The data-based inverse representation will not be perfect due to the finite repetitive control gain and finite sampling frequency. So the suppression of harmonics will be limited and the required output condition will always be approximated. But the harmonic content of the excitation force signal will be considerably lower than in the situation with linear control.

Conclusions and recommendations

10.1 Conclusions

In this thesis we presented a new approach towards the analysis of non-linear systems. The relevance of this new approach is motivated by the increase in positioning accuracy requirements in motion systems in industry, the need for advanced analysis techniques in non-linear control system design and the absence of suitable frequency domain based measurement techniques for non-linear system behavior. The class of systems for which this new technique applies, consists of causal, stable, time-invariant, non-linear systems which respond in a harmonic way to a sinusoidal excitation. The approach is frequency domain based and differs from the existing frequency based techniques in the sense that it is not a linearisation nor that it requires the system response to be analytic. This new technique is a generalization of the well established Sinusoidal Input Describing Function concept towards higher orders. The resulting framework is referred to as *Higher Order Sinusoidal Input Describing Functions* (HOSIDF). A theoretical basis for the HOSIDF was established. Hereto the concept of the *Virtual Harmonics Expander* (VHE) was presented. This non-linear function describes the transformation of a single sinusoid into an infinite amount of harmonics ($0Hz$ included), each with equal amplitude as the input signal and a phase equal to the phase of the input signal times the harmonic number. We showed that a non-linear system belonging to the class we defined can be modeled as a parallel connection of an infinite amount of weakly non-linear subsystems in series with the VHE. The functions describing the weakly non-linear input/output relations of these subsystems are the HOSIDF with the classical Sinusoidal Input Describing Function being the first order. Two non-parametric measurement techniques were presented able to determine the HOSIDF. The first technique is FFT based and relates the phase and magnitude of the individual harmonic components in the output of the system to its si-

nusoidal excitation signal. The second technique is based on digital filtering and utilizes IQ (in-phase/quadrature-phase) demodulation to determine the phase and magnitude of both the excitation signal and the harmonics in the system response. We showed through analysis and a verification experiment that by proper selection of the FFT parameters like block length, sample frequency and applied weighting function, the FFT method has ideal selectivity and dynamic range. This in contrast with the IQ method, which is hampered by limited selectivity and dynamic range due to the non-ideal characteristics of the lowpass filters. By neglecting the influence of intermodulation and desensitization an algorithm was derived to reduce the bias in the estimated HOSIDF caused by harmonic excitation which results from non-constant amplitude-time profiles. With a real experiment we proved the practical applicability of the method by showing that the transition from stick phase to sliding phase in a mechanical system can be detected unambiguously with the third order SIDF. Additionally we demonstrated that combining the information about the friction induced resonance frequency from the first order SIDF and the presliding displacement determined from the third order SIDF yields the breakaway force in a friction contact without the need of a separate force measurement. We expanded the applicability of the HOSIDF technique towards the analysis of plants operating in feedback. For this purpose two solutions were presented for dealing with the feedback of harmonic energy to the input of the controlled plant. The first technique employs a numerical compensation algorithm which calculates a first order compensation of the influence of harmonic energy. In this technique, the effects of intermodulation and desensitization on the HOSIDF estimates is neglected. The second technique effectively suppresses the feedback of harmonic energy by applying a modified repetitive controller to the feedback loop. The effectiveness of both techniques was proven in a realistic simulation experiment. We showed that HOSIDF are very sensitive to changes in the friction characteristics of a mechanical system and as such might serve as an indication of changes in the friction condition of a mechanical system caused by wear. This fact offers new opportunities in the field of machine condition monitoring. Finally we presented the dual of the HOSIDF defined as the *Higher Order Sinusoidal Output Describing Functions* (HOSODF) for the class of causal, stable, time-invariant non-linear systems with a harmonic input which results in a sinusoidal response. HOSODF describe the relations between a sinusoidal system output signal and its cause, a specific harmonic excitation signal. The theoretical foundation of the HOSODF was presented, based on the dual of the VHE, the so called *Virtual Harmonics Compressor* (VHC). Non-parametric identification of HOSODF requires a sinusoidal output of the non-linear system under evaluation. We presented a modified repetitive control scheme for controlling the sinusoidal output state of a non-linear system belonging to that class.

At the end of this thesis we conclude that our approach to use HOSIDF for the analysis of non-linear system behavior has resulted in a new and powerful measurement and identification technique. This technique enables the detection and display of very interesting

non-linear phenomena from well controllable experiments without the need for model assumptions. Moreover, this new technique reveals the information in a format which relates to the background of the professional user in industry.

10.2 Recommendations for future research

In this thesis some key aspects of the new HOSIDF approach have been presented. Evidently, the tools presented are so powerful that it is worth while exploring a number of additional aspects. These aspects are related to fundamental issues of non-linear system identification and non-linear synthesis techniques, technical issues of measurement technology and issues related to the practical applications of HOSIDF.

- A subject of further research should be to establish theories which describe the conditions under which HOSIDF uniquely describe the dynamic behavior of a specific class of non-linear systems.

- Non-linear systems with fading memory can be described with Generalized Frequency Response Functions (GFRFs). Additional investigations are necessary to determine under which condition the intermodulation and desensitization behavior of these systems, as described by the GFRFs, can be estimated from the HOSIDF results.

- Since an analytic response function is not required for a non-linear system to belong to the class of systems which can be described by HOSIDF, systems with bifurcations can belong to this class. A comparison should be made between the system information generated with well established techniques like bifurcation diagrams and Pointcaré sections and the system information derived from the HOSIDF.

- The concept of the HOSODF offers many opportunities for additional research. To identify whether a non-linear system belongs to a class of systems which can be described by HOSODF, selection criteria with regard to system dynamics should be established. Also, the interrelation between reciprocity as a system aspect and Volterra functional series as system description should be investigated.

- Present day synthesis techniques for controllers are based upon linear techniques. Research should establish whether HOSIDF, as extensions of these linear techniques, offer starting points for additional synthesis techniques for non-linear controllers based upon non-linear philosophies.

- The IQ method can be easily implemented in field-programmable gate arrays. This offers interesting opportunities for very cheap measurement equipment for real-time, on-line identification of HOSIDF. However the selectivity, dynamic range and

settling time of the IQ method is dominated by the low-pass filter characteristics. Additions research is required to optimize the trade-off between these aspects and the overall real-time performance.

- Alternative amplitude-time relations may have hidden potential with respect to the relation between harmonic content, susceptibility to noise and overall measuring time. This research has to be combined with further research into the characteristics of the FFT and IQ method with respect to noise.

- It was demonstrated that the HOSIDF are able to reveal very small changes in friction characteristics. Likewise, minute changes in the stiffness characteristics of a system will be detectable using HOSIDF, especially changes in the symmetry of the stiffness characteristic of a mechanical system. Research is required to determine the benefits of the HOSIDF technique in machine condition monitoring, for example for the purpose of crack detection.

CHAPTER ELEVEN

Appendix

11.1 Fourier coefficients of backlash

The Fourier coefficients for backlash as derived in Section 4.1 are presented in Table 11.1.

Table 11.1 / Fourier coefficients of harmonic response of backlash

n	a_n
1	C_a
3	$C_a\{-\frac{8}{3}\beta^2 + \frac{8}{3}\beta - \frac{1}{3}\}$
5	$C_a\{\frac{256}{15}\beta^4 - \frac{256}{15}\beta^3 + \frac{328}{15}\beta^2 - \frac{24}{5}\beta + \frac{1}{5}\}$
7	$C_a\{-\frac{1024}{7}\beta^6 + \frac{3072}{7}\beta^5 - \frac{10496}{21}\beta^4 + \frac{5632}{21}\beta^3 - \frac{1424}{21}\beta^2 + \frac{48}{7}\beta - \frac{1}{7}\}$

n	b_n
1	$\frac{A}{k\pi}\{\frac{\pi}{2} + \arcsin(1 - 2\beta) + 2(1 - 2\beta)\sqrt{\beta(1-\beta)}\}$
3	C_b
5	$C_b\{-\frac{32}{5}\beta^2 + \frac{32}{5}\beta - 1\}$
7	$C_b\{\frac{384}{7}\beta^4 - \frac{768}{7}\beta^3 + \frac{496}{7}\beta^2 - 16\beta + 1\}$

99

with

$$a_n = \frac{2}{T} \int\limits_{t_0}^{t_0+T} y(t)\cos(n\omega t)dt \qquad\qquad (11.1)$$

$$b_n = \frac{2}{T} \int\limits_{t_0}^{t_0+T} y(t)\sin(n\omega t)dt \qquad\qquad (11.2)$$

$$\beta = \frac{b}{A} \qquad\qquad (11.3)$$

$$C_a = \frac{4A}{\pi k}\beta(\beta-1) \qquad\qquad (11.4)$$

$$C_b = \frac{4}{3}C_a(2\beta-1)\sqrt{\beta(1-\beta)} \qquad\qquad (11.5)$$

11.2 Stick to sliding measurement setup

The applied linear bearings are Schneeberger type 2045. This type of bearing consists of two V-shaped runways which are separated by cylindrical rolling elements. The axes of rotation of two neighboring elements are mutually perpendicular. The rolling elements are separated by a cage. Although kinematically over-constrained, this setup assures low rolling friction and high stiffness. The bearings are lubricated with Molykote, a lubricant containing Molybdenum Disulfide (MoS_2). The sliding table is the mounting base of a friction finger which adds dry friction to the system. This finger is a beryllium bronze cantilever and slides over a very smooth surface ($R_a \leq 25nm$) made of silicon carbide which is mounted to the fixed world. The friction finger is pre-loaded in z-direction due to its own stiffness. The system is excited with an electro-magnetic shaker type LDS 201 coupled through a stinger. The driving force is measured with a piezo sensor type B&K8200. The acceleration of the sliding table is measured with a piezo accelerometer type B&K4326. Both charge signals are conditioned with charge amplifiers type B&K2626. The current through the shaker is measured with a current transducer type LA25-NP. All three signals are sampled synchronously with a dynamic signal analyzer type SigLab2024. Its signal generator is used to excite the shaker through a linear voltage to current converter with adequate dynamic range.

11.3 Modified Leuven friction model

The Modified Leuven friction model (Lampaert et al., 2002) is an extension of the Leuven friction model (Swevers et al., 2000). The model accurately describes the Stribeck effect, hysteretic behavior in the stick phase, friction lag, a varying break-away force and stick-slip behavior. The model consists of two equations. The first equation describes the friction force:

$$F_f = F_h(z) + \sigma_1 \frac{dz}{dt} + \sigma_2 v \tag{11.6}$$

with F_h the part of the friction force with hysteretic behavior, σ_1 the micro-viscous damping coefficient, σ_2 the viscous damping coefficient and v the relative velocity between the friction surfaces. The second equation is a non-linear state equation that describes the state variable z which can be interpreted as the average deflection of the asperities between the contact surfaces:

$$\frac{dz}{dt} = v \left(1 - sgn\left(\frac{F_h(z)}{s(v)}\right) \left|\frac{F_h(z)}{s(v)}\right|^n \right) \tag{11.7}$$

The function $s(v)$ models the constant velocity behavior in the sliding phase near zero velocity. In this velocity range, the Stribeck effect becomes noticeable and can be modeled by choosing:

$$s(v) = sgn(v)(F_c + (F_s - F_c)e^{-\left(\frac{v}{v_s}\right)^\delta}) \tag{11.8}$$

For small velocities $s(v)$ is equal to the static friction F_s, for large velocities $s(v)$ is equal to F_c, the Coulomb friction. The Stribeck velocity v_s and the parameter δ determine the transition between F_s and F_c. The hysteretic force $F_h(z)$ is modeled using the Maxwell Slip model, resulting in a piecewise approximation of the hysteresis function. The Maxwell Slip model consists of N mass-less elastoslide elements in parallel, all linked to a common displacement input z (Fig. 11.1). Element i has a linear spring-stiffness k_i, and starts to slide when its maximum spring force W_i is reached (Fig. 11.2). The position of each element is described by the state variable ζ_i . Because the elastoslide elements are mass-less, there is a static relation between the individual forces generated by the elements and their displacement relative to the input displacement z. This relation can be described by:

$$
\begin{aligned}
\text{if } |z - \zeta_i| < \tfrac{W_i}{k_i} \quad &\text{then} \quad
\begin{cases}
F_i = k_i(z - \zeta_i) \\
\zeta_i = \text{const.}
\end{cases} \quad &\text{(stick)} \\
\text{if } |z - \zeta_i| \geq \tfrac{W_i}{k_i} \quad &\text{then} \quad
\begin{cases}
F_i = \text{sgn}(z - \zeta_i)W_i \\
\zeta_i = z - \text{sgn}(z - \zeta_i)\tfrac{W_i}{k_i}.
\end{cases} \quad &\text{(slip)}
\end{aligned}
\tag{11.9}
$$

In the initial state all values of ζ_i are equal to z_i, the system is in the stick phase and the actual stiffness is the sum of all individual stiffnesses $\sum k_i$. When increasing z, at the

moment a force generated by one of the element exceeds the accompanying saturation value W_i, this element slips, its position ζ_i changes and the total stiffness decreases with the amount k_i. Eventually all elements will slide and the maximum hysteresis force W_i is reached. The total hysteresis force is:

$$F_h = \sum_{i=1}^{n} F_i = \sum_{i=1}^{n}(z - \zeta_i)k_i \leq \sum_{i=1}^{n}(W_i) \qquad (\text{11.10})$$
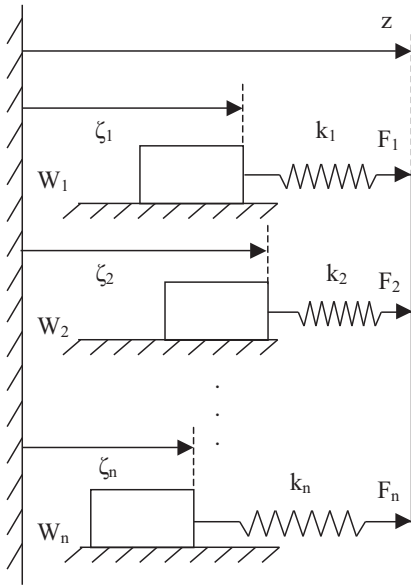
Figure 11.1 / Maxwell Slip Model for N elements
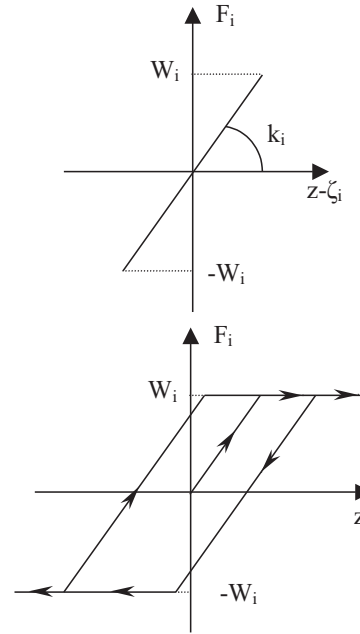
Figure 11.2 / The characteristics of an elastoslide element

The parameters of the modified Leuven model used in the simulations are:

W_i	=	[0.35 0.25 0.15 0.15 0.1]	[N]
k_i	=	[10000 10000 20000 40000 10000]	[N/m]
n	=	1	[-]
F_c	=	1	[N]
F_s	=	2	[N]
v_s	=	0.007	[m/s]
δ	=	0.5	[-]
σ_1	=	$sqrt(10e5)$	[Ns/m]
σ_2	=	1	[Ns/m]

With these parameters the model describes an odd system with symmetric friction characteristics in both directions.

Bibliography

ADAMS, D.E. and ALLEMANG, R.J. (1998). Survey of Non-linear Detection and Identifications Techniques for Experimental Vibrations. In *Proceeding of ISMA23*, 269–281.

AL-BENDER, F. and SYMENS, W. (2005a). Dynamic characterization of hysteresis elements in mechanical systems. I. Theoretical analysis. *Chaos*, **15**(1), 13105–1–11.

AL-BENDER, F. and SYMENS, W. (2005b). Dynamic characterization of hysteresis elements in mechanical systems. II. Experimental validation. *Chaos*, **15**(1), 13106–1–9.

AN, C.H., ATKESON, C.G., and HOLLERBACH, J. M. (1988). *Model-based control of a robot manipulator*. The MIT Press, Cambridge, Massachusetts.

ARMSTRONG, B. and AMIN, B. (1996). PID control in the presence of static friction: a comparison of algebraic and describing function analysis. *Automatica*, **32**(5), 679–692.

ARMSTRONG-HÉLOUVRY, B., DUPONT, P., and DE WIT, C. CANUDAS (1994). A survey of Models, Analysis Tools and Compensation Methods for the Control of Machines with Friction. *Automatica*, **30**(7), 1083–1138.

ATHERTON, D. (1975). *Non-linear control engineering*. Van Nostrans Reinhold, London.

BEDROSIAN, E. and RICE, S.O. (1971). The output properties of Volterra systems (non-linear systems with memory) driven by harmonic and Gaussian inputs. In *Proceedings IEEE*, **59**, 1688–1707.

BESANÇON-VODA, A. and BLAHA, P. (2002). Describing function approximation of a two-relay system configuration with application to Coulomb friction identification. *Contr. Eng. Pract.*, **10**, 655–668.

BILLINGS, S.A. and TSANG, K.M. (1989a). Spectral analysis for non-linear systems, Part II: interpretation of non-linear frequency response functions. *Mechanical Systems and System Processing*, **3**(4), 341–359.

BILLINGS, S.A. and TSANG, K.M. (1989b). Spectral analysis for non-linear systems, Part1: Parametric non-linear spectral analysis. *Mechanical Systems and Signal Processing*, **3**(4), 319–339.

BILLINGS, S.A. and TSANG, K.M. (1990a). Spectral analysis for non-linear systems, Part III: Case stude examples. *Mechanical Systems and System Processing*, **4**(1), 3–21.

BILLINGS, S.A. and TSANG, K.M. (1990b). Spectral analysis of block structured systems. *Mechanical Systems and Signal Processing*, **4**(2), 117–130.

BOYD, S. and CHUA, L.O. (1985). Fading memory and the problem of approximating non-linear operators with Volterra series. *IEEE Transactions on Circuits and Systems*, **CAS-32**(11), 1150–1161.

BOYD, S., TANG, Y.S., and CHUA, L.O. (1983). Measuring Volterra kernels. *IEEE Transactions Circuits Syst.*, **CAS-30-8**, 571–577.

BROCKETT, R.W. (1976). Volterra series and geometric control theory. *Automatica*, **12**, 167–176.

BUSSGANG, J.J., EHRAN, L., and GRAHAM, J.W. (1974). Analysis of non-linear systems with multiple inputs. *Proceedings of the IEEE*, **62**, 1088–1119.

CHEW, K.K. and TOMIZUKA, M. (1990). Digital control of repetitive errors in disk drive systems. In *Proceedings of the American Control Conference*, 540–548.

CHUA, L. and LIAO, Y. (1989). Measuring Volterra kernels (II). *International J. of Circuit Theory and Applications*, **17**, 151–190.

CHUA, L. and NG, C. (1979). Frequency domain analysis of non-linear systems: general theory. *IEE Journal of Electronic Circuits and Systems*, **3**, 165–185.

DEDENE, N., PINTELON, R., and LATAIRE, P. (2002). Measurement of Multivariable Frequency Response Functions in the Presence of Non-linear Distortions - Some Practical Aspects. *IEEE Transactions on Instrumentation and Measurement*, **51**(4), 577–582.

EVANS, C. and REES, D. (2000a). Non-linear Distortions and Multisine Signals - Part I: Measuring the Best Linear Approximation. *IEEE Transactions on Instrumentation and Measurement*, **49**(3), 602–609.

EVANS, C. and REES, D. (2000b). Non-linear Distortions and Multisine Signals - Part II: Minimizing the Distortion. *IEEE Transactions on Instrumentation and Measurement*, **49**(3), 610–616.

GABRI, B.S. and MATTHEWS, J.T. (1980). Normal mode testing using multiple exciters under digital control. *Journal of the Society of Environmental Engineers*, **19**(1), 25–34.

GELB, A. and VELDE, W.E. VANDER (1968). *Multiple input describing functions and non-linear system design*. McGraw Hill, New York.

GEORGE, D.A. (1959). Continuous non-linear systems. Technical Report 355, MIT Research Laboratory of Electronics, Cambridge, Mass.

GLOTH, G. and GÖGE, D. (2004). Handling of non-linear structural characteristics in ground vibration testing. In *Proceedings of the 2004 International Seminar on Modal Analysis*, Leuven.

GUVENC, L. and SRINIVASAN, K. (1994). Friction compensation and evaluation of a force control application. *Mechanical Systems and Signal Processing*, **8**(6), 623–638.

HARA, S., YAMAMOTO, Y., OMATA, T., and NAKANO, M. (1988). Repetitive control system - a new type servo system. *IEEE Transactions on Automatic Control*, **AC-33**, 659–668.

HENSEN, R. (2002). *Controlled Mechanical Systems with Friction*. PhD. Thesis, Eindhoven University of Technology.

HENSEN, R.H.A. and VAN DE MOLENGRAFT, M.J.G. (2002). Friction Induced Hunting Limit Cycles: An Event Mapping Approach. In *Proc. of the American Control Conference ACC2002*, 2267–2272.

HENSEN, R., VAN DE MOLENGRAFT, M., and STEINBUCH, M. (2002a). Frequency domain identification of dynamic friction model parameters. *IEEE Transactions on Control Systems Techn*, **10**(2), 191–196.

HENSEN, R.H.A., VAN DE MOLENGRAFT, M.J.G., and STEINBUCH, M. (2002b). Friction in Motion Systems: Performance Deterioration for Regulator Tasks. In P. SCHELLEKENS (ed.), *Proc. of the 3rd Euspen*, 167–170, Eindhoven, Netherlands.

HENSEN, R.H.A., VAN DE MOLENGRAFT, M.J.G., and STEINBUCH, M. (2003). Friction induced limit cycling: Hunting. *Automatica*, **39**(12), 2131–2137.

HILLERSTRÖM, G. (1996). Adaptive suppression of vibrations–A repetitive control approach. *IEEE Transactions on Control Systems Technology*, **4**(1), 72–77.

JONES, J.C. PEYTON and BILLINGS, S.A. (1990). Interpretation of non-linear frequency response functions. *International J. Control*, **52**(2), 319–346.

KANG, Y.S. and KIM, K.J. (1997). Friction identification in a sight stabilisation system at low velocities. *Mechanical Systems and Signal Processing*, **11**(3), 491–505.

KIM, M.S. and CHUNG, S.C. (2006). Friction identification of ball-screw driven servomechanisms through the limit cycle analysis. *Mechatronics*, **16**, 131–140.

KOSTIC, D., DE JAGER, A.G., STEINBUCH, M., and HENSEN, R.H.A. (2004). Modeling and Identification for High-performance Robot Control: An RRR-Robotic Arm Case Study. *IEEE Transactions on Control Systems Techn.*, **12**(6), 904–919.

LAMPAERT, V., SWEVERS, J., and AL-BENDER, F. (2002). Modifications of the Leuven Friction Model Structure. *IEEE Transactions on Automatic Control*, **47**(4), 683–687.

Lampaert, V., Al-Bender, F., and Swevers, J. (2004). Experimental characterization of dry friction at low velocities on a developed tribometer setup for macroscopic measurements. *Tribology-Letters*, **16**(1-2), 95–105.

Lee, H.S. and Tomizuka, M. (1996). Robust Motion Controller Design for High-Accuracy Positioning Systems. *IEEE Transactions on Industrial Electronics*, **43**(1), 48–55.

Lesiak, C. and Krener, A.J. (1978). The existence and uniqueness of Volterra series for non-linear systems. *IEEE Transactions on Automatic Control*, **23**(6), 1090–1095.

Lim, D.J. (2003). Describing function of Coulomb friction for the ramp reference input. *IEICE transactions on Fundamentals of Electronics, Communications and computer Sciences*, **E86-A**(5), 1309–1311.

Mihajlovic, N., van Veggel, A.A., van de Wouw, N., and Nijmeijer, H. (2004). Analysis of Friction-Induced Limit Cycling in an Experimental Drill-String Set-Up. *J. Dynamic Systems, Measurement and Control*, **126**(4), 709–720.

Mitchell, R.I. (1989). Creating Complex Signal Samples From a Band-Limited Real Signal. *IEEE Transactions on Aerospace and Electronic Systems*, **25**(3), 425–427.

Narendra, K. and Gallman, P. (1966). An Iterative Method for the Identification of Non-linear Systems Using a Hammerstein Model. *IEEE Transactions Automat. Control*, **11**, 546–550.

Neto, F.P. Lépore, de Mello, J.D.B., and dos Santos, M.B. (2006). Non-linear signal analysis applied to surface wear condition monitoring in reciprocating sliding machines. *Shock and Vibration*, **13**, 327–341.

Nijmeijer, H. and der Schaft, A. Van (1991). *Non-linear dynamical control systems*. Springer, Berlin.

Nuij, P.W.J.M. (2002). Measurement technique to determine modal parameters of friction-induced resonance. In P. Sasand B. van Hal (eds.), *ISMA2002*, 479–484, Leuven, Belgium.

Nuij, P.W.J.M. and Steinbuch, M. (2004). Two measurement techniques to determine Higher Order Sinusoidal Input Describing Functions. In P. Sasand M. de Munck (eds.), *Proceedings of the 2004 International Seminar on Modal Analysis*, 2145–2154, Leuven.

Nuij, P.W., Bosgra, O.H., and Steinbuch, M. (2006). Higher-order sinusoidal input describing functions for the analysis of non-linear systems with harmonic responses. *Mechanical Systems and Signal Processing*, **20**(8), 1883–1904.

Nuij, P.W.J.M., Steinbuch, M., and Bosgra, O.H. (2007a). Experimental characterization of the stick/slip transition in a precision mechancal system using the Third Order Sinusoidal Input Describing Function. *Mechatronics, accepted*.

Nuij, P.W.J.M., Steinbuch, M., and Bosgra, O.H. (2007b). Measuring the Higher Order Sinusoidal Input Describing Functions of a non-linear plant oprating in feedback. *Control Engineering Practice*, Accepted.

Olsson, H. (1995). Describing function analysis of a system with friction. In *Proceedings of the 4th IEEE Conference on Control Applications*, 310–315.

Olsson, H. and Åström, K.J. (1996). Friction generated limit cycles. In *Proceedings of the 1996 IEEE International Conference on Control Applications*, 798–803.

Oppenheim, A.V. and Schafer, R.W. (1999). *Discrete-Time Signal Processing*. Prentice-Hall International, London, 2nd ed edition.

Pintelon, R. and Schoukens, J. (2001). *System Identification: A Frequency Domain Approach*. John Wiley&Sons Inc.

Putra, D. (2004). *Control of Limit Cycling in Frictional Mechanical Systems*. PhD. Thesis, Eindhoven University of Technology.

Rader, C.M. (1984). A simple method for sampling in-phase and quadrature components. *IEEE Transactions on Aerospace and Electronic Systems*, **20**(6), 821–824.

Randall, R.B. (1987). *Frequency analysis*. Brüell & Kjær, Nærum.

Rugh, W.J. (1981). *Non-linear System Theory: the Volterra/Wiener Approach*. Johns Hopkins University Press, Baltimore, Maryland, USA.

SANDBERG, I.W. (1982). Expansions for non-linear systems. *Bell System Technical Journal*, **61**(2), 159–199.

SANDBERG, I.W. (1983a). Expansions for discrete-time non-linear systems. *Circuits, Systems and Signal Processing*, **2**(1), 77–87.

SANDBERG, I.W. (1983b). The mathematical foundations of associate expansions for mildly non-linear systems. *IEEE Transactions on Circuits and Systems*, **CAS-30**(7), 441–455.

SANDBERG, I.W. (1985). Non-linear input-output maps and approximate representations. *Bell System Technical Journal*, **64**(8), 1967–1983.

SANDBERG, I.W. (1992). Approximately finite memory and input-output maps. *IEEE Transactions on Circuits and Systems*, **39**, 549–556.

SCHETZEN, M. (1980). *The Volterra and Wiener Theories of Non-linear Systems*. John Wiley, Chichester.

SCHOUKENS, J., DOBROWIECKI, T., and PINTELON, R. (1998). Parametric and Nonparametric Identification of Linear Systems in the Presence of Non-linear Distortions- A Frequency Domain Approach. *IEEE Transactions on Automatic Control*, **43**, 176–190.

SCHOUKENS, J., PINTELON, R., DOBROWIECKI, T., and ROLAIN, Y. (2005). Identification of linear systems with non-linear distortions. *Automatica*, **41**, 491–504.

SCIAVICCO, L. and SICILIANO, B. (1996). *Modeling and control of robot manipulators*. McGraw-Hill, London.

SHELTON, R.D. and ADKINS, A.F. (1970). Noise Bandwidth of Common Filters. *IEEE Transactions on Communications Technology*, 828–830.

SHERIF, H.A. and BASSIONI, A.S (1994). Non-linear identification of mechanical systems with dynamic dry friction. *Journal of Sound and Vibration*, **178**(4), 513–533.

SKOGESTAD, S. and POSTLETHWAITE, I. (2005). *Multivariable Feedback Control, Analysis and Design*. Wiley.

SLOTINE, J. and LI, WEIPING (1991). *Applied Non-linear Control*. Prentice-Hall International, London.

SOLOMOU, M., EVANS, C., and REES, D. (2001). Crest Factor Minimisation in the Frequeny Domain. In *Conference Proceedings of the IEEE Instrumentation and Measurement Technology Conference*, 1375–1381, Budapest, Hungary.

SOLOMOU, M., EVANS, C., REES, D., and CHIRAS, N. (2002). Frequency Domain Analysis of Non-linear Systems Driven by Multiharmonic Signals. In *IEEE Instr. and Meas. Techn. Conf. Anchorage*, 799–804.

SOLOMOU, M., REES, D., and CHIRAS, N. (2004). Frequency Domain Analysis of Non-linear Systems Driven by Multiharmonic Signals. *IEEE Transactions Instrum. Meas.*, **53**, 243–250.

STEINBUCH, M. (2002). Repetitive control for systems with uncertain period-time. *Automatica*, **38**(12), 2103–2109.

SWEVERS, J., AL-BENDER, F., GANSEMAN, C., and PRAJOGO, T. (2000). An Integrated Friction Model Structure with Improved Presliding Behavior for Accurate Friction Compensation. *IEEE Transactions on Automatic Control*, **45**(4), 675–686.

SYMENS, W., AL-BENDER, F., SWEVERS, J., and BRUSSEL, H. VAN (2002). Harmonic analysis of a mass subject to hysteretic friction: experimental validation. In P. SASand B. VAN HAL (eds.), *Proceedings of the 2002 International Seminar on Modal Analysis*, 1229–1240, Leuven.

TAYLOR, J. (1999). *Electrical Engineering Encyclopedia: Describing Functions*. John Wiley & Sons Inc., New York.

TAYLOR, J.H. and JIN, L. (1995). Robust non-linear control system synthesis method for electromechanical pointing systems with flexible modes. *Journal of Systems Engineering*, **5**(3), 192–204.

TOMIZUKA, M. (1987). Zero phase error tracking algorithm for digital control. *Journal of dynamic systems, measurement and control*, **109**, 65–68.

TOMIZUKA, M., TSAO, T.C., and CHEW, K.K. (1988). Discrete-time domain analysis and synthesis of repetitive controllers. In *Proc. 1988 American Control Conference*, 860–866.

VANHOENACKER, K., SCHOUKENS, J., SWEVERS, J., and VAES, D. (2002). Summary and comparison overview of techniques for the detection of non-linear distortions. In P. SASand B. VAN HAL (eds.), *Proceedings of the 2002 International Seminar on Modal Analysis*, 1241–1256.

VOLTERRA, V. (1959). *Theory of functionals and of integral and integro-differential equations.* S.I., Dover. Reprint from the 1931 Macmillan edition.

VOLTERRA, V., TOMASSETTI, M., and ZARLATTI, F.S. (1913). *Leçons sur les équations intégrales et les equations integro-différentielles: leçons professées à la faculté des sciences de Rome en 1910.* Paris: Gauthier-Villars.

WEISS, M., EVANS, C., and REES, D. (1998). Identification of Non-linear Cascade Systems Using Paired Multisine Signals. *IEEE Transactions on Instrumentation and Measurement*, **47**(1), 332–336.

WIENER, D.D. and SPINA, J.F. (1980). *Sinusoidal Analysis and Modelling of Weakly Non-linear Circuits.* Van Nostrand Reinhold, New York.

WONG, S.C. and BARHORST, A.A (2006). Polynomial Interpolated Taylor Series Method for Parameter Identification of Nonlinear Dynamic Systems. *Journal of computational and Nonlinear Dynamics*, **1**, 249–256.

WYCKAERT, K. (1992). *Development and evaluation of detection and evaluation schemes for the non-linear dynamical behaviour of mechanical structures.* Ph.D. thesis, Katholieke Universiteit Leuven.

YAU, W. and TSAI, M. (1999). Repetitive control design for linear servo systems. In *Proceedings of the American Control Conference*, **5**, 3728–3732.

YUE, R., BILLINGS, S.A., and LANG, Z.Q (2005a). An inverstigation into the characteristics of non-linear frequency response functions. Part 1: Understanding the higher dimensional frequency spaces. *International Journal of Control*, **78**(13), 1031–1044.

YUE, R., BILLINGS, S.A., and LANG, Z.Q (2005b). An inverstigation into the characteristics of non-linear frequency response functions. Part 2: New analysis methods based on symbolic expansions and graphical techniques. *International Journal of Control*, **78**(14), 1130–1149.

ZATTONI, E. (2005). Detection of incipient failures by using an H2-norm criterion: Application to railway switching points. *Control Engineering Practice*, **14**(8), 885–895.

DE JAGER, B. (1993). Improving the tracking performance of mechanical systems by adaptive extended friction compensation. *Control Eng. Pract.*, **1**(6), 1009–1018.

DE WIT, C. CANUDAS and LISCHINSKY, P. (1997). Adaptive friction compensation with partially known dynamic friction model. *International Journal of Adaptive Control and Signal Processing*, **11**, 65–80.

DE WIT, C. CANUDAS, OLSSON, H., ÅSTRÖM, K.J., and LISCHINSKY, P. (1995). A New Model for Control of Systems with Friction. *IEEE Transactions on Automatic Control*, **40**(3), 419–425.

VAN SEGGELEN, J.K. (2007). *NanoCMM : a 3D coordinate measuring machine with low moving mass for measuring small products in array with nanometer uncertainty.* Ph.D. thesis, Eindhoven University of Technology.

Summary

Higher Order Sinusoidal Input Describing Functions
Extending linear techniques towards non-linear systems analysis

In modern positioning systems, accuracy and speed requirements have increased significantly. These accuracies can only be realized if account is given to nonlinear system behavior in both the mechanical and the control design. This requires additional tools for frequency based identification of nonlinear system behavior since existing tools either are either too limited to successfully describe nonlinear behavior or the results are very difficult to interpret and as such do not relate to the background of the intended user.

In this thesis an alternative concept for frequency based nonlinear system analysis is presented, the required measurement techniques are described and some application examples are shown. The method is applicable for the class of causal, stable, time-invariant non-linear systems which have a harmonic response to a sinusoidal excitation. This new concept is the generalization of the Sinusoidal Input Describing Function to *Higher Order Sinusoidal Input Describing Functions* (HOSIDF) as it yields the magnitude and phase relations between the individual higher harmonics in the response signal and the sinusoidal excitation signal, both as function of magnitude and frequency of the excitation signal. An essential element in the HOSIDF theory is the concept of the *Virtual Harmonics Expander* (VHE). This nonlinear function describes the transformation of a single sinusoid into an infinite amount of harmonics, each with equal amplitude as the input signal and with a phase equal to the phase of the input signal times the harmonic number. Nonlinear systems belonging to the class can be modeled as a parallel connection of an (infinite) amount of HOSIDF describing quasi-linear subsystems in series with the VHE. Two measurement methods for nonparametric identification of HOSIDF are presented. The Fast Fourier Transform based method on fast fourier transforms shows ideal characteristics due to its perfect selectivity. The IQ (In phase-Quadrature phase) demodulation method has limited performance due to non perfect selectivity.

The bias in the HOSIDF estimates caused by harmonic components in the input signal is analyzed and a compensation algorithm is presented to reduce this bias. Accept-

ing harmonic distortion in the excitation signal allows the application of non-constant amplitude-time profiles for testing. It is demonstrated that a ramped amplitude-time signal reduces the required settling time of the digital filters used in the IQ methode.

The capabilities of the HOSIDF technique are demonstrated in a real measurement in which the stick to gross sliding transition of a mechanical system with dry friction is captured as function of frequency. The odd HOSIDF clearly reveal this transition which is not possible with the Frequency Response Function technique. From the HOSIDF the pre-sliding displacement and the friction-induced stiffness are determined and the friction force which must be present in the stick-phase is calculated. Validation with force measurements shows excellent agreement.

Special attention is paid to the determination of the HOSIDF of a nonlinear plant operating in feedback. In a controlled system the harmonics generated by the non-linear system will be fed back to the input, changing the sinusoidal excitation into an harmonic excitation. Two different solutions are presented to deal with this problem. The first method applies a numerical compensatie techniques to compensate the bias caused by the harmonic components in the excitation signal. The second method uses a modified repetitive control scheme to suppress the harmonic components in the excitation signal. The effectiveness of both methods is tested in simulation experiments of a mass operating in feedback subjected to Coulomb friction, Stribeck-effect and hysteresis in the pre-sliding regime. The friction forces are modeled with the modified Leuven friction model. The results are compared with the HOSIDF measured under open loop condition and both methods yield correct results.

It is shown that by rearranging the repetitive control loop, the output signal of a class of stable, time-invariant nonlinear systems becomes sinusoidal as response to an harmonic excitation. For this class of signals *Higher Order Sinusoidal Output Describing Functions* (HOSODF) can be defined as the dual of the HOSIDF. The HOSODF describe magnitude and phase relations between the individual higher harmonics in the input signal and the sinusoidal output signal, both as function of magnitude and frequency of the output signal. The required dual of the *Virtual Harmonics Expander* is defined as the *Virtual Harmonics Compressor*. This nonlinear function describes the transformation of an infinite amount of harmonics into a single sinusoid.

Finally, an application example shows the extreme sensitivity of the HOSIDF technique for changes in friction characteristics, indicating interesting opportunities for application in the field of machine condition monitoring.

Samenvatting

De eisen die gesteld worden aan de snelheid en positioneringsnauwkeurigheid van moderne positioneringssystemen zijn significant toegenomen. Deze nauwkeurigheden kunnen alleen maar gerealiseerd worden als met niet-lineair systeemgedrag rekening wordt gehouden in zowel het mechanische als het regeltechnische ontwerp. In tegenstelling tot de tijddomein gebaseerde systeemidentificatie is de moderne regeltechniek op frequentiedomein technieken gebaseerd. Maar de transformatie van niet-lineaire tijddomein modellen naar het frequentiedomein is niet mogelijk met alleen lineaire technieken. Dit vereist extra gereedschappen ten behoeve van de frequentiedomein gebaseerde identificatie van niet-linear systeemgedrag omdat de bestaande gereedschappen ofwel te beperkt zijn om met succes niet-linear gedrag te beschrijven ofwel resultaten leveren in een formaat dat moeilijk te interpreteren is en niet aansluit bij de achtergrond van de gebruiker.

In dit proefschrift wordt een alternatief concept gepresenteerd voor een op frequentiedomeintechnieken gebaseerde niet-lineaire systeemanalyse. Eveneens worden de vereiste meetmethodes beschreven en enkele toepassingsvoorbeelden getoond. De methode is van toepassing op de klasse I gedefinieerd als de klasse van causale, stabiele, tijdsinvariante, niet-lineaire systemen welke een harmonische responsie hebben ten gevolge van een sinusvormige excitatie. Dit nieuwe concept is de generalisatie van de Sinusoidal Input Describing Function tot de *Higher Order Sinusoidal Input Describing Functions* (HOSIDF). De HOSIDF beschrijven de magnitude- en faserelaties die bestaan tussen de afzonderlijke hogere harmonische componenten in het responsiesignaal en de sinusvormige excitatie, allen als functie van amplitude en frequentie van dat excitatiesignaal. In de HOSIDF theorie wordt een essentiële plaats ingenomen door het begrip *Virtual Harmonics Expander* (VHE). Deze niet-lineaire functie beschrijft de transformatie van een zuiver sinusvormig signaal in een oneindige reeks harmonischen, elk met identieke amplitude gelijk aan de amplitude van het ingangssignaal en een fase gelijk aan de fase van het ingangssignaal maal het rangnummer van de harmonische component. Systemen die behoren tot de klasse I kunnen gemodelleerd worden als een parallel schakeling van een (oneindig) aantal HOSIDF in serie met de VHE. Twee meetmethodes voor de niet-parametrische identificatie van HOSIDF worden gepresenteerd. De op Fast Fourier

Transform (FFT) technieken gebaseerde methode blijkt ideale eigenschappen te hebben. De IQ (in fase - quadratuur fase) demodulatiemethode daarentegen heeft beperkte eigenschappen ten gevolge van niet-ideale selectiviteit. De vertekening in de schatting van de HOSIDF veroorzaakt door harmonische vervorming in het excitatie signaal is geanalyseerd en er is een compensatie-algoritme gepresenteerd om deze vertekening te verminderen. Door enige harmonische vervorming in het excitatiesignaal te accepteren is het mogelijk testsignalen met niet-constante amplitude - tijd relaties toe te passen. Er is aangetoond dat een testsignaal met een linear in de tijd toenemende amplitude de benodigde inslingertijd van de digitale filters, die worden toegepast in de IQ methode, vermindert.

De kwaliteiten van de HOSIDF techniek worden getoond middels metingen waarin voor een mechanisch systeem met droge wrijving de overgang van de kleeffase naar de glijfase frequentie-afhankelijk wordt vastgelegd. In tegenstelling tot klassieke Frequentie Responsie Functie (FRF) metingen is deze overgang zeer goed zichtbaar in de oneven HOSIDF. Uit de HOSIDF worden eveneens de elastische verplaatsing in de kleeffase en de frequentie van de door de wrijving veroorzaakte resonantie bepaald. Met deze gegevens is het mogelijk de wrijvingskracht te berekenen die aanwezig moet zijn in de kleeffase. Een validatie van de berekeningen middels een meting van deze kracht toont verregaande overeenkomsten. Speciale aandacht wordt besteed aan het bepalen van de HOSIDF van een teruggekoppeld niet-lineair systeem. In een teruggekoppeld systeem zullen de harmonischen die ontstaan ten gevolge van niet-lineair gedrag vanuit de uitgang teruggevoerd worden naar de ingang van het systeem. Hierdoor wordt de vereiste sinusvormige excitatie geweld aangedaan. Twee verschillende oplossingen voor dit probleem worden gepresenteerd. De eerste oplossing is een numerieke compensatie van de afwijking ten gevolge van de aanwezige harmonische componenten in het excitatiesignaal. In de tweede methode wordt gebruik maakt van een aangepaste repeterende regeling om de harmonische componenten in het excitatiesignaal te onderdrukken. De effectiviteit van beide methodes is getest middels een simulatie-experiment van een geregelde massa die onderhevig is aan Coulombse wrijving, Stribeckeffect en hysteresis in de kleeffase. De wrijvingskrachten zijn hierbij gemodelleerd met het gemodificeerde wijvingsmodel van Leuven. De resultaten van beide methoden zijn vergeleken met de overeenkomstige resultaten van een niet-geregelde massa en blijken betrouwbaar.

De extreme gevoeligheid van de HOSIDF techniek voor veranderingen in wrijvingseigenschappen van een niet-lineair systeem wordt in een voorbeeld getoond, hetgeen een mogelijk interessante toepassing oplevert in het veld van de machineconditie bewaking.

Tot slot blijkt het mogelijk te zijn een specifieke klasse van causale, stabiele, tijd-invariante, niet-lineaire systemen met behulp van een repeterende regelaar zodanig te regelen dat deze systemen een sinusvormig uitgangssignaal tonen ten gevolge van een harmonische excitatie. Voor deze klasse van systemen kan een duale beschrijving van de HOSIDF gegeven worden, gedefinieerd als de *Higher Order Sinusoidal Output Describing*

Functions (HOSODF). De HOSODF beschrijven de magnitude- en faserelaties die bestaan tussen de afzonderlijke hogere harmonische componenten in het excitatiesignaal en het sinusvormige responsiesignaal, allen als functie van amplitude en frequentie van dat responsiesignaal. De hiervoor benodigde duale beschrijving van de *Virtuele Harmonische Expander* is gedefinieerd als de *Virtuele Harmonische Compressor*. Deze niet-lineaire functie beschrijft de transformatie van een oneindige reeks harmonischen in een enkelvoudige sinusoïde.

Dankwoord

„Verder dient de kandidaat de bereidheid uit spreken binnen afzienbare tijd te promoveren." Dit was de afspraak die ik met de toenmalige decaan Prof. Schouten, mijn "nieuwe" oude baas Maarten Steinbuch en Twan Sens (personeelszaken) maakte in 2000 bij mijn start als universitair docent. Met veel meetervaring uit de industrie (waar Rens Kodde tijdens mijn afstuderen de basis voor heeft gelegd) en een voorliefde voor onderwijs ben ik aan deze opdracht begonnen. In het begin onwennig want de benodigde kennis was voor een deel diep weggezakt sinds mijn afstuderen in 1982. Na verloop van tijd kwamen de eerste resultaten in de vorm van een afwijzing van een bijdrage voor de ECC en een geaccepteerd paper voor de ISMA2002 (ook publiceren moet je leren). Ondertussen eisten mijn onderwijsactiviteiten steeds meer tijd op. De rol als tutor en mentor beviel me goed, de eerstejaars onderwijsproblematiek boeide me maar de gevolgen voor mijn tijdbesteding lieten zich raden. Het risico dat het promotieonderzoek stil zou vallen, was meer dan denkbeeldig en ik denk dat het ook echt gebeurd zou zijn als Maarten me niet tot de orde had geroepen. Maarten, bedankt voor de mogelijkheden die je me hebt geboden en bedankt voor jouw altijd inspirerende coaching. Zonder jouw verbod mij weer eens als tutor op te geven zou de balans tussen mijn onderwijs- en onderzoeksactiviteiten definitief geheel naar de onderwijs kant zijn doorgeslagen en had de wetenschapper in mij het nooit gered. Jouw advies om met Okko Bosgra te gaan sparren heb ik ook als zeer waardevol ervaren. De gesprekken met Okko zal ik me blijven herinneren als oefeningen in het zoeken naar de vraag achter de vraag. Ze waren als een rondvlucht hoog over mijn onderzoeksgebied: ineens bleek er achter de horizon nog een wereld te liggen. Onverwachte verbanden werden zichtbaar en antwoorden veranderden ineens in nieuwe vragen. Okko, bedankt voor de geestverruimende gesprekken die we hebben gehad, voor het openen van mijn ogen om de eigenlijke vraag achter de vraag te zien en voor de hulp bij het beantwoorden ervan. Goede hulp heb ik ook gekregen van Bram de Jager en Frans Veldpaus. Bram en Frans, bedankt voor jullie gewillig luisteren naar en meedenken over een soms nog niet helemaal coherent verhaal. Ook wil ik Johan Schoukens bedanken voor zijn aanmoedigingen om door te gaan op de ingeslagen weg. Inderdaad Johan, echte metingen kosten veel tijd maar geven ook veel voldoening.

Zonder de ondersteuning van mijn collega's zou mijn promotietraject heel moeilijk geworden zijn. Maar zonder de ondersteuning van mijn vrouw was het beslist niet gelukt. Lidwine bedankt voor je kameraadschap, je steun en geduld, speciaal de laatste jaren toen bleek dat mijn werkdagen te kort waren en veel avonden en weekends geïnvesteerd moesten worden om verder te komen, terwijl je het zelf ook steeds drukker kreeg. Ook mijn kinderen wil ik bedanken voor hun begrip: „Randi, weet jij waar papa is? Ja Oda, hij zit weer in zijn hok te promoveren. Oh, dan is 't goed." Dat zijn de momenten dat ik me een hele trotse vader voel van twee supermeiden. Net zo trots als mijn ouders waren toe ik hun vertelde van het promotieplan. Mam, bedankt voor de kansen die jullie beide voor mij hebben gecreëerd.

Terugkijkend is deze opleiding tot onderzoeker een zware klus geweest, en een mijlpaal in mijn leven. Nu is het af, het voelt goed, de angstdromen van vakken die nog afgerond moeten worden zijn weg en er ligt lekker nog een verbouwing in het verschiet.

Pieter Nuij
Ospeldijk, juni 2007.

Curriculum Vitae

Ir. P.W.J.M. Nuij received his M.Sc. degree in Mechanical Engineering from Eindhoven University of Technology, Eindhoven, The Netherlands, in 1982. From 1982 until 2000 he worked in industry both in Holland (Philips) and abroad (Brüel & Kjær, Denmark) focussing on signal analysis and system analysis applications in mechatronics development. As a lecturer of the Philips Centre for Technical Training he was responsible for the Philips course "Measurement Techniques in Mechatronics". He is assistant professor in the Control Systems Technology group of the Mechanical Engineering Department of Eindhoven University of Technology, a position that he combines with his position as the student advisor of the faculty of Mechanical Engineering. His research interests are focussed on measurement techniques for non-linear system analysis. His teaching interests are focussed on signal analysis and educational reform for the freshmen.